

UNIVERSITY OF NAPLES

FEDERICO II



Ph.D. IN STRUCTURES AND MATERIAL ENGINEERING

(XXII CICLO)

Ph.D. Thesis

**MODELING OF LIGHTWEIGHT CRASHWORTHY
RAIL COMPONENTS**

SUPERVISOR

Prof. Antonio De Iorio

COORDINATOR

Prof. Domenico Acierno

CANDIDATE

Mr. Marzio Grasso

MODELING OF LIGHTWEIGHT CRASHWORTHY RAIL COMPONENTS

Summary

As part of a research collaboration between the Department of Mechanics and Energetics of the University of Naples Federico II (IT) and NewRail Newcastle University Centre for Railway Research (UK) has been conducted a study on the applicability of composite materials for the crashworthiness design of a train cab.

The preliminary phase of work has involved the study of issues related to railway accidents and safety standards for passengers imposed by European Standards. In the next phase, we addressed the problem of redesigning the structure of an existing cab in order to reach a solution that, at the same performance, is able to increase the payload and decrease manufacturing and maintenance costs..

For this purpose, composite materials, metallic and non, has been chosen with few traditional metallic material to create virtual structures, since they are very performance and characterize by very high specific absorption energy.

After a thorough comparative analysis of the characteristics of strength, energy absorption capability and applicability to a particular component of the many materials tested, it has been selected those more suitable for this purpose: mild steel, GRP, balsa wood and rigid polyurethane foam wrapped in FRP.

For components made by these materials, except those made by the balsa wood, tests of mechanical characterization, needed to be able to model the correct behaviour before moving on to the stage of numerical simulations, were conducted.

It has followed a consistent simulation activities with the finite element code LS-DYNA ®, to reproduce, on the individual components in each design, the impact conditions prescribed by the regulations EN15227, and, on the whole structure, the load conditions prescribed by EN12663. It has been possible to define the solution that better respond to the specified requirements, by comparing the behavioral responses of the different solutions hypothesized.

The next work will consist in verifying, by static and dynamic tests on full scale prototypes of the optimized structures, the compliance between numerical and experimental results.



The train collision at Ladbrooke Grove

5 October 1999

From the report of the HSE investigation

Alla mia famiglia e a Mariamichela

RINGRAZIAMENTI

Questo lavoro di tesi è il frutto di un percorso di formazione di tre anni durante i quali ho avuto la possibilità di approfondire le mie conoscenze e crescere sotto l'aspetto umano.

Per questo ringrazio:

il Prof. Antonio De Iorio per la cura con la quale mi ha seguito in questi tre anni e per i preziosi consigli che mi ha dato,

l'Ing. Francesco Penta per la pazienza con la quale mi ha supportato e sopportato durante le mille difficoltà incontrate,

il Dott. Joe Carruthers per avermi concesso la possibilità di trascorrere un periodo di formazione presso le strutture del Centro Newrail dell'Università di Newcastle,

Conor O'Neill per la pazienza e l'assistenza giornaliera che mi ha fornito durante i mesi di formazione in UK,

e Tutti coloro che ho avuto il piacere di incontrare, grazie a questa bellissima esperienza, e per quello che ciascuno mi ha dato.

ACKNOWLEDGEMENTS

This thesis is the result of three years of training during which I had the opportunity to further my knowledge and grow under the human aspect.

For this I would like to thank:

Prof. Antonio De Iorio for the attention with which he followed me in these three years and for the valuable advice he gave me,

Ing. Francesco Penta for the patience with which he has supported and tolerated me during the numerous difficulties encountered,

Dr. Joe Carruthers for giving me the opportunity to spend a period of training at Newrail, Newcastle University's Center for Railway Research

Conor O'Neill for the daily patience and assistance that he has given me during the months in UK,

and all those who I had the pleasure to meet during this beautiful experience and for what each has given to me.

CONTENTS

1. Safety and Standards	1
1.1 Introduction	1
1.2 Active and Passive Safety	1
1.3 Railway Incidents Classification	3
1.4 Reference Standards	5
1.4.1 EN 12663 (Structural requirements of railway vehicle bodies)	6
1.4.2 EN 15227 (Railway application– Crashworthiness requirements for railway vehicle bodies)	7
1.5. Impact Scenarios	8
1.6. Control Parameters	9
1.7. Target performance	10
1.8. Absorption systems	11
2. Modeling of Material Mechanical Behavior	13
2.1 Introduction	13
2.2 Metallic Materials	14
2.3 Aluminum Honeycomb	18
2.4 Fiber Reinforced Plastic (FRP)	20
2.5 Polyurethane Foam	23
2.6 Balsa Wood	23

3. Cab Structure	26
3.1 Typical Cab Structure	26
3.2 Modular Absorption	28
3.3 Lower Absorber System	30
3.3.1 Type of Absorber	30
3.3.2 Materials	32
3.4 Upper Absorber System	32
3.5 Coupler	33
3.5.1 Three Link Coupling	34
3.5.2 Instanter Coupling	35
3.5.3 Screw Coupling	35
3.5.4 Janney Coupler	36
3.5.5 AAR Coupler	36
3.5.6 Wilson Coupler	37
3.5.7 Scharfenberg Coupler	37
4. Lower Absorber Modeling	39
4.1 Calibration of material parameters	39
4.2 Lower Absorber	46
4.3 Multi-stage model	58
4.4 Single stage model	65

5. Upper Absorber Modeling	73
5.1 Upper Absorber	73
5.2 Calibration of Material Parameters	74
5.3 Honeycomb Block Optimization	82
6. Cab Modeling	91
6.1 Composite Cab	91
6.2 Performance of the Structure	103
6.3 FE Modeling	104
6.4 Calibration of Material Parameters	109
6.5 Results of the Static Analysis	113
7. Conclusions	117
8. References	120



CHAPTER I

SAFETY AND STANDARDS

1.1. Introduction

Effects on passengers and things that the great variety of accidents occurring in rail transportation can produce are well known. Thus, it can be said that a train must be designed not only taking into account its structural resistance under applied loads but also giving specific attention to the study of systems able to absorb an adequate amount of impact energy, to preserve passengers and surrounding environment in case of collision.

Technicians, who have been dealing with this issue for years, have proposed several design solutions to increase safety on trains, based on automotive and aeronautical results, where the research is very advanced.

Since 1994, with prescriptions becoming stricter in the very complex standards, that regulate structural requirements, it is provided for using systems, which, in a controlled and reliable way, are involved during the collision and can mitigate the effects of a collision or overriding. However, because of the high energy involved, these systems are often too heavy and cumbersome. For this reason, the possibility to use composite materials, metallic or not, lighter than the traditional ones, is seen as very good option.

1.2. Active and Passive Safety

Safety as a concept is divided into two categories, the passive safety, which is achieved using devices that reduce the negative effects on a passenger during an accident, and the active safety which is achieved using monitoring devices to reduce the chances of accidents.



As far as the active safety is concerned, there are sophisticated control and warning systems that help the driver during operation, regulating the flow and avoiding those overlapping that may occur on the tracks. In addition to that, there are also some monitoring and emergency systems in the railway vehicle. It has been observed, in numerous studies, that after an accident both the incorrect functioning of the emergency disposals and the incorrect arrangement of the evacuation steps can provoke a higher number of victims than the same accident [1]. With reference to the passive safety, devices to dissipate the impact energy are installed on all railway vehicles and they allow both controlling and limiting the impact effects and reduce the consequences for the occupants.

Railway vehicles are very different from other structures of any other transportation system. Due to the typology of service and the configuration of the train, originally, it was necessary that the structure was built to resist to low speed shocks that may occur during the service. For this reason, until the Fifties, the carbody structure, which is the main element of the vehicles, was made of a very stiff floor, which ensured the necessary strength during the travel and of very light elements that had the only function of defining the passenger survival space and protect them in case of inclement weather.

After very heavy accidents and speed increase in trains, the first studies on structural resistance of railway vehicles began. ORE, European Railways' Office of Research and Experimentation, appointed a special committee, B7, who had the task of studying the current structures and create the guide lines to design the railway vehicles with safety requirements more adequate to rail transportation needs. B7 created the standard OR 567 in which it was described the typology and the entity of loads that the structure has to withstand without plastic deformation to ensure sufficient safety standards [2].

Only in 1980, studies on the dynamic strength in rail transportation began to investigate on the structure behavior during a crash. The committee B165 was appointed to study the dynamic behavior of a cab during a frontal crash. Numerical simulations of a frontal crash were done and validated with a full-scale test. At the



end of the study a document was issued with some indications on how to design a cab, focused on the structural optimization in case of impact. In particular, it was observed that, during the impact, after braking, the inertial actions push one vehicle on the proximal. Because of this action, permanent deformations occur at the ends of each railway vehicle. To minimize the extension of these deformations and concentrate them only in specific areas, in order to preserve both the passengers and the rest of the structure, it is necessary to provide for disposals which, deforming in a controlled manner, dissipate kinetic energy and maintain unchanged the survival space where the passengers stay.

The evolution of the standards brought to EN 12663 [3] and EN 15227 [4] which are reference standards for designing of railway vehicles. In particular, EN 12663 is the reference standard for designing rail vehicles in terms of static and fatigue loads, while EN 15227 describes the operational procedures to verify the passive safety requirements according to European standards.

1.3. Railway Incidents Classification

Train accidents are of such a great variety that trying to classify them is really difficult. Thus, it is very complex to identify them into categories, which would help a general approach to the issue. Generally speaking, it is possible to identify 4 steps during an impact: Pre-crash, primary impact, secondary impact, final phase (fig. 1.1) [5].

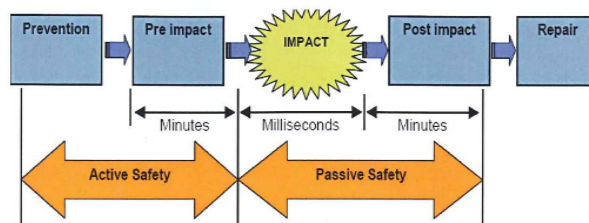


Fig. 1.1 – Sequence pattern of a railway impact [9].



In the first phase, called pre-crash, active safety systems intervene, such as the diagnostics of the boarding systems and the control systems of the railway traffic. When these systems are not efficient, an impact occurs.

The primary impact is the crash of the railway vehicle against things, of any nature, which are on the track. During this phase there are abrupt variations of the acceleration, possible overriding and, in extreme situations, a derailment may occur. The impact, which involves passengers too, is called secondary impact. We can distinguish two typologies of secondary impacts. One makes one cab crash against another one, the other is caused by the relative speed between the passengers and the vehicle. In the first case, the impact involves the structure as the collision provokes the reduction of the internal space. In the second case, the speed variation creates inertial effects that push the passengers against the interiors or against other people, but no deformation of the structure occurs. The last phase is the one that concerns track conditions and the environment after the crash. The chance of explosions or fire can interfere with the evacuation plan and obstruct the rescue [6].

As it is impossible to study and verify the behavior of the structures and the occupants in all possible impact scenarios, known or hypothetical, a systematical study identified the most common and dangerous ones compared to all the possible accidents that may occur during the operation.

Accident Category		Number of Accidents	%
1. Collision with another rail vehicle	1.1 Head-on	31	10%
	1.2 Rear-on	69	23%
	1.3 Other	21	7%
2. Collision on level crossing	2.1 With car	28	9%
	2.2 With Lorry/tractor	80	26%
	2.3 Other Vehicle	3	1%
3. Collision not included elsewhere		24	8%
4. Collision with buffer stop		33	11%
5. Collision after derailment		2	1%
6. Derailment without collision		13	4%

Fig. 1.2 – Impact scenarios occurred from 1991 to 1995.

In fig. 1.2, taken from a report of Rail Safety and Standard Board [7], the main accidents occurred on the European railway are summarized. It analyzes the 60% of



the total tracks, in a period of time from 1991 to 1995. It is highlighted that some accidents, which we can classify as on-line accidents, are repeated. Among them there are frontal impacts between two trains and impacts against road vehicles at the intersections between the tracks and the roads. Collisions not well defined, which are the 8% of the total, include also those caused by humans, which are really difficult to investigate due the complexity of factors involved.

Another important issue is the one connected with the maintenance of an infrastructure, which, falling within the track maintenance, is not taken into account during the vehicle design.

Other type of accidents, which we could classify as oblique, include, among others, a collision between two trains at an intersection and the impact that can occur on lines with two tracks, when one of the two trains have elements which come out of the shape of the vehicle and occupy the other train space.

From these studies, in terms of dangerousness, representation and damage of the structures, in Europe, five reference scenarios have been described in EN 15227.

1.4. Reference Standards

In designing every single component of a railway vehicle there is a specific standard which validity is extended to all EU Countries. For structural verifications on the carbody and to verify the conformity of a railway vehicle to the European prescriptions on crashworthiness, the reference standards are EN12663 [3] and EN15227 [4]. Following, the content of these two standards have been analyzed in general.



1.4.1. EN 12663 (*Structural requirements of railway vehicle bodies*)

The standard defines the structural requirements that a railway vehicle body must have in terms of static and fatigue loads, the methodologies used to quantify these loads and all the tests to make the verification.

Among the requirements that the structure must satisfy, the most significant ones are that it has to withstand the maximum loads correspondent to the service conditions and it has to ensure the survival level under loading which is supposed to be adequate. Moreover, in case of plastic deformation due to an overloading or to a fatigue loading, dangerous structural collapses must not be noticed.

The railway vehicles are divided into two categories:

- Freight vehicles (F)
- Passenger vehicles and locomotives (P)

The Freight vehicles can be divided into 2 subcategories:

- Vehicles which can be shunted without restriction; (F-I)
- Vehicles excluded from hump and loose shunting (F-II)

The Passenger vehicles and locomotives can be divided into 5 categories:

- Coaches and locomotives; (P-I)
- Fixed Units; (P-II)
- Underground and rapid transit vehicles; (P-III)
- Light duty metro and heavy duty tramway vehicles; (P-IV)
- Tramway vehicles; (P-V)

As a matter of facts, the standard identifies the typologies, entity and loading combinations for each category and subcategory.

Other loading typologies or specific applications can be evaluated by the designer and by the customer in case of further investigations were necessary.



1.4.2. EN 15227 (*Railway applications – Crashworthiness requirements for railway vehicle bodies*)

The Standard [4] defines the requirements to ensure a sufficient protection when all primary systems are inefficient. However, as it is very difficult to create systems that ensure a protection for the passengers against all possible impact scenarios, the ref. [2] identifies most likely and significant risk scenarios against which the structure must ensure the required protection level.

Railway vehicle reliability evaluation, in terms of safety, is checked through parameters, which characterize the dynamic of the phenomenon such as the dissipated energy, deceleration level measured during the impact and the structural resistance of the designed parts to withstand without plastic deformations.

The chance of making all the physical tests on all configurations is rare, being these too expensive. For this reason they are often substituted with virtual experiments, with numerical analysis, every time they result significant. The respect of the prescriptions can be verified through a scenario simulation, paying attention to calibrate the model and verifying its reliability with some tests. These ones do not necessarily have to include the whole structure, as it is possible to isolate some subsystems to study if they are correctly working and the interaction of the parts they are composed by.

It is mandatory though, to make them so that the energy level involved are the same of the scenario of a frontal impact between two identical trains or of the impact between a passengers train against a wagon. To ensure that the calibration and validation proofs are accepted it is necessary to document in details the experimental stage reporting all the significant parameters acquired and the evaluation of the uncertainty connected to the measurement of different quantities.

1.5. Impact Scenarios

With reference to the Standard [4] mentioned in the previous paragraph, the prescribed scenarios are (fig. 1.3):

- A front end impact between two identical train units;
- A Front end impact with a different type of railway vehicle
- Train Unit front end impact with a large road vehicle on a level crossing
- Train unit impact into low obstacle.

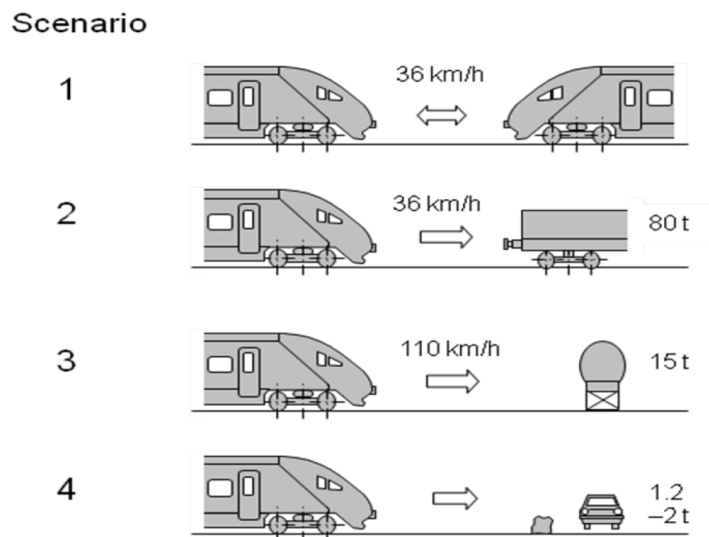


Fig. 1.3 – Impact scenarios from EN 15227.

In the following table the aforementioned impact scenarios are described according to the categories indicated in the standard and according to the operational conditions that must be respected for the validation.

The Standard describes in details the railway vehicles configurations, the impact speed and the entity of the moving masses for each scenario (fig. 4).



	Short description	Special requirements	Global requirements (valid for all scenarios)
Scenario 1	Collision train set – train set at 36 km/h	Prevent anti climbing, verification at 40 mm vertical offset, no lift-off of all wheel sets of one bogie → minimize risk of derailment	<ul style="list-style-type: none">• mean acceleration <5g (up to 7.5 g permitted)• 0.75 m survival space for driver inside the cab• In passenger areas deformations <1% at 5m length or plastic strains <10%• At end vestibule deformations <300 mm or 30% of original length• Standard method of validation: Test – Calibration – Simulation
Scenario 2	Collision train set - 80 t freight wagon at 36 km/h	Input for freight wagon (prEN 15227)	
Scenario 3	Collision train set – obstacle (equivalent to 15t lorry) at 110 km/h (for 160 km/h)	Input for obstacle (prEN 15227) <ul style="list-style-type: none">• Boundary conditions (Geometry)• Requirements (F/s – characteristic)	
Scenario 4	Collision train set – small obstacle (e.g. animal, car)	Special (static) load cases	

Fig. 1.4 – Short description of the requirements for the impact testing from EN15227 [7].

To take into account the limited number of scenarios prescribed compared to the variety of conditions that can happen during the travel, the Standard takes into account the chance of evaluating additional scenarios. In this case it is necessary a risk analysis connected to the configuration analyzed in order to decide how critical the situation is and the procedure to follow to perform that scenario.

Since it is possible to make the validation numerically only if supported with a validation test, the annex C of the reference [4] describes in details the characteristics to be used to build numerical models of the trains and of the obstacles to be simulated in different scenarios.

1.6. Control Parameters

Testing has two goals: validating the numerical models, in order to ensure that the collapse mechanisms and the estimated energies correspond to the ones observed in the simulations and verifying that all the disposals work properly.

Ref [4] describes all the operational conditions to execute the tests in terms of available energy, absorbed energy and minimum speed during the test. As a warranty for a correct execution of the test, a detailed report is required describing a test set-up and the quantities measured, as for instance the force, the impact speed and the deceleration. Moreover, it is necessary to create a simulation movie of the test, with



high speed camera to evaluate the correct collapse sequence and the dynamic of the folding.

For those components subject to large deformations, as for instance absorption systems, it is necessary to make some dedicated characterization of impact tests

1.7. Target performance

Conditions to verify both via numerical and experimental are:

- ✓ Reduction of overriding risk
- ✓ Structural integrity of the space occupied by passenger and by driver
- ✓ Vertical displacement of the wheelset of the frontal bogie and the decelerations in the survival space.

As far as the overriding reduction is concerned, in case of a frontal crash caused by high levels of energy and consequently by the forces that the two crashing trains mutually exchange, the vertical component of the force in the contact areas is very high and this may cause the train body being lifted and chance of a derailment. For this reason, it is necessary to verify the good behavior of the absorber in an on-line impact condition and with vertical offset to ensure that, in case of impact with a vertical offset of 40 mm, the system does not lose its functionality. Moreover, it is necessary that the vertical movement of the wheel be limited into certain limits to avoid the derailment.

The structure must withstand to all described impact conditions. Any failure or local buckling are allowed if they do not invalidate the structure functionality. In the cab, for instance, around the seat a safety region is defined so that the driver can leave his seat without being the egress blocked by the structure deformation.

One way of evaluating the injury factors for a train occupants is the maximum deceleration. Kinetic energy, at low speed too, in a train is very high, because of the considerable mass. Since the stop spaces are very small, the inertial actions on occupants are very high. Thus, the absence of restrained systems which tie up



passengers' motion to the seat may cause violent impacts of the passengers against the interiors injuring them to death.

1.8. Absorption systems

Since the first studies on the dynamic behavior in railways, it was well understood the advantageous effect that plastic deformation areas have on passengers' safety through which absorbing the impact energy and limiting the effects on the remaining part of the vehicle. At this purpose, suitable areas at the edge of the vehicle were identified, as they are the first ones involved and the farthest from the passenger area.

To respond to this requirements, the typical structure of a train is composed of a main structure, which has the function of transferring the loads to the carbody without any plastic deformation, of a energy absorption system and of a thin shell.

In particular, an absorption system that satisfies the standard regarding crashworthiness, generally consists of three elements:

- Coupler, which has also the function to connect the vehicles of a train unit;
- Lower absorber systems, which is the main absorption elements in scenarios 1 and 2;
- Upper absorber systems, whose main function is to accommodate the impact with the deformable obstacle.

The contribution of the coupler to dissipate the energy is very low and in some cases, like the impact against small road vehicles, can increase the damage factor for the road vehicle occupants. To obviate to these inconveniences, it is required an uncoupling system that allows the coupler to move back and ensure the functionality when traveling.

To perform their function, the lower absorbers are mounted behind the buffer and their activation occurs when the mutual actions among the buffers of the trains impacting one against the other go over the established value. The peculiarity of these elements is that they must get deformed under the impact loads but, at the same time, they must have the necessary stiffness to ensure that the contact force



components in the plane orthogonal to the travel direction do not provoke excessive movements causing the derailment.

Regarding the upper absorbers, in most of the applications they reproduce in small scale the lower absorbers both in shape and in materials. Since in case of impact against large obstacles the involved area is the one over the buffer area, it is necessary provide a disposal which, absorbing the impact energy, protects the area occupied by the driver.

In addition to these systems, which are in the frontal area, there are those ones placed in the intercommunication areas among the rail vehicles, since an amount of the kinetic energy that the vehicles behind the heading have, must be dissipated in the deformation of the frontal areas of the single vehicle.

This dissipation occurs both as a plastic deformation of the carbody and through absorption systems placed at buffers level which are among the vehicles.



CHAPTER II

MODELING OF MECHANICAL BEHAVIOR OF MATERIAL

2.1 Introduction

Although the availability of computing resources and numerical strategies unthinkable until a few years ago to be of great help to the technician who is confronted with impact problem, allowing them to experiment and test in a virtual and shortly time a rather large number of design solutions, a central aspect of the problem of assessing the requirements of crashworthiness is still open as problematic and awaits a comprehensive and robust solution: the formulation of the constitutive model for materials, a task made particularly difficult or tricky is the multiplicity of variables that can influence the mechanical response of the material, both on the size of the domain in which these can vary, both aspects of the problem that force from time to time to formulate models "ad hoc" rather than particularization for the special case constitutive law of general application.

Generally, a constitutive models must have the following characteristics: capability to describe important aspects of material behavior, and to require a reasonable amount of experimental effort to obtain material parameters. No matter how complex mathematical model is, it will be possible, at least in principle, to incorporate such a model into computer code. Instead, the difficulties in obtaining experimental data and identifying material parameters can determine the practical value of the model.

From this it follows immediately that the choice of constitutive model optimal for a given crashworthiness problem is also affected by the available test equipment for characterization of materials and to validate the model.



Indeed, the simplest method for determining strain-rate sensitivity of a material is to increase the speed of a uniaxial tension and compression tests. Those tests are ideal, because the state of stress is purely uniaxial. Various types of machines are designed for performing tests at intermediate strain rate, and it is possible to achieve strain rates up to approximately 10^1 s^{-1}

The most complex rate dependent models define the flow stress as a function of strain, strain rate, and temperature. These work hardening models are usually classified as empirical or phenomenological (also physically based). Today the tendency of researchers is to develop more physically based models, since this approach should enable application of the model to a broader range of strains and strain rates, opposite the restriction to specific strain and strain-rate ranges when using the less physically sound models.

2.2 Metallic Material

In the case of metallic materials, it is well known that different mechanisms govern the deformation behavior of different strain rate regimes (a quite general classification of strain rate regimes is presented in fig. 1.1)

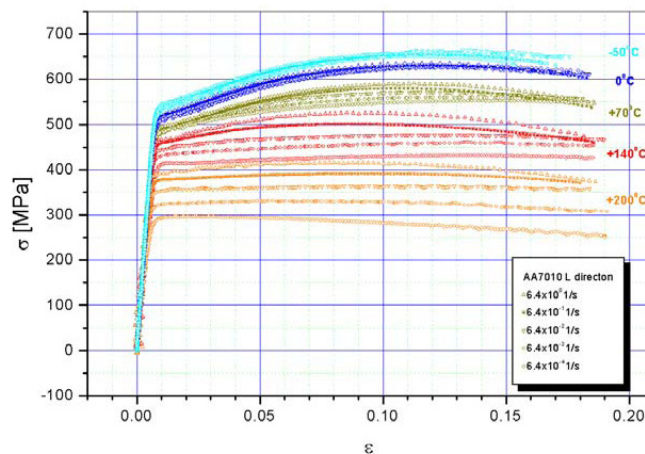


Fig. 1.1 - AA7010 stress-strain curves for L direction at different strain rates and temperatures[8]



The range of strain-rate between 10^{-6} to 10^{-5} s^{-1} correspond to the creep behavior of materials, usually observed at high temperatures and creep type laws are used to describe the mechanical behavior. At strain rates of the order of 10^{-4} to 10^{-3} s^{-1} , quasi-static stress-strain curves are obtained from constant strain rate tests such as uniaxial tension or compression. Those quasi-static stress-strain curves are used as an inherent property of materials. One should be aware that they are valid descriptions of materials only at the strain rate at which test was performed.

The most widely used models today, for crashworthiness applications, are the Johnson-Cook (JC), Zerilli-Armstrong (ZA) and Mechanical Threshold Stress (MTS) models. While JC and ZA have a simpler structure and require a smaller number of constants, the MTS model is of quite general validity and consequently is a very complex model. Simpler models, such as ZA and JC models, are more widely used in simulations, as it is easier to obtain the material parameters required for the models. On the other hand, the MTS model offers better accuracy in predicting the response at higher strains and represents a model of greater importance for the future.

Material testing procedures for the Johnson-Cook and Zerilli-Armstrong models do not require low temperature tests and therefore are simpler than required for the MTS model. The main advantage of the Johnson-Cook model over the Zerilli-Armstrong and MTS models is in the great number of materials for which the parameters are known. At the same time the advantage of the Zerilli-Armstrong and MTS models over Johnson-Cook model is in the fact that they are based on physical processes taking place in the deforming material and therefore can more accurately represent the behaviour of the material.

The Johnson-Cook [8] material model is an empirical model. As most of the models of this type, it expresses the equivalent von Mises tensile flow stress as a function of the equivalent plastic strain, strain rate, and temperature. This model is applicable for the range of strain rates from 0.001 to 1000 s^{-1} . Typical applications include explosive metal forming, ballistic, and impact.



In the presence of low and constant strain rates conditions, metals work harden along the well-known relationship which is known as parabolic hardening rule:

$$\sigma = \sigma_0 + k \cdot \varepsilon^n,$$

where σ_0 is the yield stress, n , the work hardening exponent, and k are material parameters. Dynamics events often involve increases in temperature due to adiabatic heating, because of this thermal softening must be included in a constitutive model. The effects of temperature on the flow stress can be described with the following relation:

$$\sigma = \sigma_r \left[1 - \left(\frac{T - T_r}{T_m - T_r} \right)^m \right],$$

here T_m is the melting point, T_r is a reference temperature at which σ_r , the reference flow stress, is measured, T is the temperature for which σ , the flow stress, is calculated, and m is material dependant constant.

The strain rate effect can be simply expressed with the following relationship, which is very often observed at intermediate strain rates:

$$\sigma \propto \ln \varepsilon.$$

Johnson and Cook, based on the above dependencies, proposed the following equation for the work hardening law :

$$\sigma = [A + B \cdot \varepsilon^m] [1 + C \cdot \ln(\dot{\varepsilon}^*)] [1 + (T^*)^m],$$

where A , B , C , n and m are material constants, T^* is a function of the absolute temperature given by:

$$T^* = \frac{T - T_r}{T_m - T_r},$$



with T_r reference temperature, at which σ_0 is measured, and $\dot{\varepsilon}^* = \dot{\varepsilon}/\dot{\varepsilon}_r$ is the dimensionless strain rate. This equation describes very well the response of a number of metals and structural alloys.

However, one of the problems with this constitutive equation is that strain rate and temperature effects on the flow stress are uncoupled. This implies that the strain rate sensitivity is independent of temperature, which is not generally observed for most metals. Because the empirical constitutive equations are basically a curve-fitting procedure, they are relatively easy to calibrate with minimum of experimental data in form of few stress-strain curves at several strain rates and several temperature.

This models incorporates simple modifications to the JC model to better represent the strain rate effect. There is evidence that strain rate influence on the flow stress of some materials is better represented by a power law rather than a linear function of $\ln(\dot{\varepsilon})$.

On the basis of this observation, the flow stress can be expressed as:

$$\sigma = [A + B \cdot \varepsilon^m] [(\dot{\varepsilon}^*)^C] [1 + (T^*)^m].$$

A model with a greater capacity to fit the experimental data and able to take into account separately isotropic and kinematic hardening, but neglects the effects of temperature, was finally brought by Hopperstad and coworker [9]:

$$\sigma = \left\{ \sigma_0 + \sum_{i=1}^2 Q_{(r)i} [1 - \exp(-C_{(r)i} \varepsilon)] + \sum_{i=1}^2 Q_{(x)i} [1 - \exp(-C_{(x)i} \varepsilon)] \right\} \cdot (1 + \dot{\varepsilon}^{*C}),$$

where $Q_{(r)i}$ and $C_{(r)i}$ are isotropic hardening parameters, while $Q_{(x)i}$ and $C_{(x)i}$ are kinematic hardening parameters, both to be experimentally determined.

From the comparison of the characteristics of various models briefly described, we have drawn the conclusion that, within this thesis, it was preferable to use the last



model in the simulations of the behavior of the metal components making up the absorption systems.

2.3 Aluminum Honeycomb

The honeycomb is a cellular solid consisting of an ordered set of cells with well-defined form. The cells are usually hexagonal, but can also be square, triangular and diamond. The metal honeycomb is mainly used as core material in sandwich panels and systems bounded to the absorption of energy.

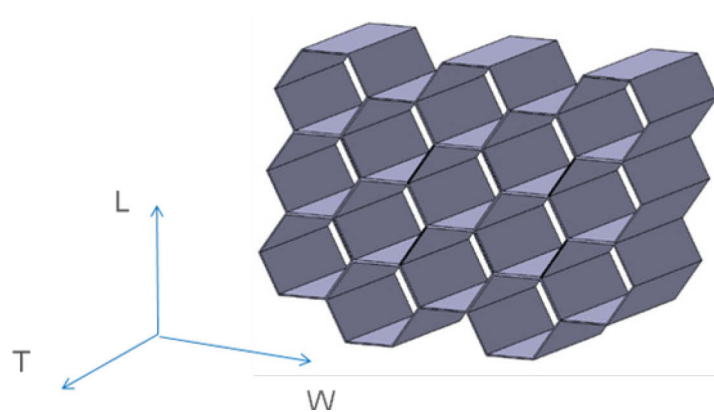


Fig 2.2 - Definition of the orthotropic axis for the honeycomb.

The shape of the elementary cells (fig. 2.2) gives the structure a different behavior in the three directions, and for that reason the description of macroscopic behavior must be done through an orthotropic model.

The main directions of orthotropic material are indicated with WLT. In particular, the T-direction coincides with the axial direction of the cells, the L-direction coincides with the direction of development of the foam sheets to create the cells, and the W-direction is orthogonal to T and L.

In the direction T is identified the "stabilized compressive strength", which represents the ultimate value of the stress at which the walls deform plastically. Since the determination of this value is made by applying a compressive load on a



sandwich consisting of an honeycomb core and two plates glued on the faces and normal to the direction T, is distinguished the “Stabilized compressive strength” and the “Bare compressive Strength”. The first is the value determined by the compression test. The second refers only to honeycomb core.

For the determination of “Stabilized compressive modulus”, because some materials have a linear behavior in the elastic phase, such as those made of carbon fiber, while others, such as Nomex, have a strong non-linearity, it refers to the stress-strain curve obtained from the previous test and the “elastic modulus” is determined as the slope of the curve in the first part [9].

Reached the “stabilized compressive strength” the core material plasticizes and starts a regular folding of the cells with an initial fall in the load curve and a subsequent stabilization around a value known as “Crush strength”. Because of the folding, stress undergoes fluctuations around the stabilized compressive strength, which can be constant or less depending on the density and the material itself. Each wave encountered in the load curve corresponds to the formation of a plastic hinge that forms in the wall of the unit cell.

Upon reaching the condition of fully compacted, the stress rises rapidly and the material behaves as if it were a single block of aluminum (fig. 2.3).

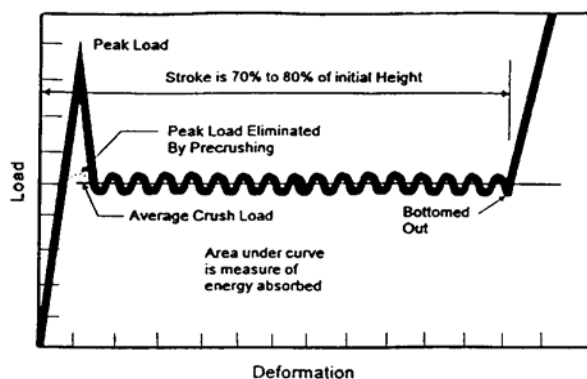


Fig 2.3 - Proper honeycomb characteristic curve [10].



For the determination of shear modulus tests are carried out on sandwich with honeycomb core. The direction of load application is chosen coincident with L, for the determination of the properties in the LT plane, or with W, for the determination of the properties in the WT plane.

The stress at which the material of the core reaches plasticization is defined “shear strength”. By determining the slope in the origin of stress-strain curve, acquired during the test, it can be determine the value of the shear modulus.

For the estimation of yield stress in the T-direction, we can assume that it is coincident with the stress corresponding to the treatment with no slope in the fig. 2.3. This value is not to be confused with the Bare or Stabilized compressive strength.

Since the datasheets do not provide all the material parameters for the complete determination of the constants needed to describe the behavior of orthotropic material, it is possible to estimate the missing ones on the basis of observations conducted on the experiments. In particular, to estimate the elastic modulus in the W and L directions, for example in the description of mechanical behavior of materials for a finite element simulation, you can use 0.1% of the value of elastic modulus in the direction T [10].

For the estimation of shear modulus in the LW plane it can be considered 0.1% of the average in the other two tangent modulus [10].

The yield stress in the T and W directions may finally be assumed equal to 0.1% of the value calculated in the T direction [10].

2.4 Fiber Reinforced Plastic (FRP)

The FRP (Fiber Reinforced Plastic) is a composite material made of fiberglass or carbon or aramid fibers in a polymer matrix of a different nature, such as polyester, vinyl ester or epoxy. The ability to vary the amount of fiber and the nature of the matrix allows making a composite with mechanical properties according to



requirements of the particular application. This variability affects not only the mechanical properties, but also the ability to absorb energy. In fact you can increase the specific absorption energy using a composite with carbon fibers compared to a fiber glass or aramid, or using an epoxy resin. The variation of mechanical properties can also be achieved by changing the method of treatment of the resin itself.

The FRP, unlike metals, does not shows the mechanisms of ductile failure, as the main failure mechanism is essentially brittle.

Referring, for simplicity, to a hollow cylindrical geometry made by FRP under compressive load the failures are mainly three: Euler buckling, progressive folding and brittle fracture. The most interesting are the progressive folding and brittle fracture. For the first, the configuration assumed under the load is similar to that taken by the metallic materials, namely, a configuration called a concertina. It occurs when aramid fibers are used or when glass or carbon fibers with an interlaminar shear stress much lower than the strength of the matrix.

Regarding brittle fracture, it manifests as a sudden loss of functionality of the component and can be controlled using devices such as initiators, which stabilize the progression of crushing, and then the energy absorption more constant and predictable. A stable brittle fracture process can absorb much more energy compared to progressive folding.

FRP behavior under axial compressive loading is essentially of two types: *Lamina Bending* and *Transverse Shearing* (fig. 2.4) .

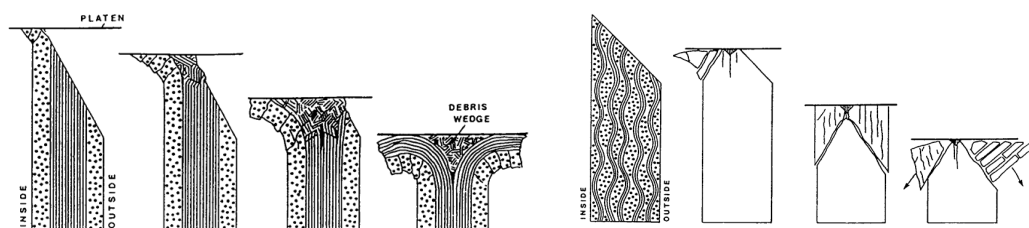


Fig 2.4 - Lamina Bending and Transverse Shearing [11].



In both cases the energy is absorbed through the propagation of cracks, which are formed between the layers and inside of the layers themselves, and by the friction between the layers.

Also, the failure mechanisms and the absorbed energy depend on the orientation of the fibers to the direction of the load and the orientation of the fibers in the composite lamina. This factor is combined with the characteristics of the matrix influencing the global behavior of the composite.

Concerning the strain rate sensitivity, the data available in literature are very conflicting. In particular, some experimental studies underline an increased absorption energy with increasing load speed, while others highlight a decrease. One explanation to this problem can be found in the diversity of the geometry of the specimens tested and compared.

For applications which are referenced in this thesis, it is essential to know the behavior of materials under dynamic conditions, since the correct evaluation of the structural behavior of the used composite depends on this.

At present, because of multiple factors, it is not yet fully described the dynamic behavior of composites but it was only established, with experimental evidence, the occurrence of different behavior in static and dynamic condition.

2.5 Polyurethane Foam

Foams are made by introducing pores in different materials such as polymers, metals or ceramics, in order to have a relative density less or equal to 0.3. The energy absorbed by the foam depends on many factors, such as density, homogeneity and the type of cell. From a mechanical point of view, unlike honeycomb, it is a material that exhibits similar behavior in different directions and so it is possible to hypothesize an isotropic behavior. The failure mechanism can be divided into three distinct phases. A first phase, in which the behavior is linear elastic. A second phase, in which there are small increments of load for large values of displacement due to



the failure and the stretch of the cells. A third stage in which the cells are completely compacted and the behavior of the material is close to that of the material which forms the foam. For different material types it can be seen a different behavior in the plateau region. In particular, for rigid foam, cracks that nucleate and propagate determine load fluctuations even substantial (fig.2.5).

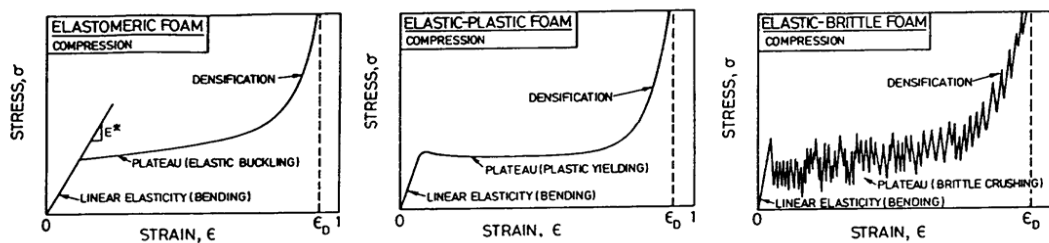


Fig. 2.5 - Polyurethane foam characteristic curves with different behavior[11].

Due to this behavior foams are able to absorb large amounts of energy in a controlled and predictable manner, and this explains the reason for their massive use in making absorption systems.

The correct modeling of the material behavior requires the complete knowledge of all parameters that characterize the state of the material in the three phases described above. In our model, based on the possibility to consider the behavior essentially isotropic and being interested to the structural strength rather than dynamic effects, it has been considered only the linear elastic phase, ignoring what happens in the following two stages.

2.6 Balsa Wood

Balsa is a tree of the Bombacaceae family, very popular for the high specific values of stiffness and strength. The microstructure of balsa, like all wood, consists of prismatic cells with nearly hexagonal section, that remind honeycomb structure. The predominance of one dimension of the cell than the others two gives the material a strong anisotropy.



A block of balsa wood, subjected to a compressive force in the axial direction of micro cells, exhibits a linear elastic behavior until failure, which occurs for localized collapse. The behavior in post failure is characterized by an almost constant value of the force until the final collapse (fig. 2.6).

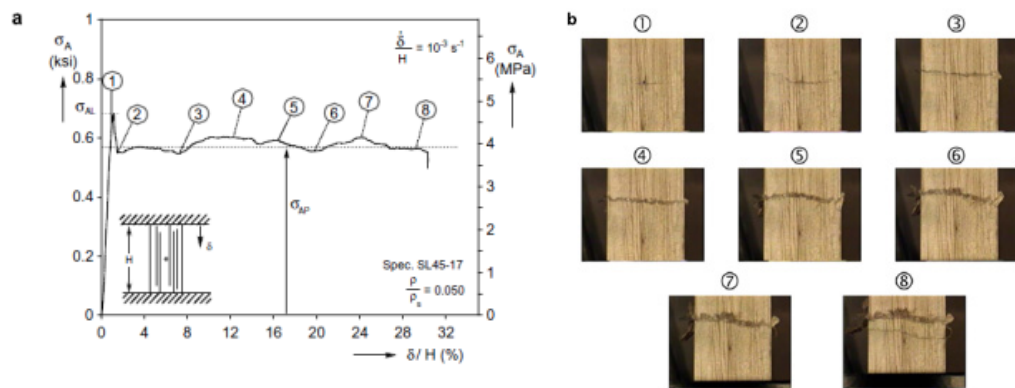


Fig. 2.6 - Characteristic curve of the balsa with sequence of photographs to describe the failure mechanisms [12].

Through micrographs (fig. 2.7), it is noted that the walls of the cell, in the area affected by collapse, assume the configuration to concertina.

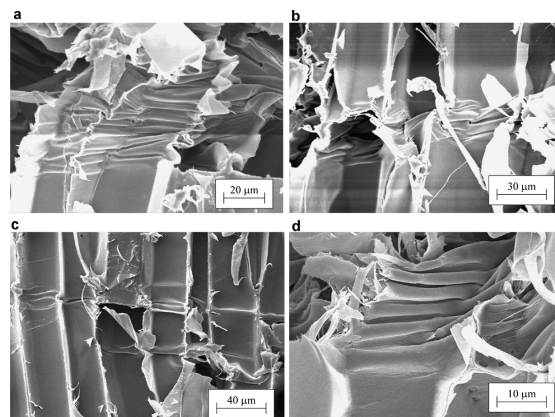


Fig. 2.7 - Micrographs of the balsa cells in the final collapse phase [12]

For reasons similar to those described for foam, even in this case it has been limited to model the material as isotropic and without taking into account the failure. The



results of linear analysis carried out have been analysed to ensure that the maximum stress did not exceed the critical values of the considered material.



CHAPTER III

CAB STRUCTURE

3.1 Typical Cab Structure

The cab (fig. 3.1) define the extreme part of the vehicle put to use as control and driving systems for the movement of the train.



Fig. 3.1 - External view of the Minuetto cab.

The main part of the space is dedicated to the control console (fig. 3.2), which takes all the disposals of which the driver needs.



Fig. 3.2 - Control panel of the Minuetto.



To the aforementioned components, auxiliary services and electric, pneumatic and hydraulic systems are added. For the definition and protection of the area of the cab, this is wrapped in a thin shell of appropriately shape to reduce aerodynamic effects. This shell has a removable part, called nose, in the frontal area, since in service frequently damaged occur due to the small impact of the stones of the ballast on the cab, it becomes necessary to replace this part. Absorption energy systems and coupler are positioned in the front area of the cab. All these components are assembled on a supporting structure (fig. 3.3) which is in turn connected to the carbody. The main structure has not a fixed scheme but the different configurations depend on the absorption system and the type of vehicle. However, one can say that, since all vehicles must comply with the EN15227 Standard, the tendency of designers is to create a cab with a very strong structure at the floor level on which is going to fix the absorb systems and the coupler. To prevent intrusion and guarantee the survival space of the drivers, two beams, shape and size of which are optimized for the specific case, are connected with one end to the front of the floor and the other end on the carbody.

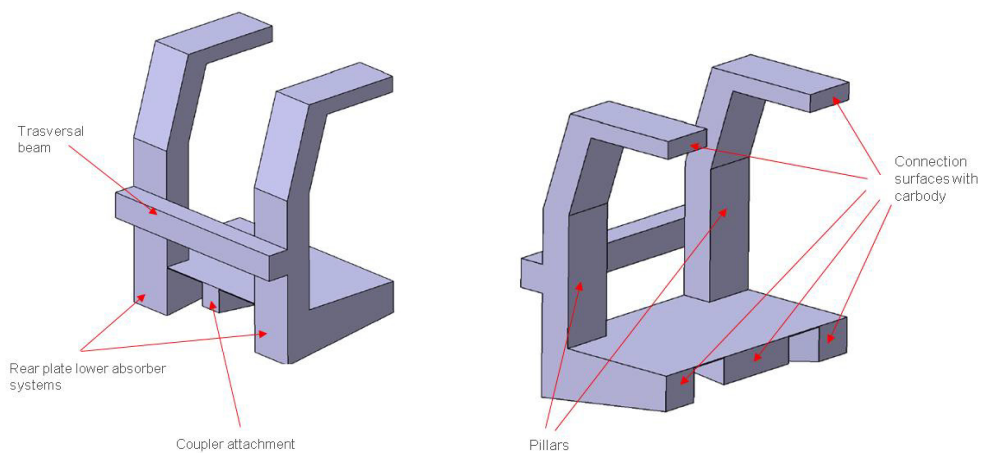


Fig. 3.3 - Schematic representation of the structural parts of a typical cab.

To ensure the necessary stiffness of the structure the two vertical beams are usually connected with a transversal beam, which also acts as a further support element for the connection of the interiors. The floor has a central beam, which transfers the load acting onto the beam on the front of the carbody, and two boxes, arranged



symmetrically with respect to this beam, which allow to transfer to the carbody the loads acting on buffers.

The space occupied by absorption systems depend on the type of train as a vehicle for high speed will have absorption devices that are much longer than a vehicle for regional transport.

3.2 Modular Absorption

To avoid abrupt changes in the values of contact forces during the collision between two vehicles, devices are taken to completely absorb kinetic energy of the vehicle and in a gradually way, as sudden deceleration would lead to structural collapse and occupant injury. the cab and the absorption systems are designed by distributing the masses in order to have a gradual increase in stiffness in the longitudinal direction. This is reflected in a profile of the reaction force increased with increasing the total area affected by plastic deformation and then a gradual increase in energy absorbed.

According to this variation of stiffness, there are three main areas. One is the front area (fig. 3.4), i.e. the nose, which absorbs a very low amount of impact energy. It is usually a very light structure, easy to replace, most often used to break down after impact so as not to interfere with the phase of engagement of the absorption systems of the two impacting vehicles.

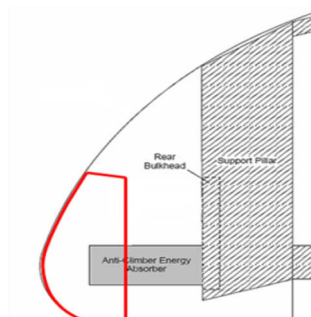


Fig. 3.4 - First module of the cab.



The second part (fig. 3.5) is that in which generally are placed the devices to absorb energy and then there are the highest deformation and, consequently, the maximum absorption energy.

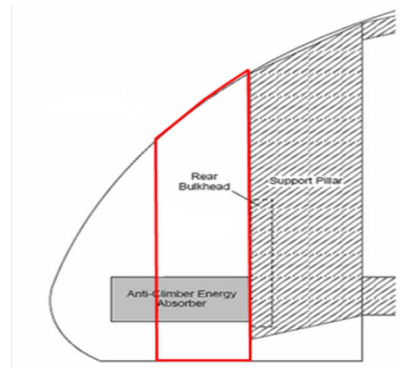


Fig. 3.5 - Second module of the cab.

A third part of the cab (fig. 3.6) matches the security area and is the part that needs to be undeformed at the end of the collision to ensure the conservation of survival space of the driver. Also has the function of keeping in place the absorbers and to distribute the loads to the rear area.

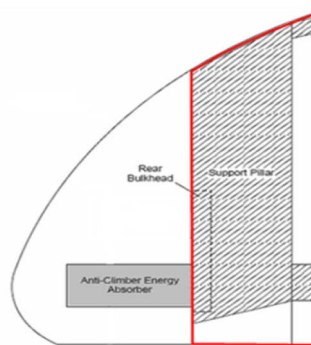


Fig. 3.6 - Third module of the cab.

The contribution of individual parts can be evaluated after a preliminary phase in which the total energy during the impact has been estimated. This energy depends on the mass of the vehicle and the investigated scenario. After that these parameters have been estimated, it can be identified the contributions of individual devices and thus the contribution of the primary absorption system and, where defined, of the secondary systems.

3.3 Lower Absorber System

3.3.1 Type of Absorber

The absorption system employed on all trains is the primary absorber or lower (fig. 3.7), so called because it is mounted in series with the buffers and is fixed to the supporting structure of the cab.

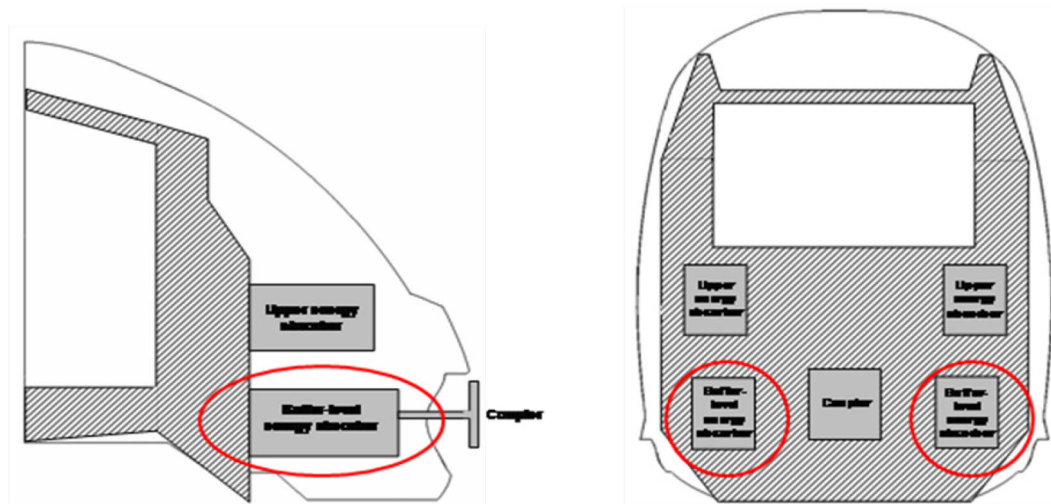


Fig. 3.7 - Lower absorber level.

Many technical solutions are adopted to build the absorption systems. The most common and most widely used are those made of welded rectangular or circular plates, which they collapse under axial load, dissipating energy by plastic deformation.

Other devices, like pneumatic systems, dissipate energy by exploiting the leakage of fluid through holes created in the mantle of the cylinder.

Some are made of pipes seated on each other: when the force acting on the inner tube exceeds a certain value, the relative motion is triggered and the inner tube flowing into the outer tube deforming it. Other special applications dissipate impact energy through the permanent deformation of a strip of material from the outer surface of the cylindrical buffer.



Mixed systems are also worth mentioning that use a combination of some of the listed devices, such as multistage system which uses pneumatic components placed in series with a welded box that collapses plastically. In this way it can adapt the absorber response to the operating conditions.

For the verification of compliance of the device with the standards, it is necessary to carry out numerical simulations and their validation tests. The tests must be conducted so that the energy absorbed is at least 80% of that expected. To ensure the sufficient level of energy during the test, the impact velocity must be at least 50% as it is in the reference scenario. The mechanisms involved in the operation of the device must activate during the test to verify the correctness of the sequence and interaction between different systems.

The two configurations in which the system must be tested are the impact against an identical train, positioned, in the first configuration, both at the same height from the rail level, and in the second one, with 40 mm vertical offset. In any case, the absorber must have the same behavior as that determined by the simulations and in particular there must be correspondence between the sequence of collapse and the energy absorbed. The comparison of force and displacement level must be executed.

The simulations of the complete structure are added to the tests described above. The model for this type of simulations must include the whole cab and its subsystems modeled in detail. For the remainder is possible to approximate the structure maintaining the masses and stiffness of individual elements to have the same dynamic effects of real structure. The objective of these simulations is to verify the behavior of the absorption devices, particularly in the configuration with offset. Indeed, under these conditions the absorption system must ensure that anticlimbers remain in contact throughout the duration of impact and that the vertical displacement of the structure, as measured by movement of the wheel compared to rail, does not exceed 75% of total flange height of the wheel. Then, it can be verified that during the collision the train does not have excessive movements that could lead to conditions of derailment.



3.3.2 Materials

The correct simulation of the dynamic behavior of the structure cannot ignore the detailed knowledge of the mechanical material properties. The totality of the devices currently in use employs metallic materials, for which it is known with high confidence the behavior in both static and dynamic conditions. The materials used are mild steel and aluminum. Their massive use is due to the fact that, for aluminum, the mechanical properties do not vary significantly with strain rate, while for mild steel the range of variation of strain rate in service is such that have very high values of toughness.

The operational method, geometry and materials used for the absorbers are quite varied, which explains why there is a need to define a parameter that allows us to compare performance of different devices. The most used parameter for this purpose is the specific absorption energy, which is defined as the absorbed energy per unit mass deformed [11]. This parameter is used to investigate the behavior of the system as a function of mass and then optimize the absorption system in terms of mass. The need to reduce vehicle mass, increase payload and carry out an eco-system has prompted research to study the applicability of materials that allow the same absorption properties with reduced masses, i.e. with an higher specific absorption energy.

3.4 Upper Absorber System

The Upper absorber (fig. 3.8) is the element delegate to accommodate the impact against the large obstacle contemplated in the scenario 3 of EN15227. This type of device is not present on every train units, but unlike the primary absorption system, is present only on those vehicles for which the service involves the intersection with road.

The main purpose of this device is to prevent the collapse of the main structure of the cab under the action of loads due to impact against the obstacle and protect the survival area within the .

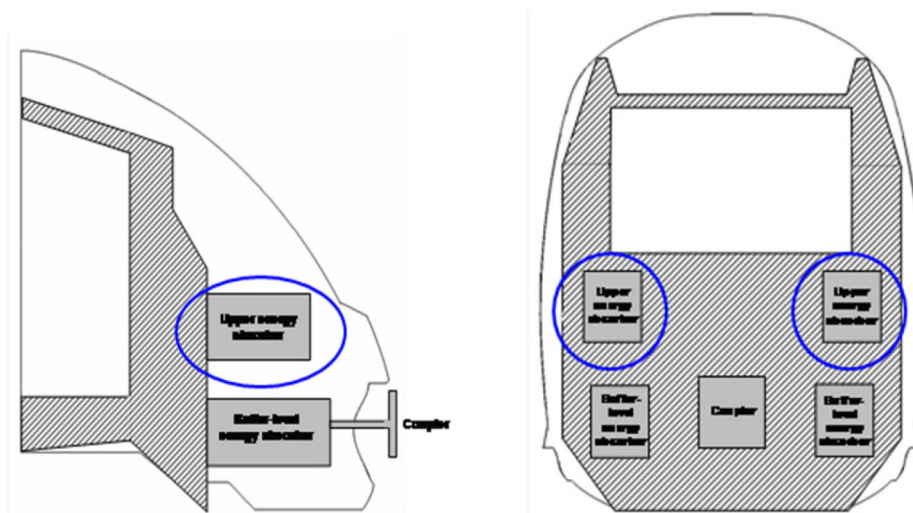


Fig. 3.8 - Upper absorber level.

The upper absorber geometry generally reproduces the primary absorbers, but on a small scale since the energy to be absorbed is lower. The location of these systems is in front of the transversal beam, at the windscreen sill level, set on pillars delimitating the survival space of the driver.

For these systems, when the amount of energy that they must absorb is defined, the testing phase has to be conducted with the same requirements described for the primary absorption system. As for the configurations to be simulated and then tested, only the impact between two absorbers of the same type is expected.

The validation of the numerical model is carried out by comparing the accuracy in estimating the sequence of collapse and force levels.

3.5 Coupler

To connect the vehicles that composed a train, the ends of each vehicle are equipped with a system, coupler, which allows the transmission of longitudinal forces. There are two types of coupler, the manual coupler and automatic coupler, of which we describe, briefly, the most important.



3.5.1 Three Link Coupling

The "Three link coupling" (fig. 3.9) is a system that provides to use a chain of three links for the connection, one end of the chain is fixed on a vehicle the other end is free to be connected to another train. In the composition of the train, each vehicle is connected to the others, placed in sequence, with its link at one end and with the link of the near vehicle at the other end. This type of coupler is unsuited with configurations for which there is an automatic braking. Since the connection allows traction only during braking, each vehicle is braked by a ballast and the braking system partially operating.

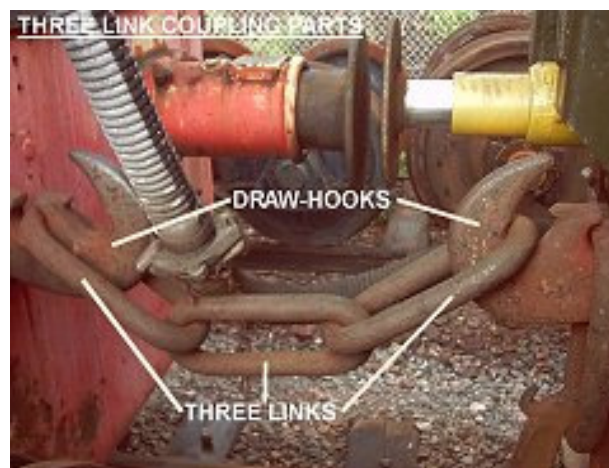


Fig. 3.9 - Schematic representation of the Three link coupling [13].

3.5.2 Instanter Coupling

The "Instanter coupling" (fig. 3.10) is an evolution of the "Three link coupling," in which the connection is composed of a central forged element with a triangular hole, which allows to adjust the relative position of the vehicles in a quick way. Remains the slack that, in the early stages of braking, causes the collision between the buffers..

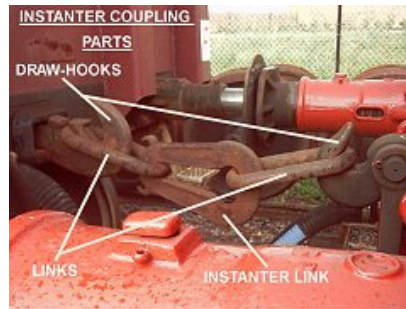


Fig. 3.10 - Schematic representation of the Instanter coupling [13].

3.5.3 Screw Coupling

The "Screw coupling" (fig. 3.11) consists of a linking bar and a turnbuckle. The linking bar has the function of transmitting traction, while the turnbuckle allows to pull together the buffers and apply a compressive load that can damp the shock occurring in service. The docking system is connected to the carbody through a particular system, which besides giving a high elasticity coupling, through a system of springs contained in it, allows the rotation of the hook around a vertical axis standing away from the front plane of the carbody.

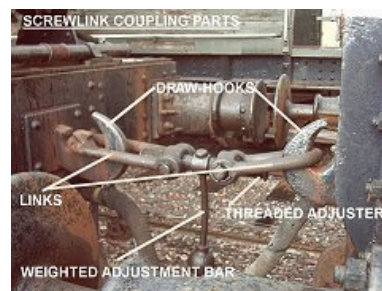


Fig. 3.11 - Schematic representation of the Screw coupling [13].

During coupling, a railworker had to stand between the cars as they came together and guide the link into the coupler pocket and they run serious risks linked to the operations of hooking and release. For this reason, automatic and fully automatic systems have been developed. Among those automatic, which have in common to allow higher maximum tonnage compared to the manual coupler, we mention below the most known.



3.5.4 Janney Coupler

This is a coupler with non rigid jaws (fig. 3.12), which allows reciprocal vertical movements of the two heads in order to connect vehicles with different suspension behavior. The limit of this system is that at least one of the two heads must be open in order to achieve the coupling. There are also rigid systems, but in this case the linking bar is articulated in vertical and horizontal direction. During the coupling, in order to guarantee the perfect lock is necessary that one of the two terminals is driven with a certain speed against the other.

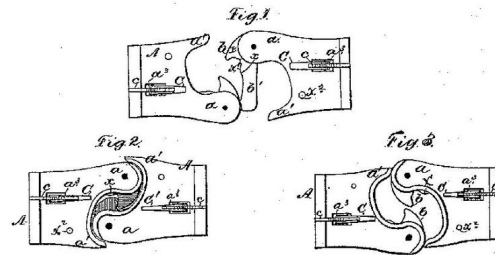


Fig. 3.12 - Janney system as in the inventor's drawing [13].

3.5.5 AAR Coupler

This system (fig. 3.13) is an evolution of the Janney coupler. There are two versions, "full-size" and "three-quarter". The characteristic of this automatic system is that it allows greater security in the closure and the possibility to withstand higher loads. The locking system consists of a pin. It is necessary to apply a compressive force on the cars involved in the device to release it..

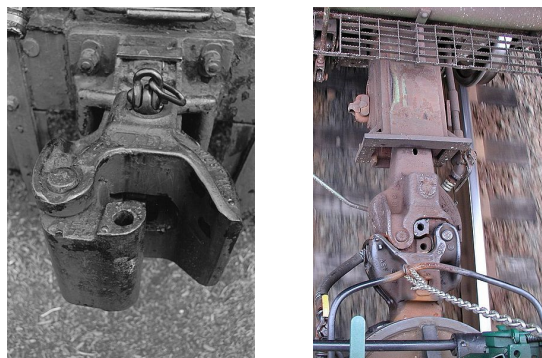


Fig. 3.13 - One of the ends of the AAR coupler and the coupling configuration [13].



3.5.6 Wilson coupler

This type of coupler, very old in the USA, is mainly applied today in the Russian railroads and others. The functioning system on which this disposal is based is described in fig. 3.14.



Fig. 3.14 - Wilson system in the coupling configuration [13].

The interlocking system is very safe, it is not affected by temperature variations and allows to transfer compressive and tension loads of order of magnitude of 250t.

The coupling systems are also fully automatic, requiring no intervention from the railworkers during docking. These systems use pneumatic and electrical devices for the handling of locking mechanisms. It is worth mentioning the following system.

3.5.7 Scharfenberg coupler

The device (fig. 3.15) consists of a pneumatic system and electrical equipment that allows the rotation of the coupling head ensuring its locking. The main advantage of this system is that it does not require high-speed during docking, as the closure is determined by the system itself. However, the system withstands low tension load, so is used mostly in light passenger vehicles.



Fig. 3.15 - Automatic coupler Scharfenberg [13].

Because of the variety of coupling systems and the frequent incompatibility between them, systems such as the double coupler or coupling adaptor are used. In the first case the car is set up with two types of couplers, the second of which is generally a manual coupler. Alternatively, there is a device that interfaces with the two different systems makes possible the connection. The problem of this solution is the excessive weight of the device.

Moreover, interface elements that make compatible different types of coupling systems are used, mounted on the vehicles which are to be coupled.

The contribution of the coupler during the impact is crucial, because it ensure a further element of engage and then a further element of prevention of undesirable phenomena, such as derailment, apart from contributing to the absorption of impact energy.



CHAPTER IV

LOWER ABSORBER MODELING

4.1. Calibration of material parameters

Before the phase concerning modeling solutions alternative to that of the existing absorption system, it was necessary to determine the set of constants defining the constitutive model of the chosen material.

The general approach to determine these parameters is characterising the material through tests having different strain rate [14]. In our case, a different approach has been chosen: parameters determination was performed using the results of quasi-static compression tests, on mild steel tubes and a campaign of numerical simulations, through which the set of parameters minimizing the gap between the experimental and numerical results was searched [15].

Tests were performed at the labs of the University of Gdansk in Poland. The geometry of tested tubes is a round section with different lengths. On some tubes radial holes in the extreme areas were performed in order to evaluate the effect discontinuities have on the collapse load and the folding.

Specimens to be tested are shown in fig. 4.1.

Tests were performed using a machine having a load capacity of 4000 kN, equipped with the Peekel Autolog 2180 measurement system connected to a laptop for data recording (fig. 4.2). Measuring the force was performed through the C1/250 load transducer by HBM, while measuring the displacement was performed through the 1-WA/500 MM-L displacement transducer, by the Hottinger as well.



Fig. 4.1 – Mild steel samples for compression tests.



Fig. 4.2 – Test machine used for compression tests.

In an initial stage, tests were performed using equipment allowing the insertion of axial loads only without preventing edges rotation (“a” configuration in fig. 4.3). Afterwards, equipment was modified (“b” configuration in fig. 4.3) to prevent such rotation, to which the Eulerian instability of the tubes detected during the previous phase had been associated.

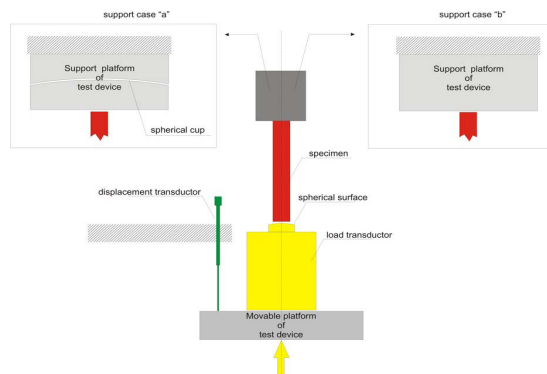


Fig. 4.3 – Configurations of the test machine.



The results of the tests performed on specimen n.1, n.4 and n. 5 are reported below. Specimen n.1 was tested in configuration **a** in fig. 4.3, while specimens n. 4 and n. 5 were tested in configuration **b**.

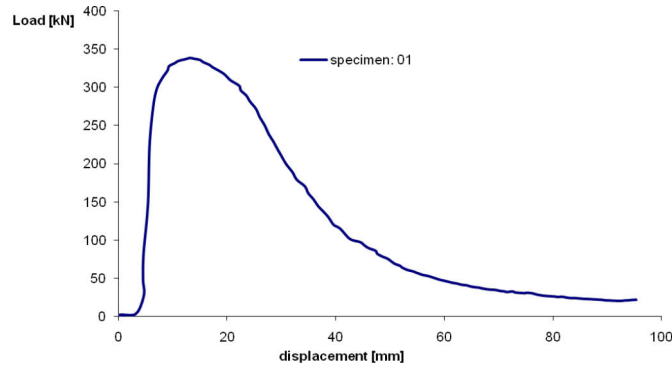


Fig. 4.4 – Results obtained with specimen n. 1.

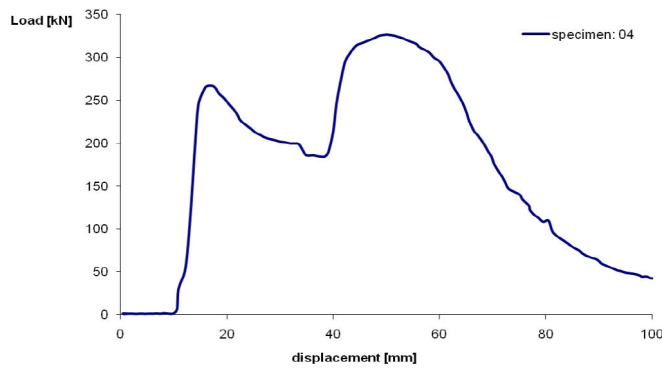


Fig. 4.5 – Results obtained with specimen n. 4.

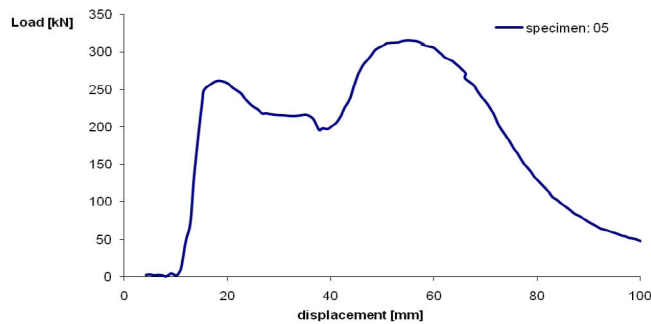


Fig. 4.6 – Results obtained with specimen n. 5.



For each one of them, the phenomenon of collapse due to the Eulerian instability at the maximum load equal to 350 kN, 256 kN e 261 kN respectively for specimens n. 1, n.4 and n.5 was observed.

Analysing the results (fig. 4.4÷6), it is possible to note that the presence of the hole has the effect to reduce the maximum load and to cause a localised collapse in the area nearby the discontinuity, before the global instability.

In fig. 4.7 ÷ 4.12 displacement load and final configuration obtained through the specimens on which length reductions have been performed are reported.

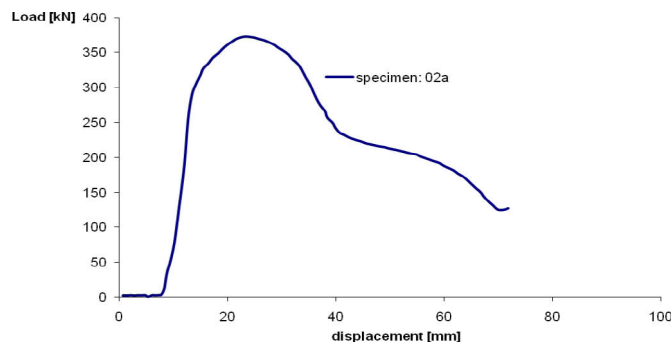


Fig. 4.7 – Results obtained with specimen n. 2, configuration “a”.

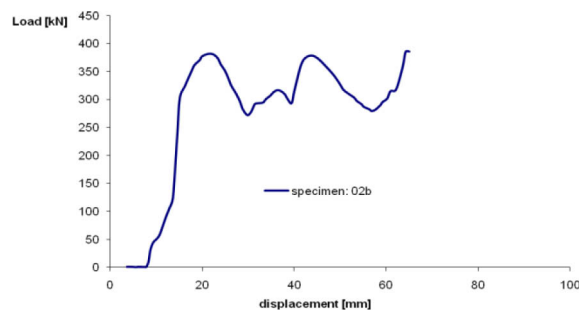


Fig. 4.8 – Results obtained with specimen n. 2, configuration “b”.

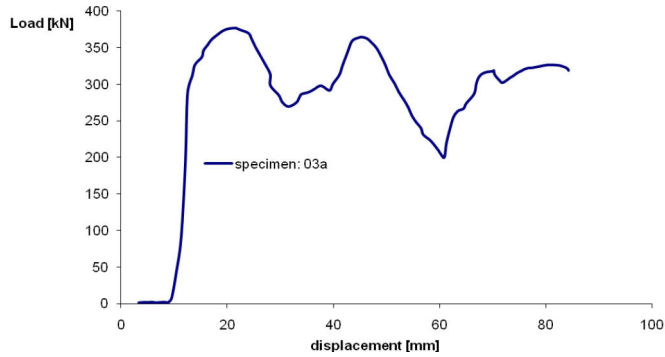


Fig. 4.9 – Results obtained with specimen n. 3, configuration “a”.

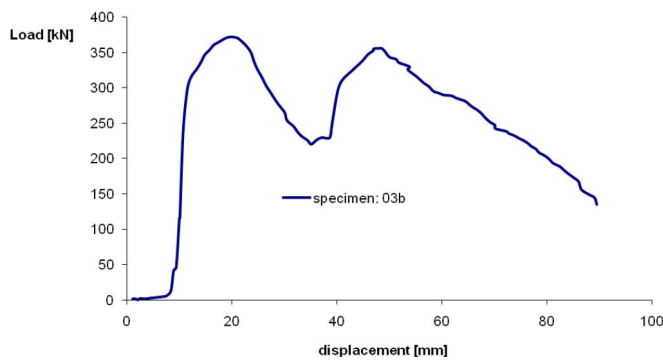


Fig. 4.10 – Results obtained with specimen n. 3, configuration “b”.

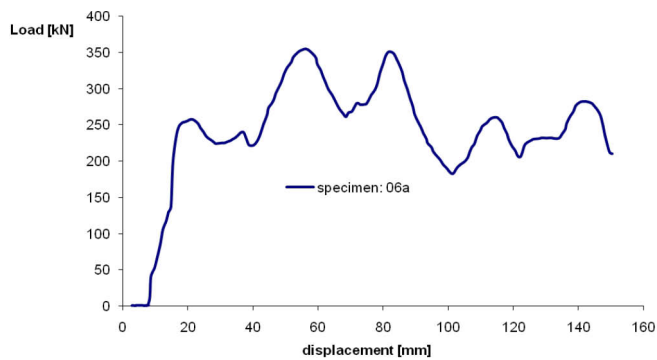


Fig. 4.11 – Results obtained with specimen n. 6, configuration “a”.

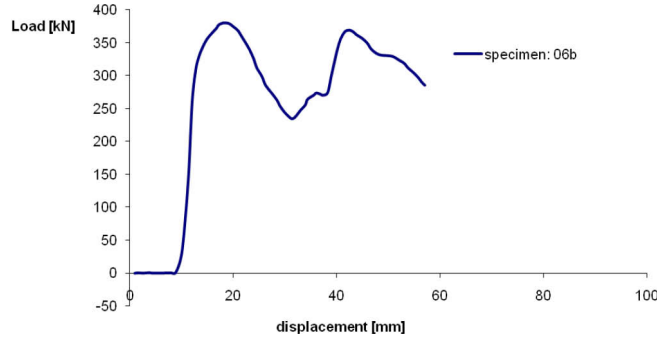


Fig. 4.12 – Results obtained with specimen n. 6, configuration “b”.

For calibrating the parameters of the material, a model for the finite elements in LS-dyna environment was created and one of the compression tests was reproduced.

The model (fig.4.13) uses shell elements, with Belytschko-Tsay formulation [16], with a node in the plane and n. 5 integration points through the thickness. After a sensitive analysis of the mesh, the characteristic size of the shell elements equal to 5 mm has been chosen.

The material model used is MAT ANISOTROPIC VISCOPLASTIC (*MAT_103), which has already been implemented in the LS-dyna calculation code.

In order to describe hardening, the *MAT_103 uses an bilinear elastoplastic model, which takes into account both isotropic and kinematic hardening. The function connecting the effective value of deformation to the actual stress is the following.

$$\begin{aligned} \sigma(\varepsilon_{eff}^p, \dot{\varepsilon}_{eff}^p) = & \sigma_0 + Q_{r1}(1 - \exp(-C_{r1}\varepsilon_{eff}^p)) + Q_{r2}(1 - \exp(-C_{r2}\varepsilon_{eff}^p)) \\ & + Q_{\chi1}(1 - \exp(-C_{\chi1}\varepsilon_{eff}^p)) + Q_{\chi2}(1 - \exp(-C_{\chi2}\varepsilon_{eff}^p)) \\ & + V_k \dot{\varepsilon}_{eff}^p V_m \end{aligned}$$

In such a connection, three contributions can be mainly observed, the first one related to the isotropic hardening, the second one related to the kinematic hardening and the third one reads the viscous behaviour, until V_k is annulled [17][18][19].



Being the model a non linear one, it is not possible to perform direct measurements to determine the characteristic parameters of the material. For such a reason, the “inverse approach” calibration method is used, that is to say optimizing parameters by reducing the gap between experimental and numerical results.

The contact with the edges plates was modelled with a “node to surface” contact.

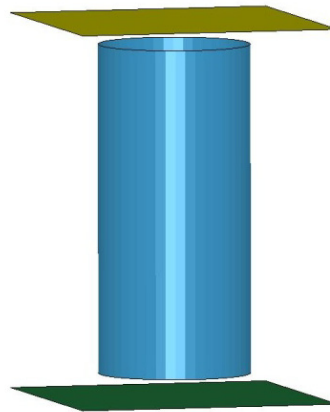


Fig. 4.13 – FE Model used for calibration simulations.

In tab. 4.1, the parameters for the material obtained during the optimization phase are shown.

Tab. 4.1 – Optimized material parameters.

Density (kg/mm ³)	Young's Modulus (MPa)	Yield Stress (MPa)	Hardening Coefficient a	Isotropic Hardening Parameter Q _{r1}	Isotropic Hardening Parameter C _{r1}
7.85 x 10 ⁻⁶	206,000	275	0.5	0.02	76.0
Isotropic Hardening Parameter Q _{r2}	Isotropic Hardening Parameter C _{r2}	Kinematic Hardening Parameter Q _{e1}	Kinematic Hardening Parameter C _{e1}	Kinematic Hardening Parameter Q _{e2}	Kinematic Hardening Parameter C _{e2}
0.03	10	0.2	76	0.3	10



In fig. 4.14 the overlapping of the load displacement curve obtained from the compression test and the one obtained from the simulation performed with the parameters reported in the table are shown. It is possible to note that there is a good compliance between modelling and experimental results, even though parameters may be improved so that to try to reduce the gap. For the purposes of our modelling, the degree of approximation reached is considered sufficient.

For what concerns modelling the material in simulations performed to optimize the lower absorber the parameters shown in tab. 4.1 will be used.

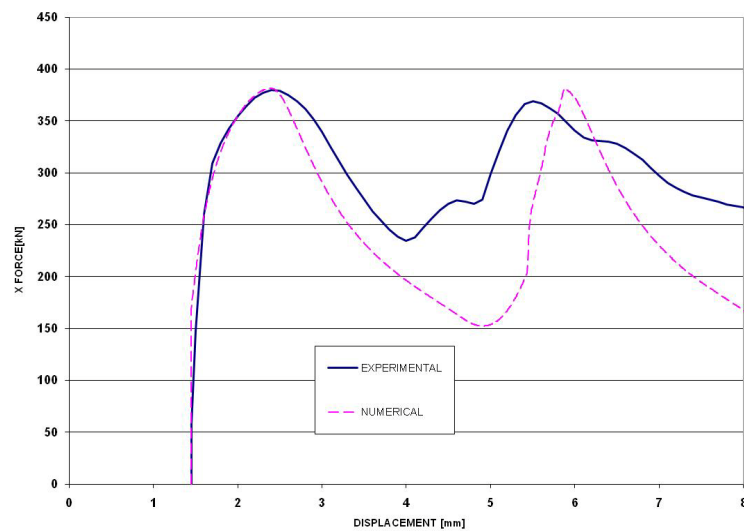


Fig. 4.14 –Overlapping of the numerical and experimental curves.

4.2. Lower absorber

The basis for designing the new lower absorber was the study of an existing absorber. It is made up of a tube having a rectangular section, with a deep-drawing on the frontal part, which acts as a starter to guide the formation of the first wave. The frontal plate, the anticlimber, has two prismatic blocks guiding the axial translation within the internal plates fixed to the external tube fig. 4.15.

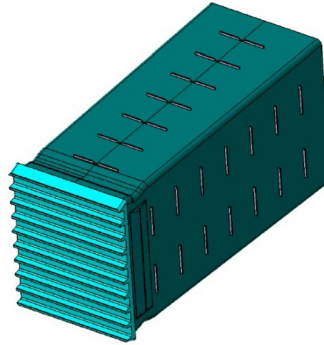


Fig. 4.15 – Modified initial model.

Performances of the existing absorber, in terms of absorbed energy and load, are shown in fig. 4.16.

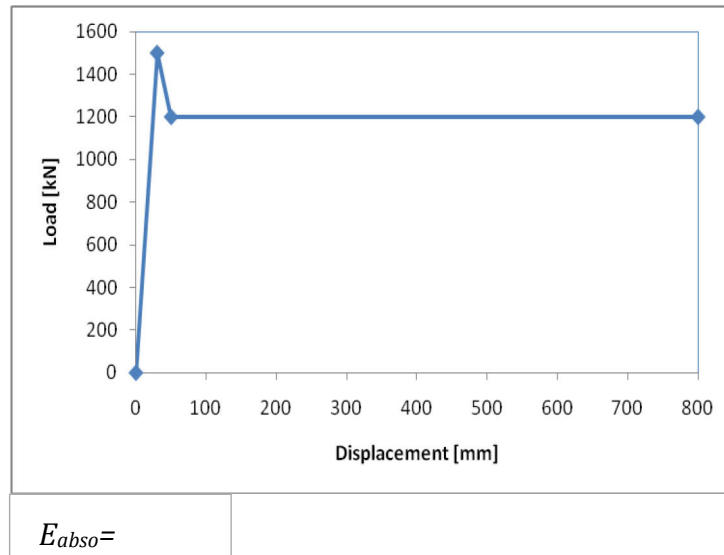


Fig. 4.16 – Load displacement reference curve and Energy target.

The overall dimensions only has been taken from this component. Unlike the existing one, the new model is based on the use of tubes [20] with a square or circular section welded between two plates so that the axial direction matches with the direction of loads application. The first analyzed solution is the one shown in fig. 4.17.

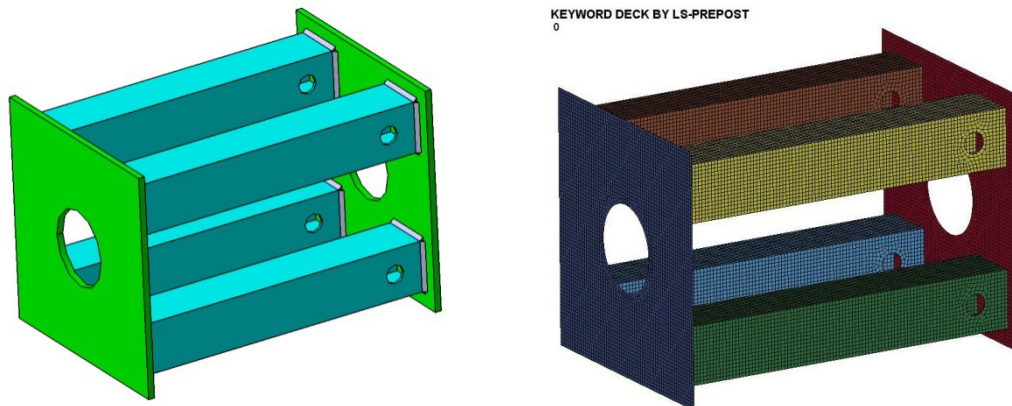


Fig. 4.17 – CAD and FEM model of the first study hypothesis.

As the absorber is made up of two modules having the same length, the energy absorbed by each module is equal to 550 kJ, that is the half of the total one.

As the use of tubes with rectangular or square section has a drawback connected to the possible breaks which might occur on edges with the subsequent reduction of their own capability to absorb energy, solutions using tubes with circular sections have also been evaluated. Different hypothesis have been examined, each one of them reproduced with dynamic simulations, through the Ls-Dyna, to evaluate the global behaviour of the structure in conditions of frontal impact with an impact mass of 25t at 36km/h.

Some of the analyzed solutions with relevant post-crash configurations are shown below. In the considered hypothesis, we have studied configurations with a longitudinal development of the tubes that, in some hypothesis, covers the whole length and, for others, the half of the total length of the initial module.

The model, shown in fig. 4.18, due to the tube's excessive slenderness, collapses under a relatively low peak load, as a matter of fact resulting ineffective for the goal.

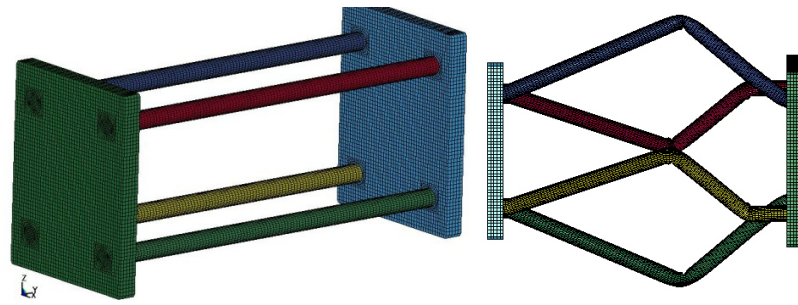


Fig. 4.18 –Second study hypothesis.

On the basis of the results of the previous model the section tubes was modified, for what concerns both shape and dimensions, without changing the distance between tubes. Post-crash configuration shown in fig. 4.19 underlines that changes performed resulted effective, allowing an axial tube collapse, but the absorbed energy is lower than the minimum required.

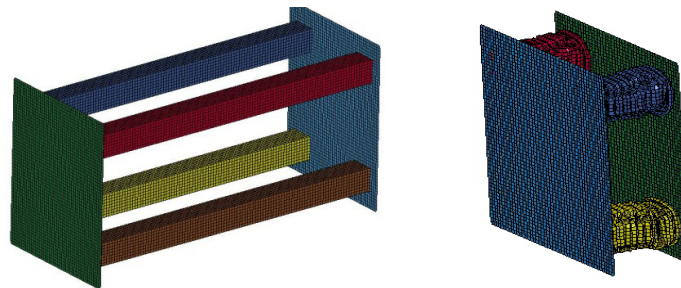


Fig. 4.19 – Hypothesis with tubes having rectangular section.

In order to increase absorbed energy, the position of the tubes has been changed so that to evaluate its effects on the component global behaviour. Fig. 4.20 shows non-deformed and deformed configuration.

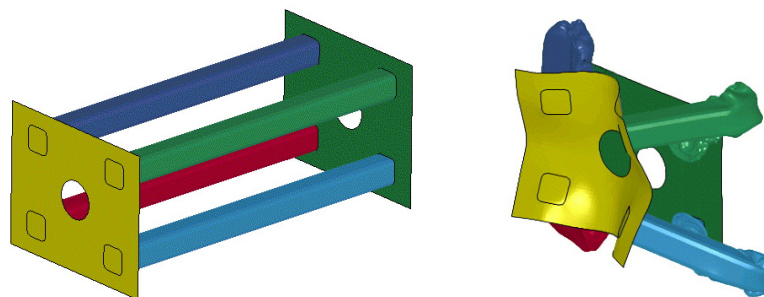


Fig. 4.20 – Hypothesis with rectangular section and rounded-out edges.

Due to the inefficacy of the solution, the possibility to use tubes with circular section but having bigger diameter and thickness has been evaluated. The result, shown in fig. 4.21, in terms of folding progress and typology, seems satisfactory but the reaction force is too high.

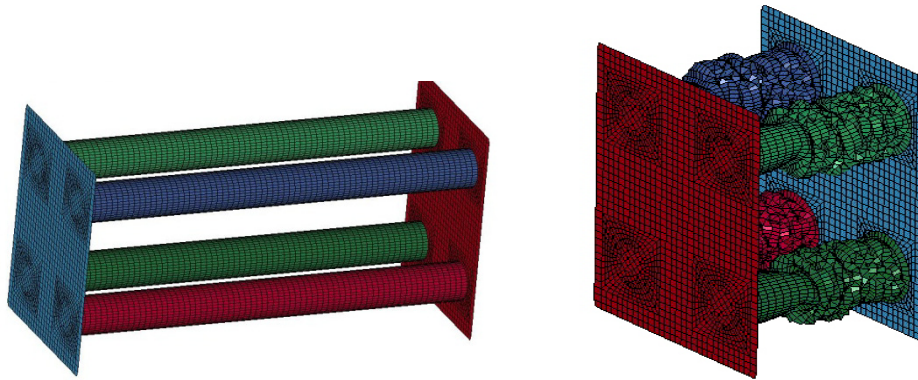


Fig. 4.21 – Solution with tubes having circular section.

In order to check reaction force and elements collapse, the total module has been divided into two parts. The results in terms of deformed configuration are positive, but the absorbed energy is once again too low (fig. 4.22).

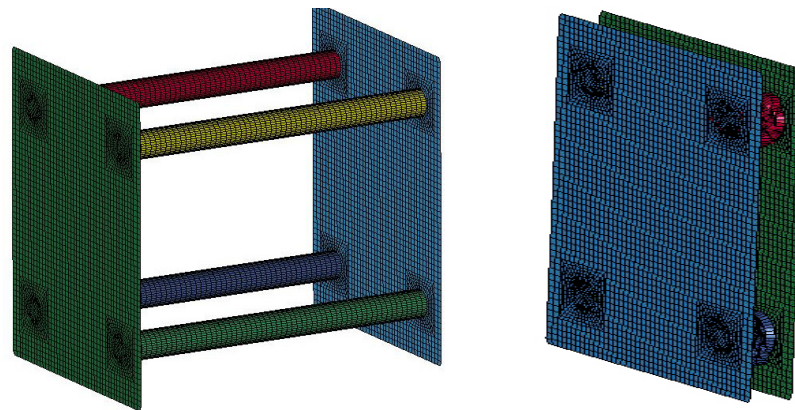


Fig. 4.22 – Results obtained with a single module.

Along with the previous solutions, an alternative solution (fig. 4.23) using a single longitudinal element composed by different modules spaced out by steel plates has been studied. The excessive mass caused the rejection of this solution.

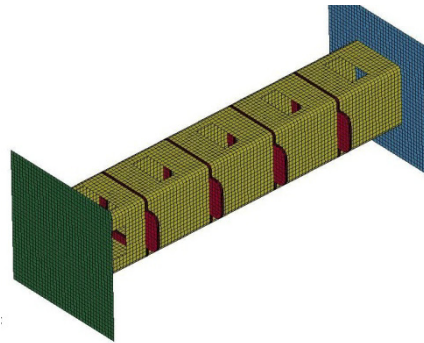


Fig. 4.23 – Alternative hypothesis with a single stage.

Simulations performed on models shown in fig. 4.17÷4.23 show that planned solutions do not give satisfactory levels of force and therefore energy.

However, for the solutions for which no global instability occurs, energy levels are close to those requested and the force displacement curve has a course which is very close to the one chosen as a target.

On the basis of such information, attention was paid to the model closer to the target conditions (fig. 4.24).

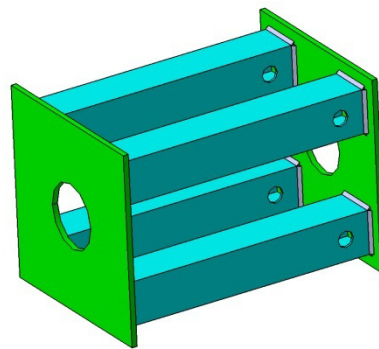


Fig. 4.24 – Solution to develop.

The energy absorbed by the device goes beyond the required value and the load-displacement curve corresponds with the one used as a reference (fig. 4.25). As too high force levels cause unbearable decelerations for occupants it is necessary to act on geometry so that to reduce reaction force even if absorbed energy is equal.

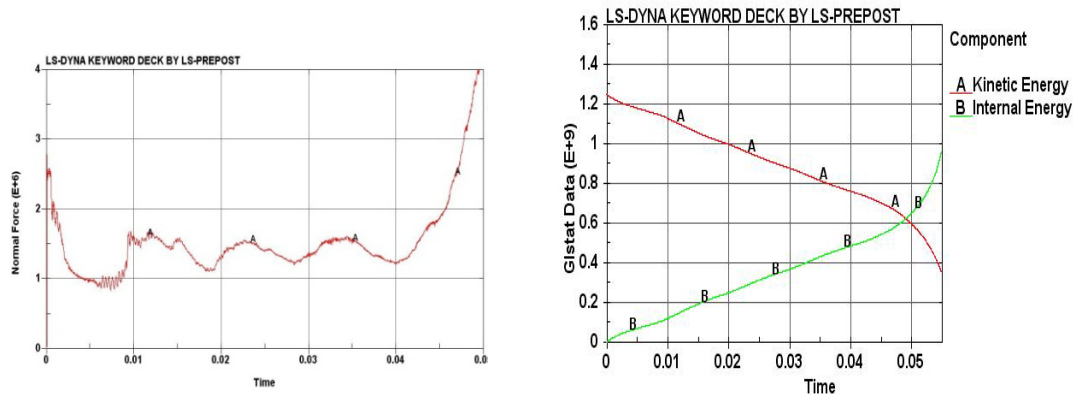


Fig. 4.25 – Load displacement curve (a), energies profile (b).

Experience acquired during the experimental step suggested to modify primer elements, the so-called starters [21], and thickness tubes, as geometry and position of the starters effect on critical load and formation of the first wave. The following images show some of the analyzed solutions.

The first image, fig. 4.26, shows the solution with the double starter: the variation of the section of the tube is linked to the holes performed on the tube's wall.

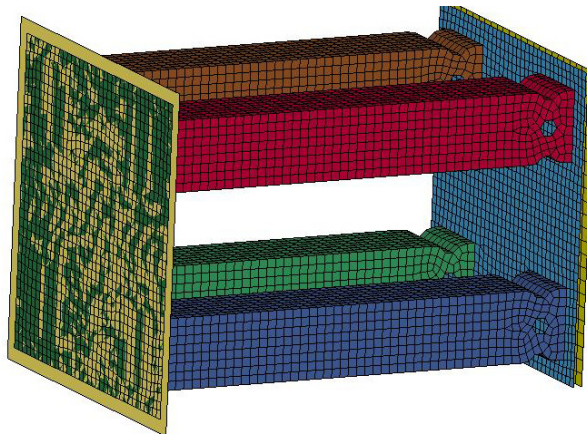


Fig. 4.26 – Model with holes and variation of the section.

The second solution (fig. 4.27) does not have the holes and uses only the variation of the section as primer element and collapse check.

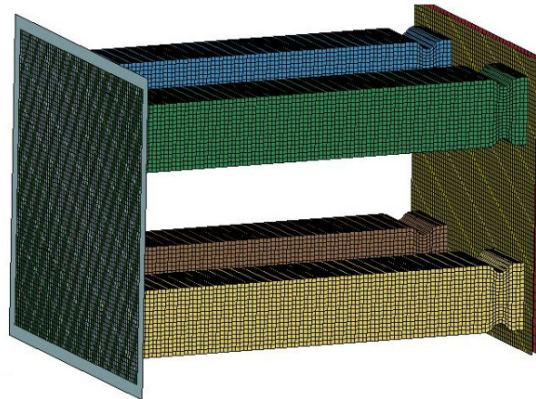


Fig. 4.27 – Model without holes and with variation of the section.

The last solution (fig. 4.28) uses a grid of properly placed holes having a very small diameter.

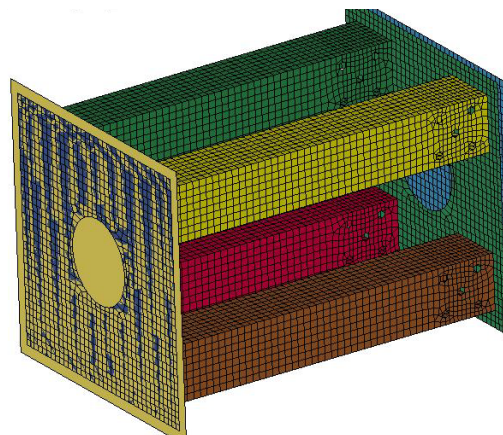


Fig. 4.28 – Model with a grid of holes.

The combination starter tube thickness by itself does not allow finding the optimal solution. As a matter of fact during the manipulation of such parameters an excessive reduction in the load level, when using a too small thickness and a too big starter, or an excessive reaction force, when using a bigger thickness with a starter having a too small diameter, occurs. As the optimal combination is not easy to be found, it was thought to use aluminium honeycomb elements allowing to increase absorbing capabilities, without excessively increasing reaction force and structure weight and in the meanwhile allowing to check load levels in the plateau area following the initial peak [22].



One of the solutions using aluminium honeycomb is shown in fig. 4.29. It is possible to observe that the honeycomb has been inserted in the internal space between the tubes so that to contribute to absorb the spurious components, due to the non perfect axially of the load acting upon the frontal plate and to the more consistent one deriving from the impact condition with offset (fig 4.30).

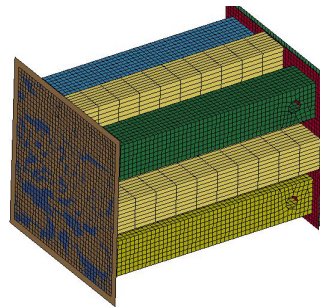


Fig. 4.29 – Solution with aluminum honeycomb.

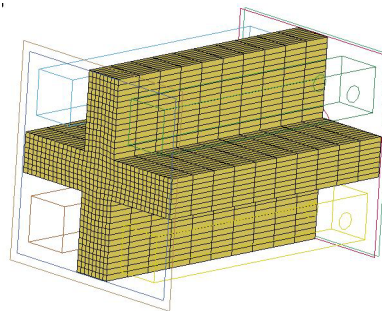


Fig. 4.30 – Detail of honeycomb block.

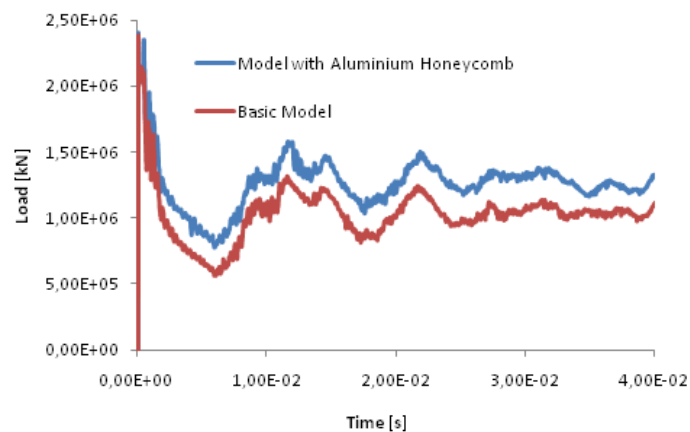


Fig. 4.31 – Overlapping of the load displacement curve with and without honeycomb.



The graph in fig. 4.31 shows the overlapping of the load displacement curves connected with solutions with and without honeycomb. The curve concerning the solution with honeycomb shows that the use of cellular material allows increasing reaction force and absorbed energy without altering the initial peak.

In order to look for a solution allowing to reduce the initial peak, it was thought to replace the square section with the circular one (fig. 4.32), leaving tubes' position and length unchanged. This choice derives also from considerations connected to the tubes with a circular section's availability and cheapness.

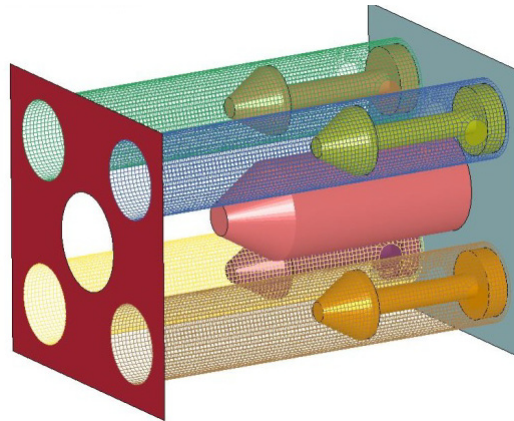


Fig. 4.32 – Solution with circular tubes and alignment system.

As the absorber must guarantee proper functioning even when the impact is not centred, that is with a 40 mm vertical offset, it was convenient, even in this preliminary phase, to study the systems allowing to drive the crushing phase while tubes collapse in the axial direction only.

In order to guide the crushing phase some guides have been inserted into the tubes (fig.4.33), while to react to the vertical component arising during the crushing final phase, causing a relative displacement of the edges plates which damages the tubes, a central guide was inserted which by being inserted in a hole made in the back plate, allows to link the relevant displacements of the two plate. The guides are coaxial with the tubes and have the central part of a reduced section so that they do not interfere with the waves generated during tubes.

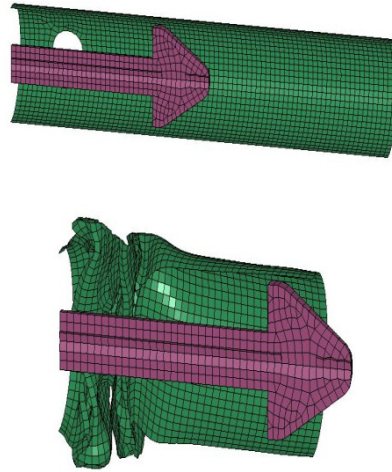


Fig. 4.33 – Sections of the tube and the guide in pre and post crash configuration.

In the following graphs (fig. 4.34 – 4.35) the profile of the reaction force and the profile of the operating energies during the impact is shown. Moreover, fig.4.36 shows the configuration of the absorber after the crash.

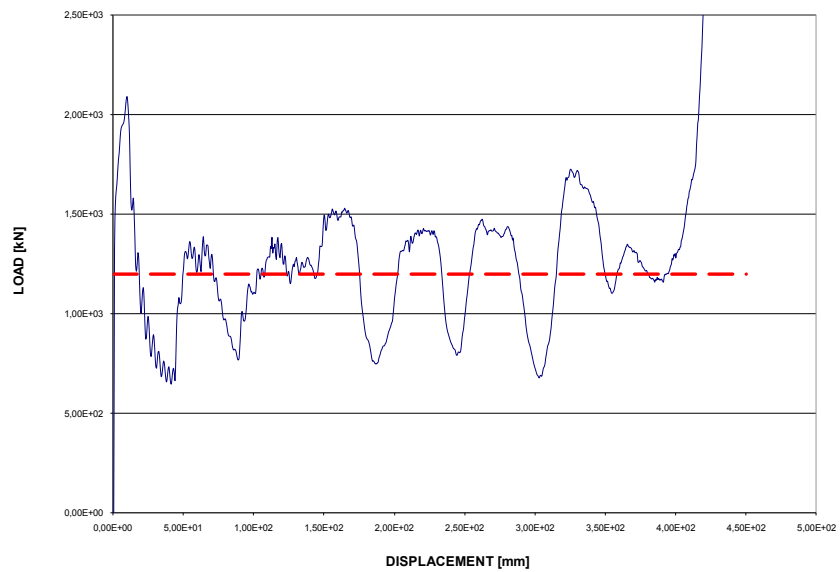


Fig. 4.34 – Load displacement curve obtained by the simulation and target curve.

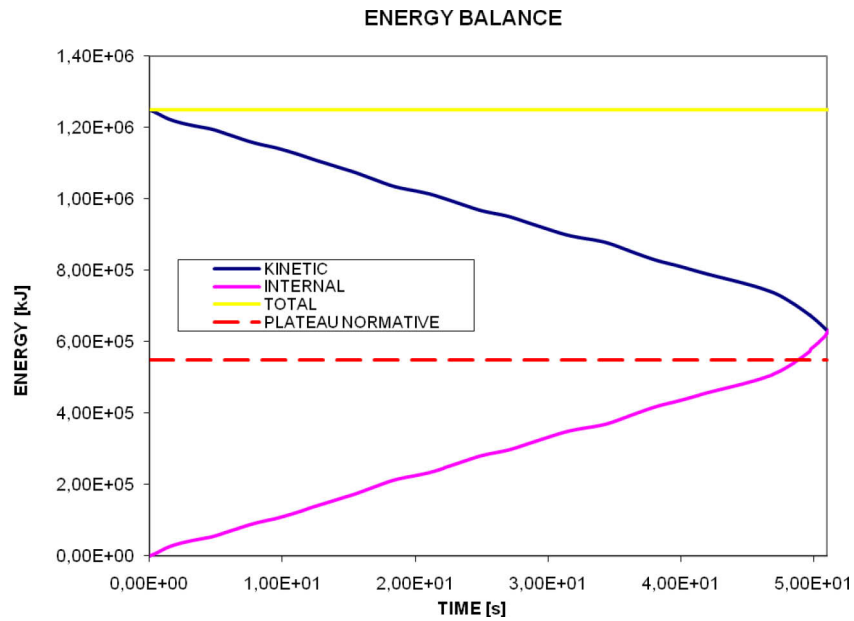


Fig. 4.35 –kinetic energy, internal energy and total energy obtained by numerical simulation.

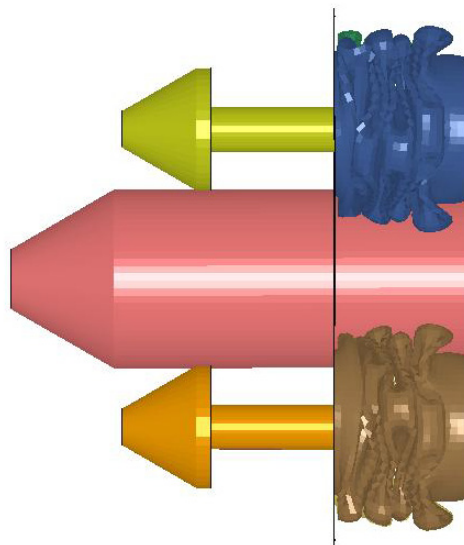


Fig. 4.36 – Absorber configuration at the end of the crushing.

It is possible to note that, both in conditions of aligned impact or impact with the offset, the absorber shows a good behaviour keeping alignment.

4.3. Multi-stage model

The element modelled in the previous paragraph is one of the two components constituting the complete absorber. The absorber complete configuration requires two sequentially elements so that to cover the total length of the existing absorber, which is equal to 1070 mm (fig. 4.37).

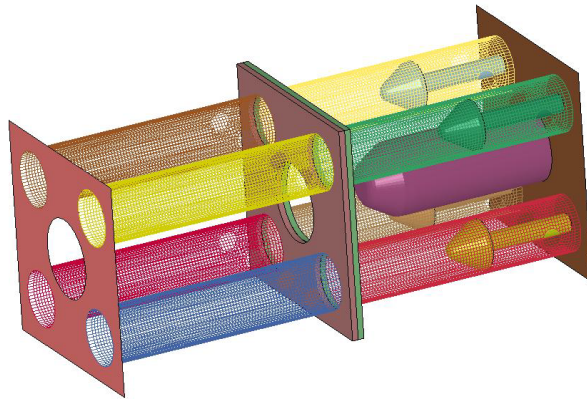


Fig. 4.37 – Two stages model.

However, this solutions interferences with the modular solution for overlapping of the second module to the ideal cutting line between the nose and the second absorption area (fig.4.38), as a consequence it was necessary to reduce the length of the two components to 400 mm.

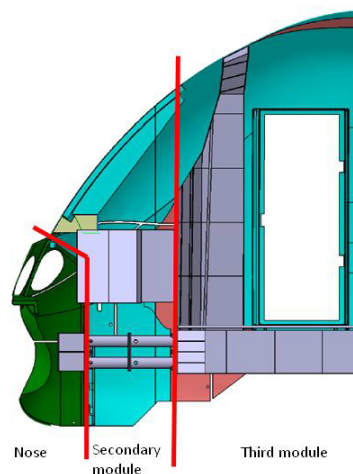


Fig. 4.38 – Localization of the three absorption areas.



In order to compensate the reduced length, another honeycomb element was added (fig. 4.39).

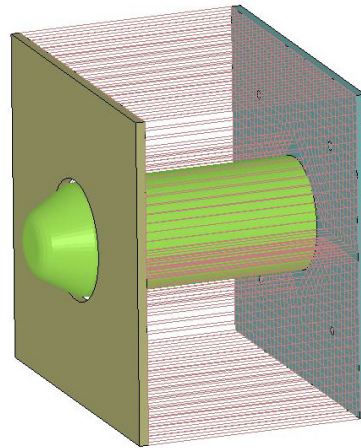


Fig. 4.39 – Honeycomb block on absorber front.

In order to check the aluminium honeycomb block crushing and ensure the parallelism of the opposite faces of the block during the crushing phase, the central guide was moved on the frontal plate, connecting it to the anticlimber, while guides inside tubes kept the previous position. Weight reduction obtained with this absorption system compared to the initial one is equal to 60%.

The whole of all these changes has led to the solution shown in fig. 4.40.

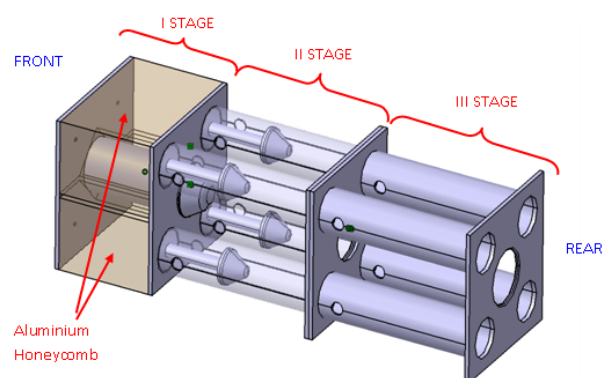


Fig. 4.40 – Complete model of the multi-stage absorber.



For this final configuration, numerical simulations reproducing impact conditions planned in scenario n.1 of the EN 15227 were performed. Fig. 4.41 shows post-crash configuration for the align crash condition.

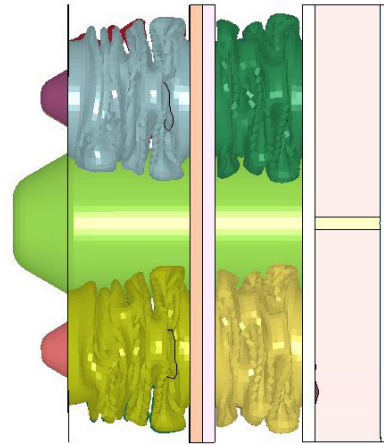


Fig. 4.41 – Configuration of the multi-stage absorber at the end of the impact.

In the following graphs (fig. 4.42 – 4.43) the load displacement curve and the curves relevant to the energies operating during the impact are shown. It is possible to see that the device is able to absorb the amount of energy required with load levels corresponding to the ones planned.

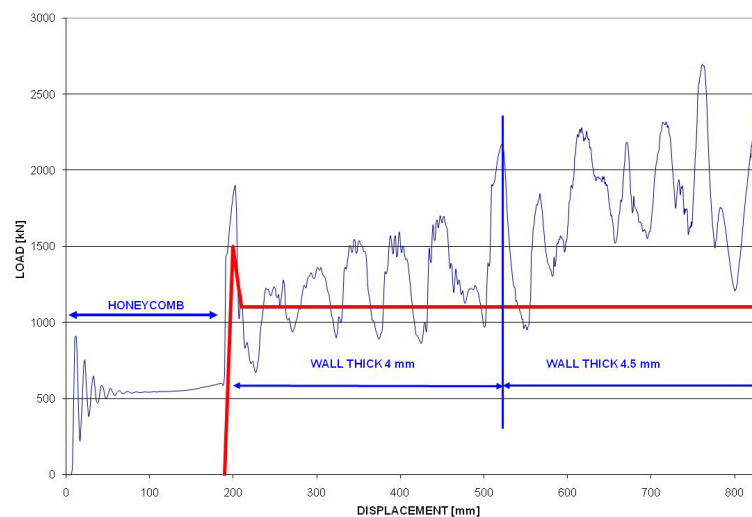


Fig. 4.42 – Load-displacement curve obtained by numerical simulation.

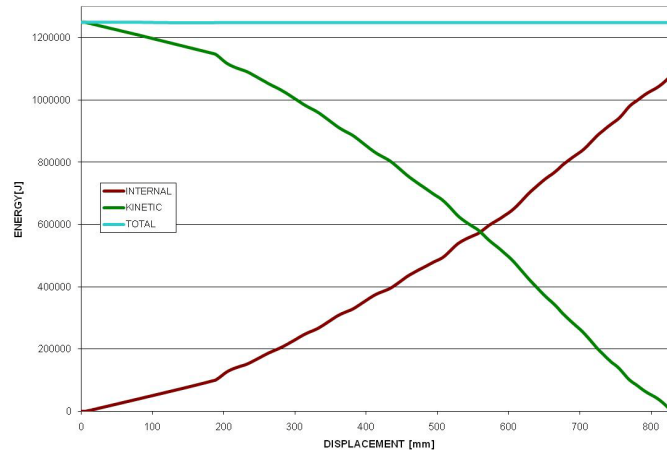


Fig. 4.43 –kinetic, internal and total energy during impact.

However, the offset configuration (fig. 4.44) did not give positive results due to the guides inefficacy. In fact, due to the overturning momentum, created by the 40 mm offset, tubes bend on the vertical plane and the system loses its functionality (fig. 4.45).

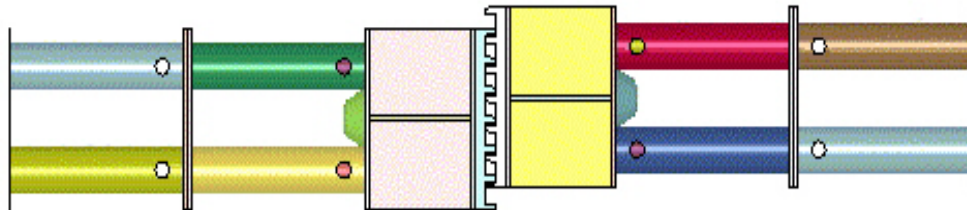


Fig. 4.44 – Initial configuration with non aligned crash.

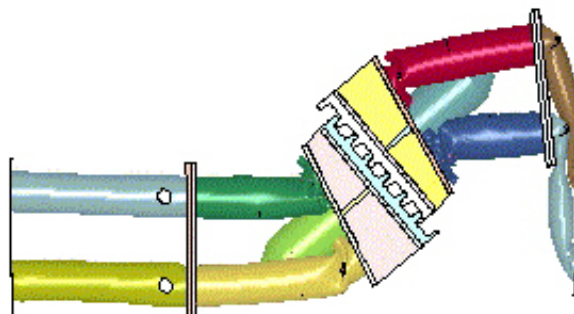


Fig. 4.45 – Configuration obtained by numerical simulation.



In order to counter this drawback, different alternative solutions allowing to keep edge plates parallelism and the tubes to be crushed keeping axis perpendicularity with edge plates were studied.

As the unchecked collapse of the structure is due to the inefficacy of the alignment systems and the chosen configuration, the alignment system was changed in an initial stage. However this approach resulted in a failure, as a consequence configuration was changed until it was possible to get one having expected performances and reduced weight.

Figures 4.46÷4.48 show first attempts in which the tubes inclination was changed when compared with the edge plates.

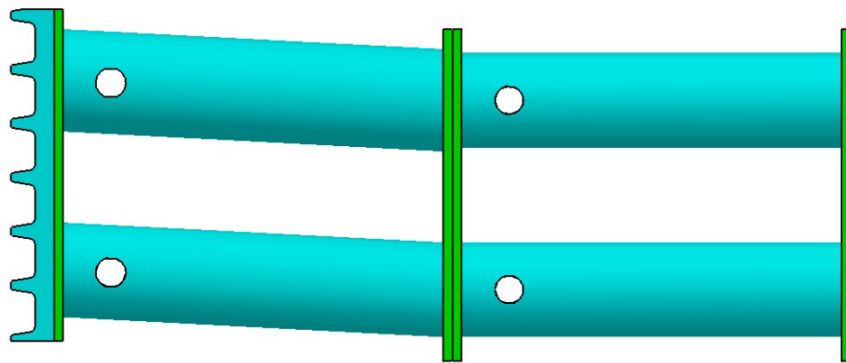


Fig. 4.46 – Solution with tubes axis of the first module inclined and vertical anticlimber.

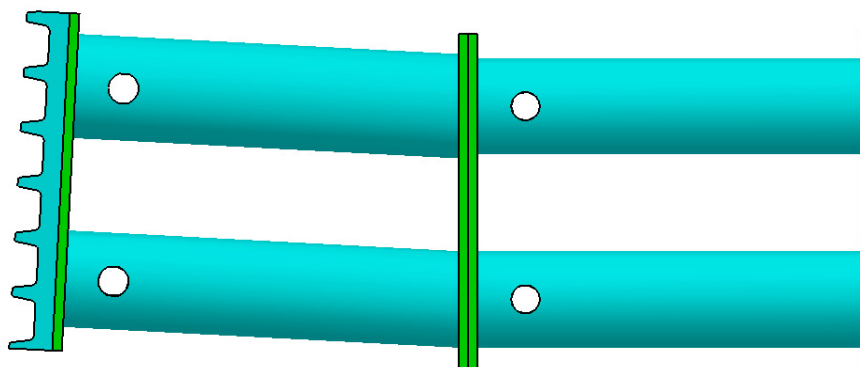


Fig. 4.47 – Solution with tubes axis of the first module inclined.

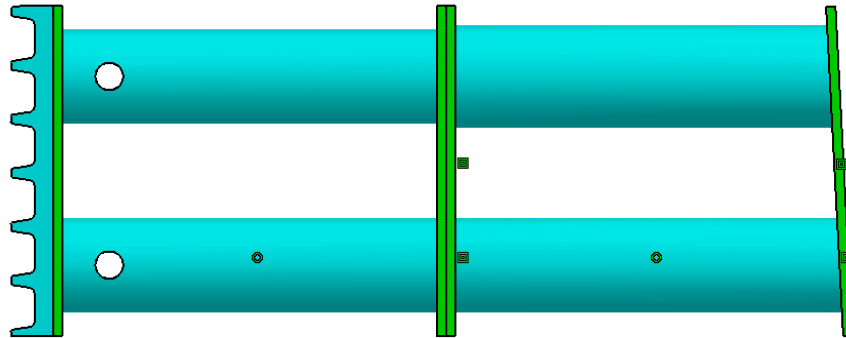


Fig. 4.48 – Solution with tubes axis of the first and second modules inclined with respect to the plate with rear coupling.

However, solutions shown were not resolving, as a consequence a different solution was evaluated, with the starters nearby the edge of the tube opposite to the one corresponding to the impact area and with the volume delimited by edge plates and external to the tubes and filled in with an aluminium honeycomb block (fig. 4.49).

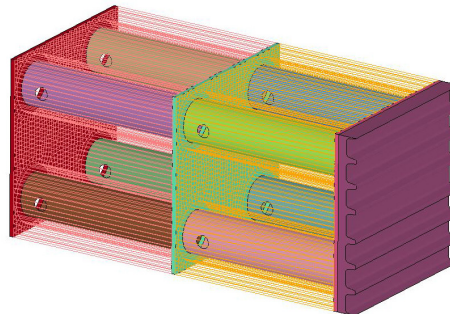


Fig. 4.49 – Solution with starters in the opposite side and filling honeycomb.

Being this solution ineffective, operations focused on the central guide, hypothesizing for it a telescopic system (fig. 4.50).

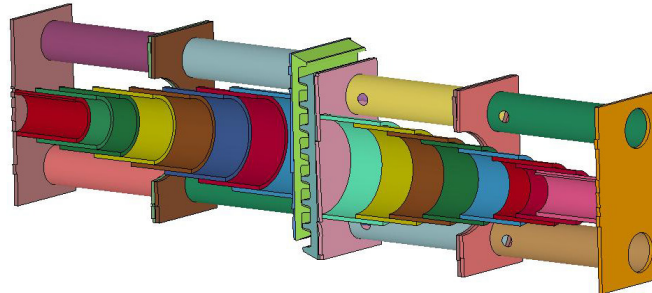


Fig. 4.50 – Solution with telescopic guide.

As this failed too, there was the attempt to insert components acting to avoid effects due to the offset. In particular, it was hypothesized to use other two elements placed on the symmetry plan, which collapsed under the axial load and contributed to avoid the effects of the overturning moment. The three following images (fig.4.51 ÷ 4.53) show some of the hypothesized solutions.

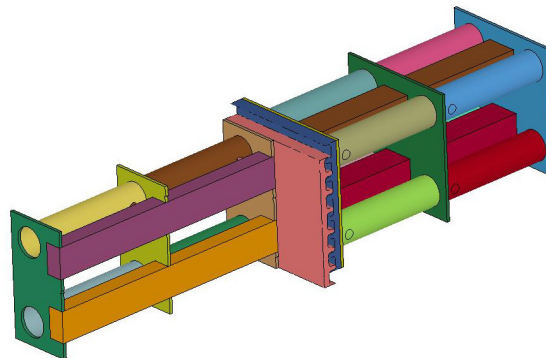


Fig. 4.51 –Solution with supplementary sacrificial tube.

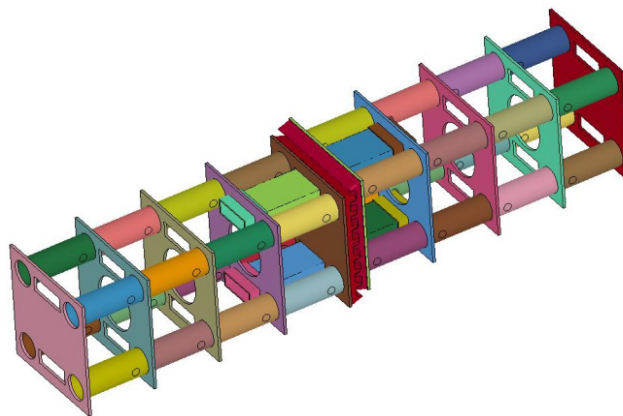


Fig. 4.52 – Solution with upper and lower guides.

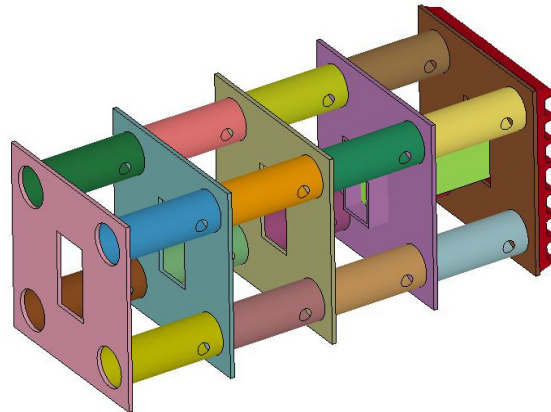


Fig. 4.53 – Solution with central rectangular guide.

All these solutions and others which were not shown, did not solve the drawback connected to the anticlimber rotation in impact condition with offset. For such a reason the geometry of the absorber was changed to the detriment of the modular concept.

4.4. Single stage model

For redesigning the absorber according to the single-stage concept, only the impact condition with offset has been considered because, if the considered solution ensures a good behaviour towards this condition, it will surely ensure it in the case of aligned impact too.

Different models have been created, the first of which is made up of two tubes with rectangular section with plastically deformed areas in the rear zone acting as a primer for localised collapse (fig.4.54).

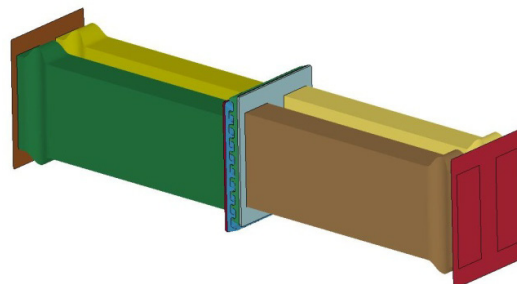


Fig. 4.54 –First single-stage solution.



The second solution replaces the previous deformed areas with a line of circular holes (fig. 4.55).

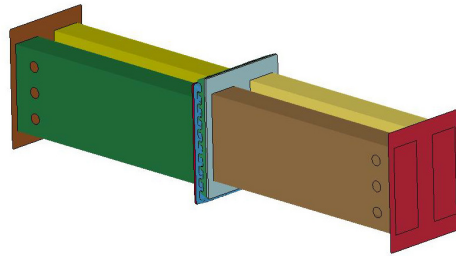


Fig. 4.55 –Second single-stage solution.

As cellular materials, because of their own structure, are very well-performing even in non aligned impact conditions, it was thought to reproduce such structure, but in a very enlarged scale, when building a new model of absorber (fig. 4.56).

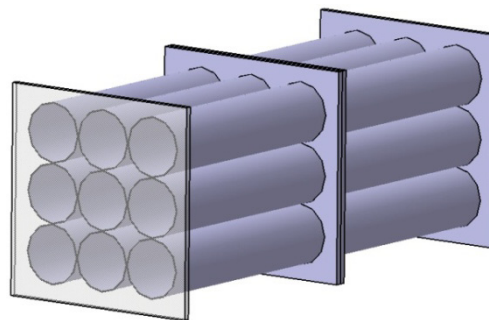


Fig. 4.56 – Solution with multiple tubes.

The solution with macrocells made with tubes having a big diameter is not effective, but a reduction in the diameter would imply a structural complexity which is not believed profitable. As a consequence it was chosen to change the shape of the single components and include a system for internal alignment (fig.4.57).

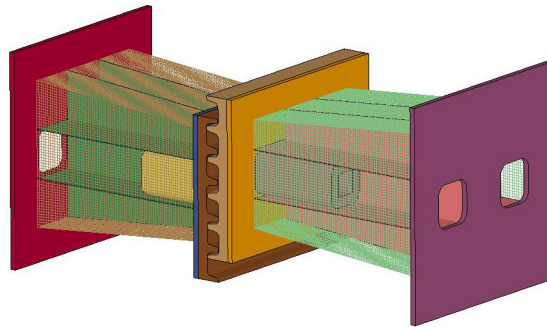


Fig. 4.57 – Solution with multi tubes having rectangular section.

Results relevant to this configuration show that the internal guide, when attempting to keep orthogonality between the anticlimber and the axis of the single tubes, damages the walls contributing to the uncontrolled collapse of the structure.

Determining the geometry which allowed to solve the problems connected to non aligned impact involved not only the shape of the tubes but also the primer device and the position hold by the device itself (fig.4.58 ÷ 4.59).

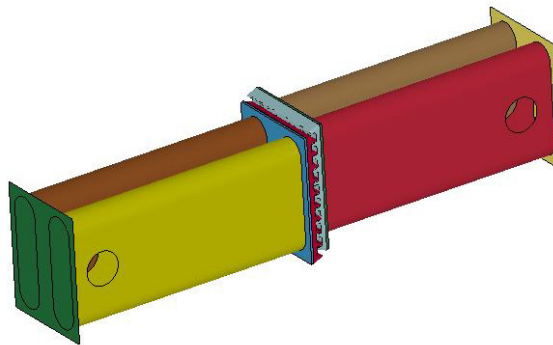


Fig. 4.58 – Single-stage solution with circular starters.

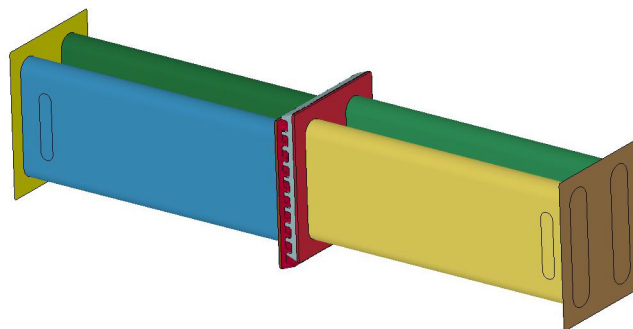


Fig. 4.59 – Single-stage solution with elliptical starters.



As the goal of redesigning was to reduce the mass of the absorption system leaving performances unchanged, composite materials were used as they allowed to make the structure simpler and reduce the weight of analogue solutions made up of conventional materials.

The basis was a solution allowing to distribute on the biggest surface possible the contact force between the two impacting absorbers. In order to do that, it was thought to use a set of sequentially placed honeycomb blocks and oriented so that the direction of the material cells was aligned with the longitudinal direction of the absorber. In order to prevent cells penetration and damage, aluminium plates having small thickness have been inserted between blocks. Moreover, the presence of the plates allow the uniform distribution of the load on all block surface. The number of blocks has been decided according to their commercial dimensions and such that the sum of single block thickness covers the length of the entire absorber (1070 mm).

The aluminium honeycomb used is of the 5052 series. Densities of each single block are variable. However, this solution, even though it allows solving the offset problem, does not react to the necessary load and energy levels. For such a reason the blocks transversal dimensions were increased.

Being such a solution far from the target, everything was inserted inside a mild steel tube (fig. 4.60), whose thickness was optimized with numerical analysis. In fig. 4.61 the load-time curve obtained from the impact simulation of this model.

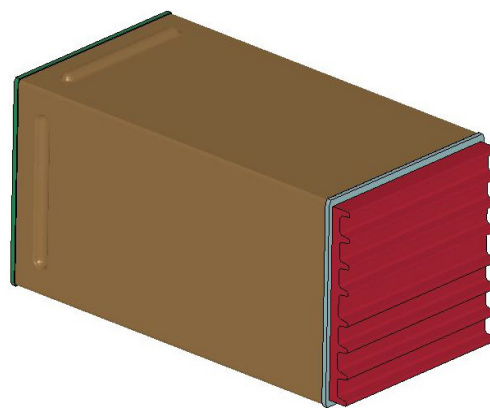


Fig. 4.60 – Solution with honeycomb and external tube.

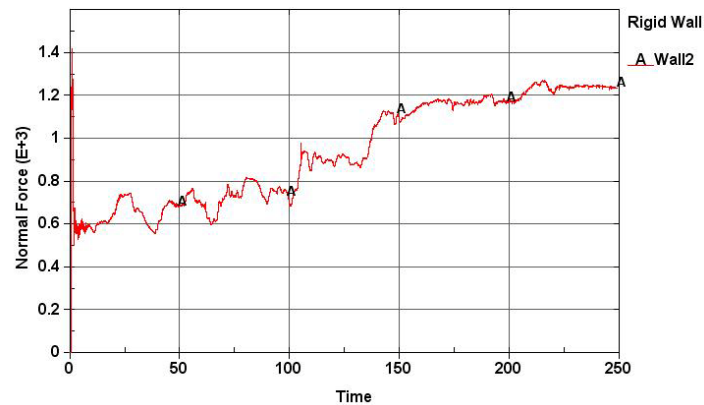


Fig. 4.61 – Progress of the force concerning the solution in fig. 4.60.

This solution was improved by changing the external tube and the internal aluminium honeycomb blocks. In fig. 4.62 the final model and fig. 4.63 ÷ 4.64 relevant results after a simulation of an impact at 18km/h with a vertical offset of 40mm is shown. Fig. 4.65 shows the final configuration after frontal impact.

The model of the complete elements was built using shell and solid elements. The external tube was connected to the rear plate and the anticlimber by merging the coinciding nodes of the contacting edges. As an internal contact between the aluminium honeycomb and the edges plates a SURFACE-TO-SURFACE [16] contact was used. In order to simulate the contacts between the tube's lobes which generate during the folding, the tube and internal blocks and the tube and edge plates, a SINGLE-SURFACE [16] contact type was used. For modelling honeycomb material, an anisotropic model implemented in LS-DYNA as *MAT_26 [16] was used. Material parameters are taken from the HEXCEL datasheet [9]. For modelling the external aluminium box material, the *MAT_103 was used, taking data necessary for parameters determination from literature.

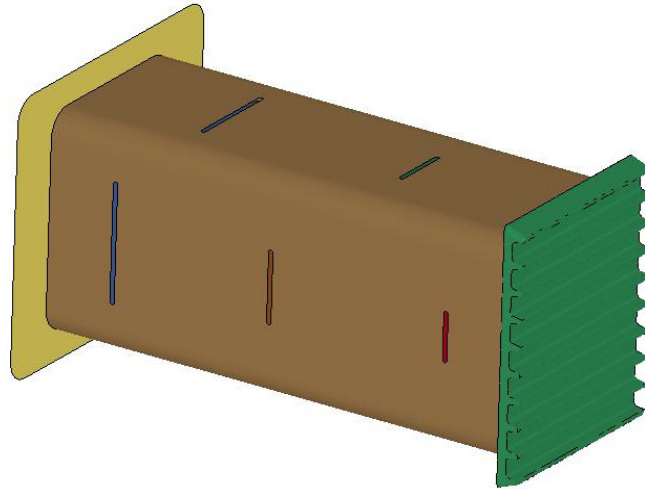


Fig. 4.62 – Optimized final solution.

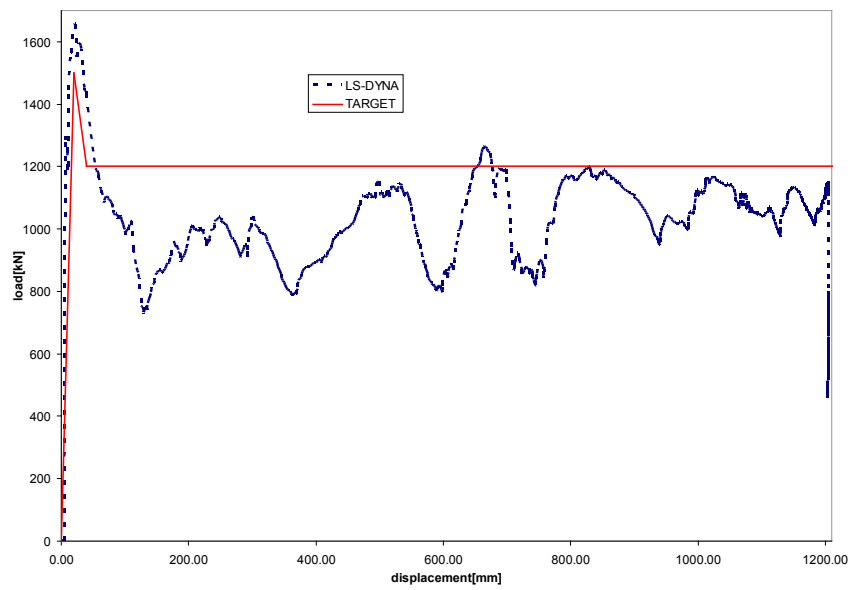


Fig. 4.63 –Force displacement curve for the optimized solution.

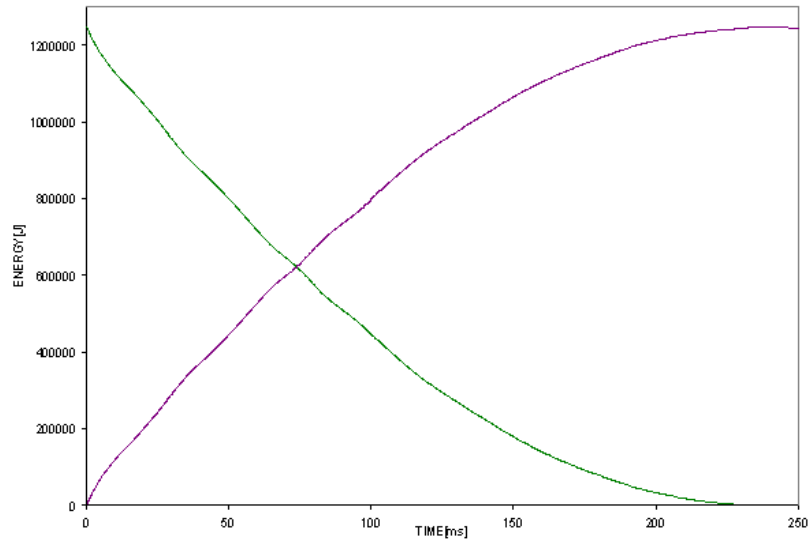


Fig. 4.64 – Energies profile during impact.

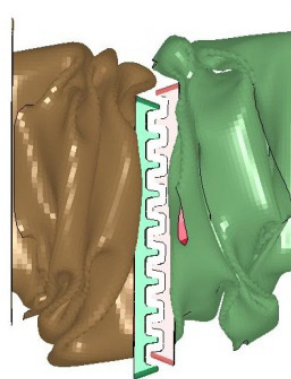


Fig. 4.65 – Post crash configuration.

The image in fig. 4.66 shows the position of the two absorbers in the re-modelled cab. The interface surface and the joint techniques will be described in the chapter dealing with cab modeling.

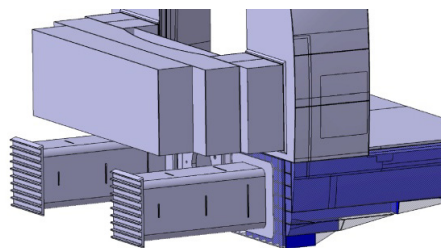


Fig. 4.66 – Position of the absorbers on the cab.



Through a long and complex process including several hypothesis which did not entirely solve the problem, it was possible to find a geometry allowing to reduce by more or less 50% the weight of the single absorber, leaving performances unchanged in terms of absorbed energy and force levels used. The only question which has not been answered is connected to the compatibility of the last solution with the modular units in which the cab is supposed to be divided. In fact, the absorber geometry is not included in the secondary module of the introduction phase (fig. 4.67). A further step could be changing this solution in order to allow the complete integration of the modular cab.

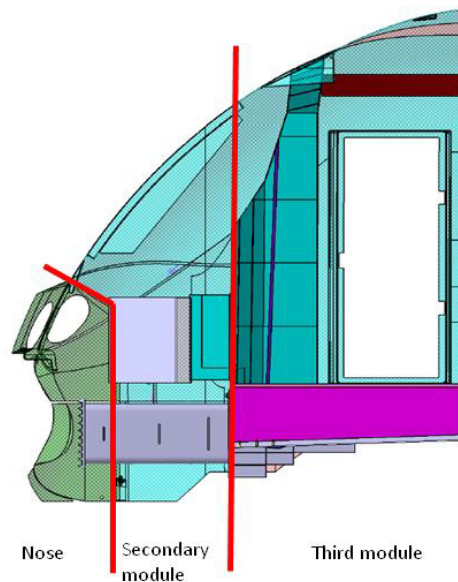


Fig. 4.67 –Interference of the lower absorber with the ideal split lines of the different absorbing zones



CHAPTER V

UPPER ABSORBER MODELLING

5.1 Upper absorber

As it has already been done for modelling the lower absorber, for the upper one too the basis was the geometry of the existing one (fig. 5.1) and, evaluated the overall dimensions, the chance to use alternative solutions allowing its mass reduction were evaluated.

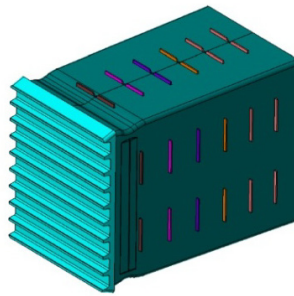


Fig. 5.1 – Upper absorber benchmark.

Reference performances identify a value with constant force during the impact and equal to 1400 kN, with a corresponding absorbed energy equal to 700 kJ (fig. 5.2).

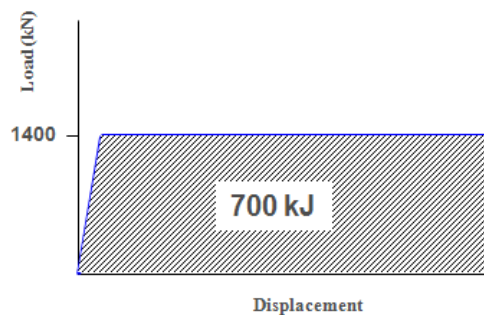


Fig. 5.2 – Reference performances.

The existing solution uses two identical absorbers placed on two frontal pillars. During the impact, the central area between the two absorbers does not have any

element taking active part in energy absorption, but presents a sort of shield protecting the driver. For such a reason [23], it was thought to introduce an element that, by covering the central area too, increased the absorption area spreading on a larger surface the action of impact forces (fig. 5.3).

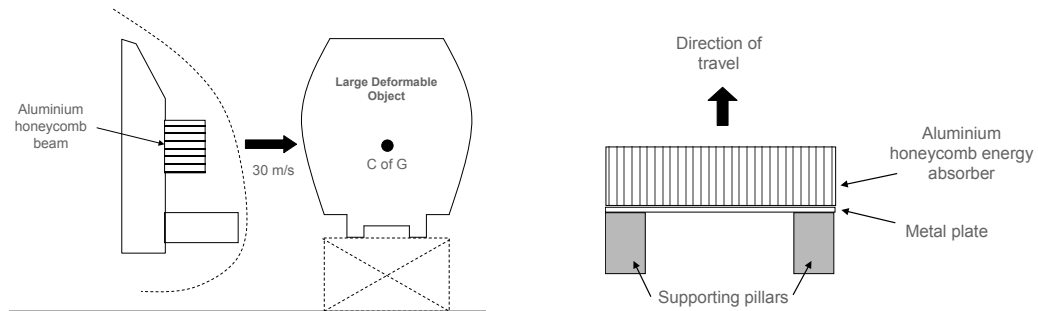


Fig. 5.3 – Position of the upper absorber.

As the transversal dimension is 2300 mm for a height of 500 mm, it would not be suitable using conventional materials to build this structure as the mass component would be much bigger than the existing one and the goal of weights reduction would be lost. The solution to this problem was found in the use of the aluminium honeycomb, as it can be easily shaped and is characterized by a very high specific absorption [10].

However the feasibility study to this solution, undertaken in this thesis with the Ls-Dyna calculation code, required the knowledge of a set of parameters for modelling the chosen material, which were not available in literature. In order to identify them, tests on components made with this material were performed.

5.2 Calibration of the material parameters

For characterizing the aluminium honeycomb behaviour, two typologies of tests have been performed. In the first typology, the behaviour of the single honeycomb block subjected to a compression force in the direction of the cells has been evaluated. In the second typology, the behaviour of a sandwich made up of a honeycomb block with two aluminium plates glued on the two opposite faces and leaning on two steel



blocks placed at a distance of 60 mm so that to create a non continuous support was evaluated.

For what concerns the first test typology, two aluminium honeycomb blocks having dimensions of $100 \times 70 \times 50 \text{ mm}^3$ were used. Fig. 5.4 shows one of the tested specimen.



Fig. 5.4 – Aluminium honeycomb block tested.

Compression tests were performed using the DARTEC Universal Test Machine for static and dynamic tests at the labs of the University of Newcastle (fig. 5.5).



Fig. 5.5 – DARTEC - Testing machine for static and dynamic test.

The specimen was loaded at a rate of 0.5 mm/s until the honeycomb reached a fully compressed state, supervised through the visual check of the specimen itself and the value of the instantaneous load read by the acquisition system. The specimen was placed between the machine heads so that to be uniformly loaded on the upper face

and continually supported on the opposite face. In the following graph (fig. 5.6) the load displacement curve and the configuration of the specimen at the end of the test is shown in fig. 5.7.

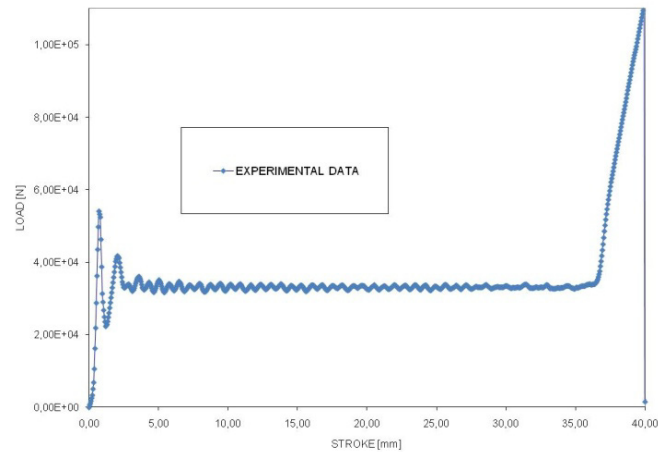


Fig. 5.6 – Characteristic curve obtained from compression test on the honeycomb block.

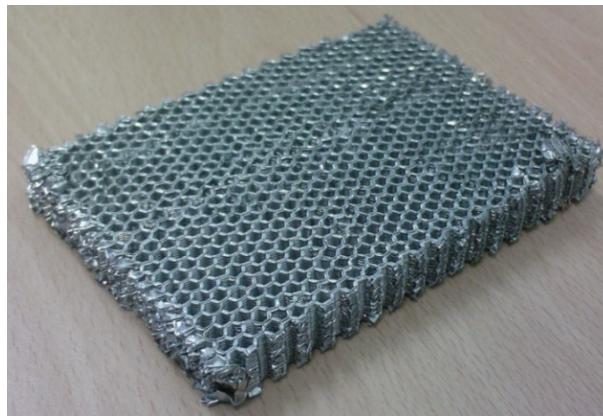


Fig. 5.7 – Final configuration of the specimen.

For determining material parameters describing its behaviour, the described test was simulated by finite element code, using as starting conditions a set of parameters supplied by the HEXCEL production factory. The model, created in HyperMesh and then imported in LS_Pre_Post for cards compilation and check, is shown in fig. 5.8.

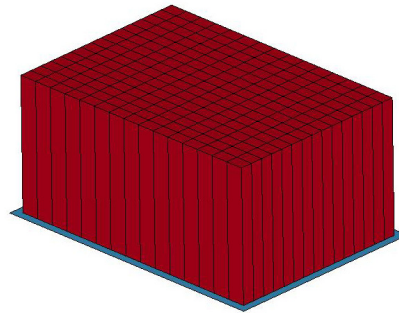


Fig. 5.8 – FE model implemented in Ls-Dyna.

Optimized parameters are shown in tab. 5.1.

Tab. 5.1 – Material parameters optimized with numerical analysis

Density (kg/m ³)	Young's Modulus of Compacted Honeycomb (MPa)	Yield Stress of Compacted Honeycomb (MPa)	Relative Volume at Full Compaction	Honeycomb Crush Strength (MPa)	Young's Modulus of Uncompacted Honeycomb (MPa)
48	70000	130	0.2	0.875	482

Other properties necessary to completely define the material orthotropic behaviour were evaluated with the non continuous support test. In fig. 5.9 the final configuration resulting from the analysis is reported, while in fig.5.10 the experimental curve was overlapped to the one obtained in the numerical way.

LS-DYNA KEYWORD DECK BY LS-PREPOST
Time = 80.8

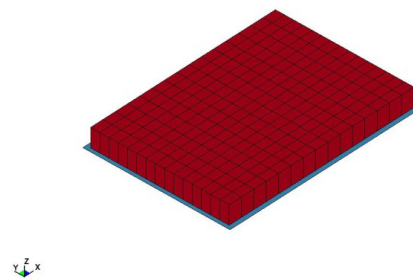


Fig. 5.9 – Configuration of the honeycomb block after simulation test.

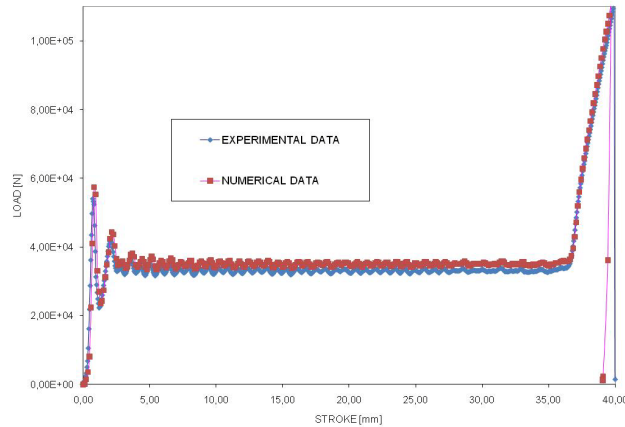


Fig. 5.10 – Overlapping of characteristic experimental and numerical curves.

The second test typology allowed the evaluation of honeycomb behaviour when it is glued between the two plates to form a sandwich. The geometrical characteristics of tested sandwich are:

Tab. 5.2 – Characteristic dimensions of the tested specimen

Length:	99 mm
Width:	49 mm
Depth:	15 mm
Skin thickness:	0.9 mm
Cell wall thickness:	0.05 mm

The set-up for the test is shown in fig. 5.11

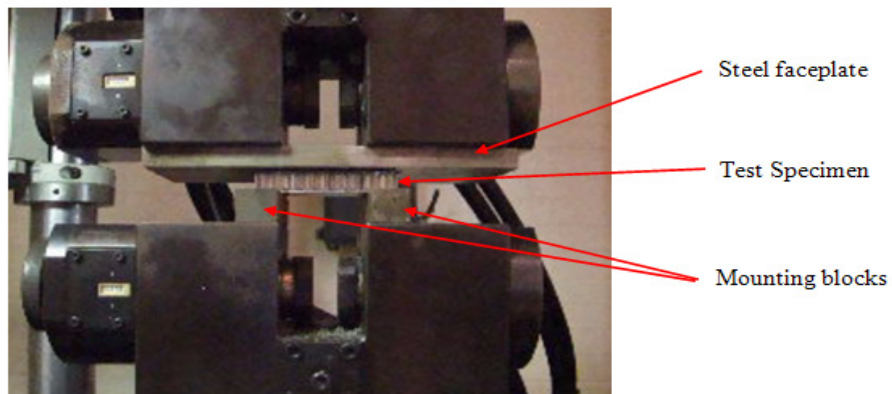


Fig. 5.11 – Set-up for tests with non continuum support.

The sandwich panel, manufactured by Alcore Brigantine, object of the test was placed on two steel blocks to create a non continuous support, while the compression load was applied in a distributed way by mean of a plate, at a rate of 0.5 kN/s. This test typology is very significant for absorber modelling, as it reproduces in small scale the condition in which the real system will have to work, glued to the two edges on pillars and not supported in the central part.

The acquired load displacement curve is shown in fig. 5.12, while the specimen configuration at the end of the test is shown in fig. 5.13.

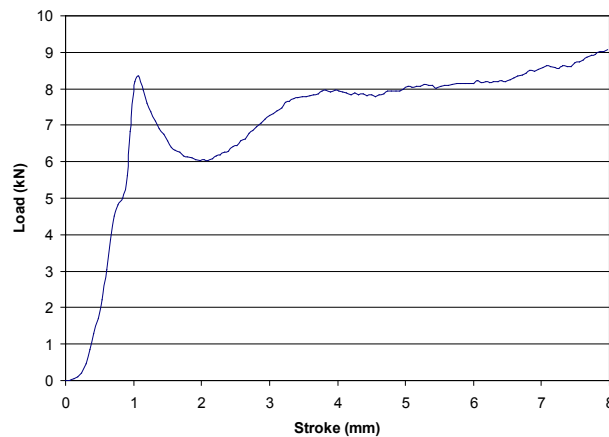


Fig. 5.12 – Characteristic curve obtained with continuum support.



Fig. 5.13 – Specimen configuration after test with non continuum support.

The test has shown that the unsupported portion of the panel, i.e. the region between the mounting blocks, did not exhibit any crushing in the honeycomb (fig.5.13A) leading to a hemi-spherical protrusion. Those regions of the panel which did crush were significantly weakened by the lateral deformation caused by the movement of



the sandwich skin (fig. 5.13B). In FE environment the sandwich model has been created and simulation were carried out to calibrate the orthotropic properties of the material. In fig. 5.14 the created model is shown. Parameters of the material were taken from HEXCEL Datasheet and Tests Results [9]. Elements used for mesh creation are SOLID95, solid elements with 8 nodes, which can tolerate distortions with a good degree of accuracy.

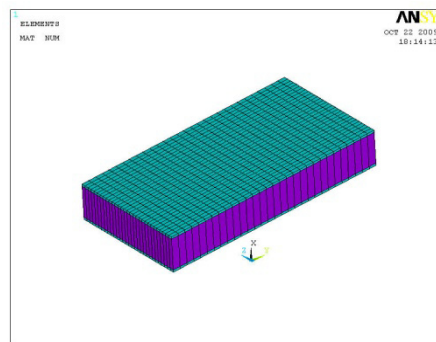


Fig. 5.14 – FE Model implemented in Ls-Dyna.

The modelling has provided results matching with the observed physical reality. As showed in fig. 5.15, in fact, by reproducing the test restraining conditions and by displacing the upper surface of 1 mm and then 3mm, the deformed configuration of the sandwich matches with the one reported on the specimen during the test.

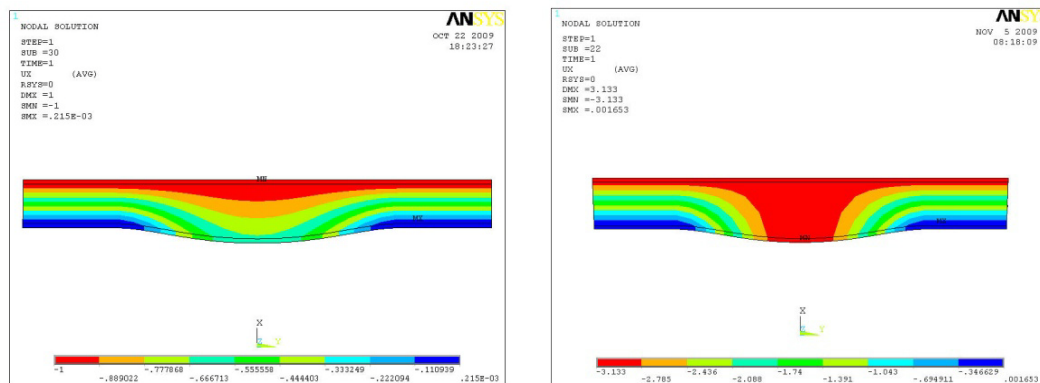


Fig. 5.15 – Displacement pattern corresponding to imposed vertical displacement of 1mm and 3 mm.

Furthermore, the reaction value, related to the FEM model, which has been taken in correspondence to the supporting surfaces for a displacement of the sandwich surface



of 1 mm is 6.8 kN, against a value of 6.9 kN registered during the test. Based on these considerations, the choice procedure for the parameter set used for describing the material behaviour in the numerical modelling of the upper and lower absorber has been considered reliable.

Now we need to specify that the calibration of the material parameters has been carried out using compression tests under quasi-static conditions. However, by increasing the impact speed, the crush-strength increases and the absorbing features of the material change. In the fig. 5.16 from [10] we can observe how, due to an impact speed of 100 ft/s, equal to about 110 km/h, the crush-strength increases by about 3%. Since the impact conditions for the upper absorption system provided by [4] foresee speeds of 100 km/h, we can approximate the honeycomb properties defined under static conditions with those related to the impact conditions at 90 km/h.

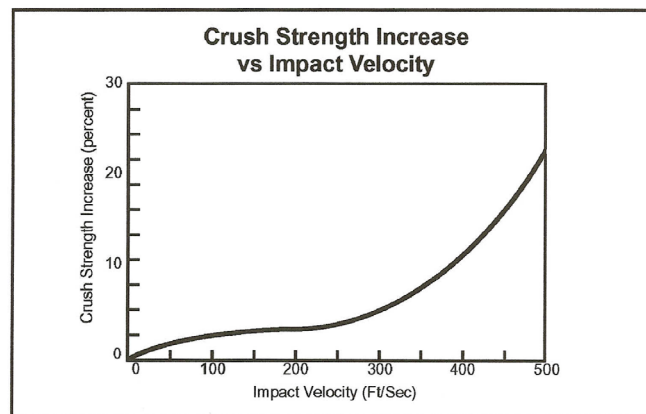


Fig. 5.16 – Crush strength vs impact velocity [10].

Another very important factor is the direction to which the crash occurs. In fact, larger is the angle between the impact direction and the typical honeycomb L-direction, lower is the absorption capability. Just think that for angles near to 35° the absorbed energy is reduced by 50% [10]. If rule-compliant, the impacting direction of the obstacle against the absorber is to be considered as coinciding with that of L-direction and, then, in this case this property decay is negligible.

5.3 Honeycomb Block Optimization

For determining the shape of the absorber, we have exploited what observed in the compression tests on not-continuous support. In fact, to avoid that the central part remained undeformed to the detriment of the absorbed energy and the system efficiency, the backplate, interfacing with the supporting pillars, has been modified by creating a curved zone in the central portion (fig. 5.17) which will create load paths from the centre of the sandwich to the pillars. The size of the bend radius for this portion is 2000 mm and the depth of the bend radius, as measured from the contacting surface with the pillars, is 100 mm (fig. 5.18).

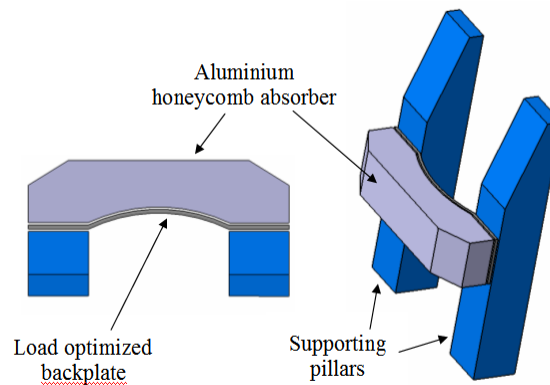


Fig. 5.17 – Upper absorber position on the pillars.

The dynamic simulations carried out in the preliminary step have showed that this arched solution allows modifying the load path by driving them to the supporting zones and making the whole block active during the compression step.

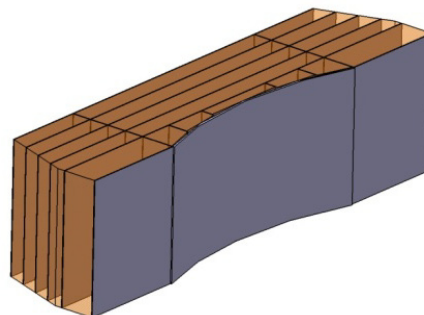


Fig. 5.18 – Multi-stage model of the Upper absorber.



The first examined model took into account a series of glued honeycomb blocks alternated to aluminium plates with a small thickness. The complex carrying out of such a device has forced to search for alternate solutions. Due to the availability of very thick honeycomb blocks, even hundred millimetres, the fragmentation showed in fig. 5.19 has been replaced with a single block.

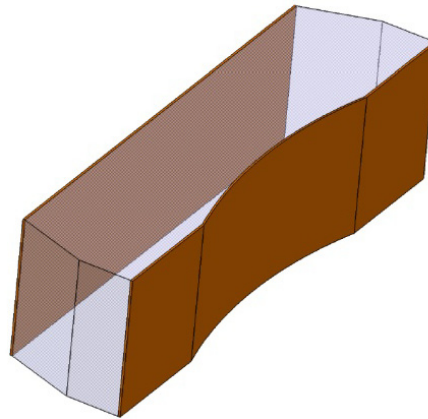


Fig. 5.19 – Single-stage model of the upper absorber.

For calculating the way such a device behaves under dynamic conditions, we have simulated, with the aid of the LS-Dyna calculation code, the crash against a road obstacle of big dimensions. For the preliminary study phase, the obstacle has been modelled like a prismatic block with an appropriate density, in order to obtain an impact mass of 50 t. For building the core FE model we have used one only element in the thickness. The contact between the core and the faces has been modelled with a tied-break contact, in order to simulate the failure occurring in the glue at the interface. The aluminium honeycomb has been modelled by using an anisotropic model implemented in LS-Dyna as *MAT_26. In order to model the plates we have used the Hopperstads's viscoplastic model [17] [18] [19] implemented in LS-Dyna as *MAT_103. The material used for the core is the aluminium Honeycomb with a density equal to 3.0 pcf, with the cell dimension of 3/8"-and wall thickness of 0.002". The aluminium honeycomb is made by 5052 series. Considering the optimization of the available spaces, the model has two side blocks which allow following the cab's contour geometry, by using the maximum available space in the cab front.

The simulated boundary conditions are all degree of freedom constrained on the rear side, in order to reproduce the rigid connection between the backplate and the pillars, and a rigid block of 50 t impacting at 25 m/s on the front face fig. 5.20.

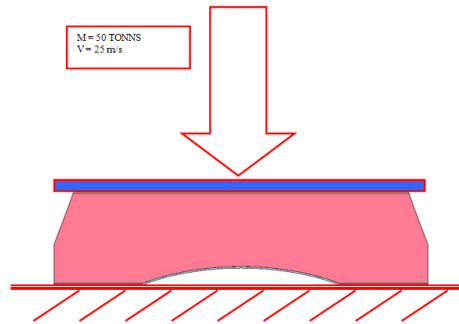


Fig. 5.20 – Boundary conditions referred to frontal impact simulation.

Fig.5.21 shows the end-of-impact configuration, where the introduction of the curved part in the backplate ensures a more uniform collapse in the central zone. Fig. 5.22 shows the load-displacement profile.



Fig. 5.21 – Absorber in the final configuration.

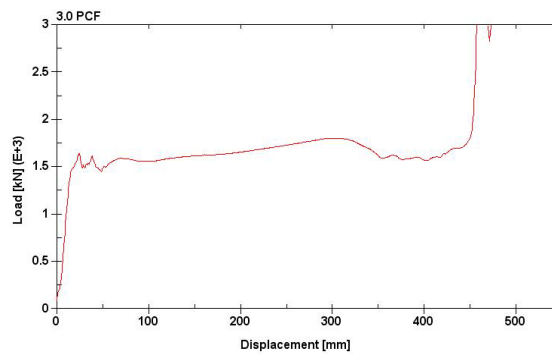


Fig. 5.22 – Load-displacement curve obtained from dynamic simulation.

Since side smoothing implies to be worked in a way such that it could cause the cells on the honeycomb block to be damaged, the geometry has been simplified using a single central block and other two blocks glued to the central one (fig. 5.23).

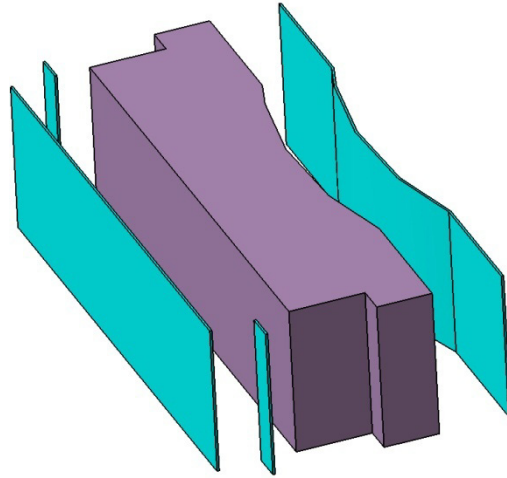


Fig. 5.23 – Absorber model with lateral blocks.

Fig. 5.24 shows the FEM model carried out for simulating the behaviour of this latter hypothesis, with the same contour conditions as the former. For simulating the gluing between the central block and the two side blocks we have used a tied-break contact, implemented in LS-Dyna, by introducing a shear failure stress value equal to the shear failure of the used honeycomb.

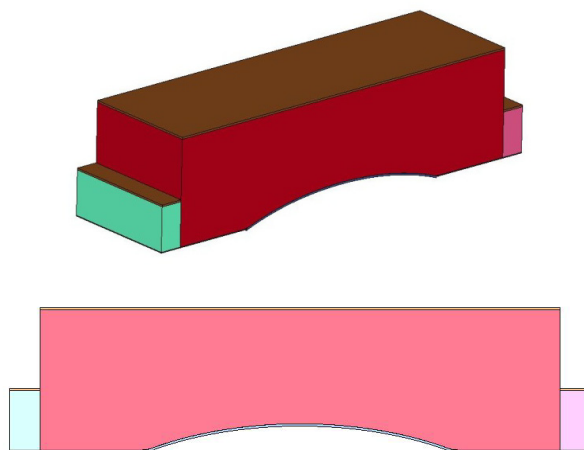


Fig. 5.24 – FE model of the upper absorber with lateral blocks implemented in Ls-Dyna.

Fig. 5.25 shows the deformed configuration, while fig. 5.26 indicates the comparison between the displacement load curve obtained from the simulation with the reference curve defined for this scenery.

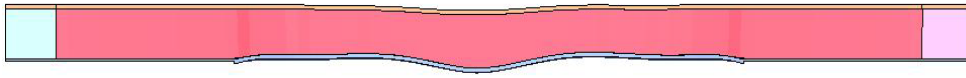


Fig. 5.25 – Final configuration assumed by the absorber.

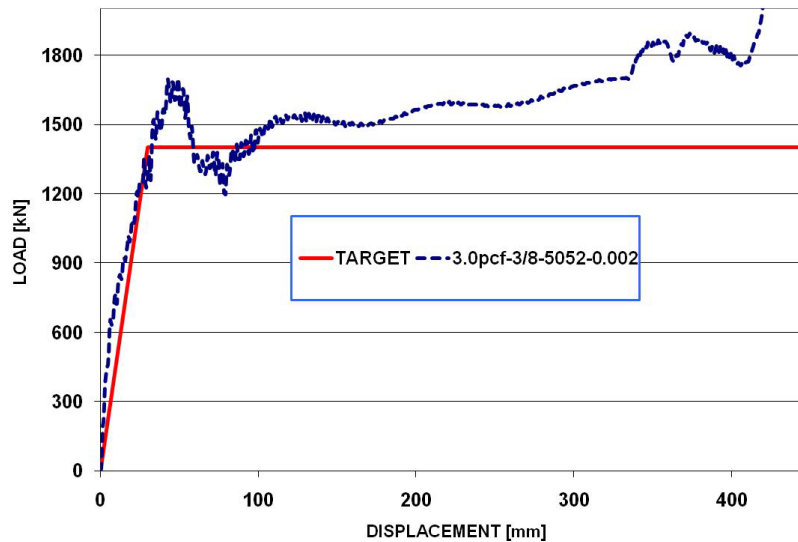


Fig. 5.26 – Comparison of load displacement curve obtained from simulation with target.

If we evaluate the feasibility of the previous solution, a problem arises for carrying out a $2150 \times 675 \times 580 \text{ mm}^3$ honeycomb block. Since a block with these dimensions is not commercially available, to make this material available we have decided to split the block into two parts, by interposing an aluminium plate in order to prevent the two block cells from penetrating into each other. Furthermore, since the two side blocks are hard to be connected to the main block, carrying out the layers allows incorporating these two blocks in the central one. Fig. 5.27 shows an isometric view of the CAD model and fig. 5.28 shows the FE model implemented in LS-Dyna for simulating the impact against a rigid 50 t obstacle.

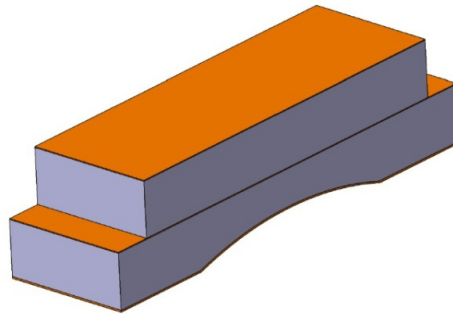


Fig. 5.27 – Absorber model with two stages.

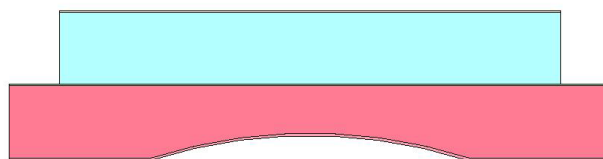


Fig. 5.28 – FE model of the two stages absorber.

To make the system carrying out easy and economical, for the dimension in L-direction we have used the value of 290 mm commercially available. The honeycomb density to be used was determined by comparing the values of the obtained force depending on the displacement, for the different honeycomb densities of the 5052series (fig. 5.29).

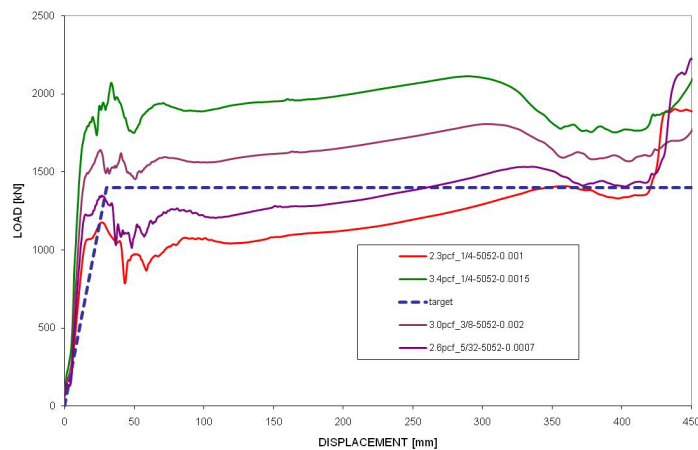


Fig. 5.29 – Load displacement curve referred to different aluminium honeycomb densities.



The density providing a force advancement that is nearer the reference one is 3.0 pcf. For this reason, we have used this density as final value. Fig. 5.30 shows the system configuration in the fully compressed condition.

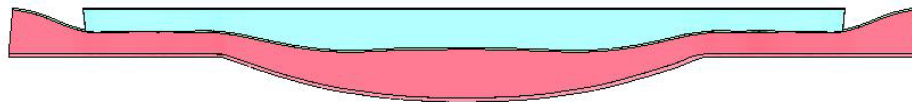


Fig. 5.30 – Final configuration of the absorber from simulation.

Due to restraint conditions, in the final compression phase the backplate is subject to very high stresses in the central area, particularly in the area connecting the bend and the flat parts (fig. 5.31).

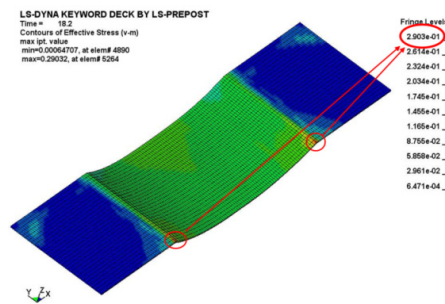


Fig. 5.31 – Von Mises equivalent stress pattern in the rear aluminium plate.

To avoid that these high stress levels could cause the plate to brake and make the system ineffective, the aluminium plate has been replaced with a 5mm-thick mild steel plate.

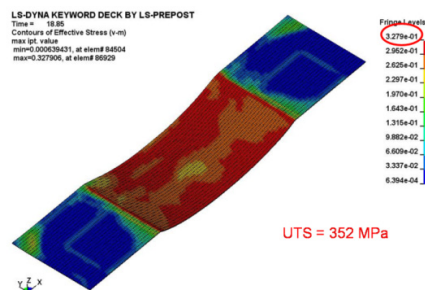


Fig. 5.32 – von Mises equivalent stress pattern in the rear mild steel plate.

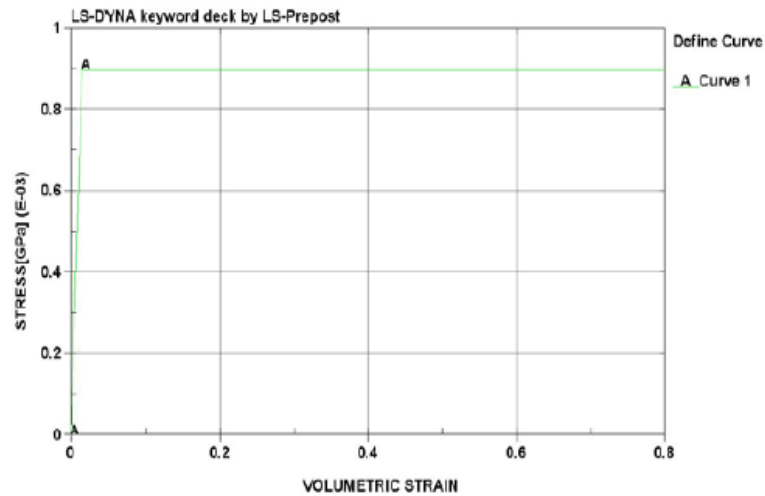


The modification resulted in a more uniform stress distribution (fig. 5.32), but its maximum value is very close to the break load. Furthermore, the total force in correspondence of the restraint area on the backplate is very far from those which have been set as reference. To overcome these difficulties, honeycomb blocks have been used with density different from that optimized in the previous phase.

The tab.5.3 summarizes the properties of the different components in the final configuration.

Tab. 5.3 – Material properties used for the simulation

	Density[kg/mm ³]	E[GPa]	ν	Y[GPa]	V _F	EAAU
ALUMINIUM SERIES 6106-T6	2.7e-6	70	0.33	0.210		
HONEYCOMB CFR-3/4-ACG-.003-1.8	2.88e-8	70	0.33	0.124	0.2	0.165
MILD STEEL	7.85e-6	206	0.27	0.275		



The charts in fig. 5.33 ÷ 5.34 show the load-displacement curve and the absorbed energy from the last configuration.

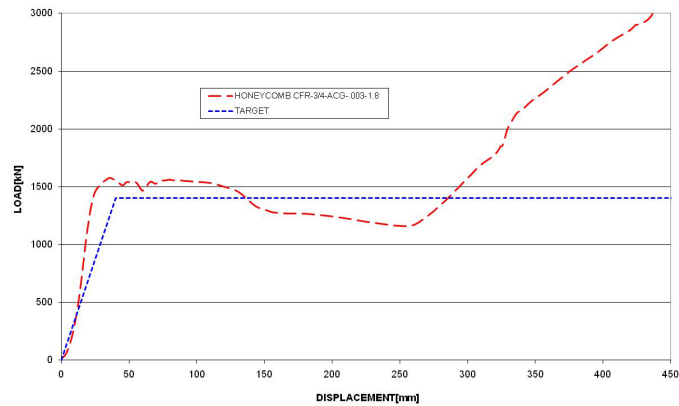


Fig. 5.33 – Load displacement curve obtained from numerical simulation.

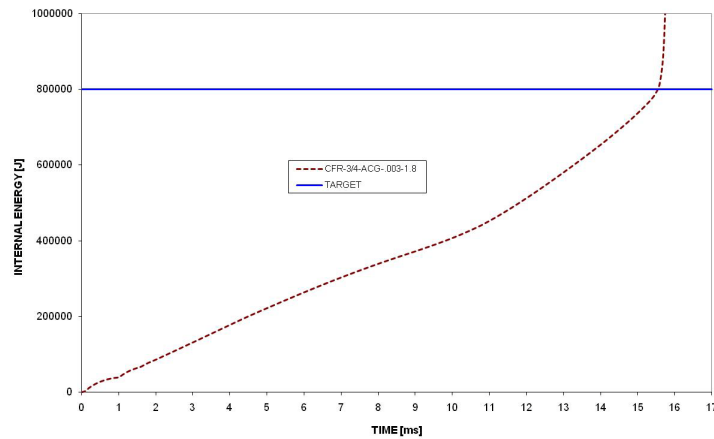


Fig. 5.34 – Internal Energy absorbed during the simulated impact.

The obtained results show that the choices being made, in terms of materials and geometries, allow designing a component with the same features as the existing solution, but with a mass that is 40% smaller. Since the new solution also covers the central area of the cab front, the new component performances are even better than the initial reference component, in terms of specific energy absorbed per unit volume.



CHAPTER VI

CAB MODELLING

6.1. Composite cab

In the last three decades the mass of rail vehicles has increased by 40% due to different factors, such as: - enhanced performances; - introduction of new passive security systems; - enhanced accessibility; - as well as enhanced comfort. The whole has caused an increased energy consumption, increased production and maintenance costs, a reduced transportable payload and reduced passenger safety. These matters induce the manufacturing firms to develop new solutions which allow reducing vehicles mass, preserving current vehicles performance level.

The best way seems to be the use of composite materials, which allow carrying out even very complex forms, with a remarkable gain, in terms of weight and numerosness of the component parts, compared to the related metal structures if performances are equal.

A feasibility study for this solution has been the main activity for the Author of this PhD thesis during his stay at the University of Newcastle's Newrail group, where he took part to the DE-LIGHT project activities developed in partnership with other European Partners.

The basic model examined to create the composite structure, provided by BOMBARDIER, is the cab used for the IDF, a regional train currently operational in France (fig. 6.1).



Fig. 6.1 – External view of the IDF cab.

The main structure and the absorption systems are completely made by metal, thus causing a remarkable burden to the total mass of the vehicle. The study conducted on this structure had two main purposes. The first purpose was to evaluate the possibility to completely replace the metal parts with composite parts. The second purpose was to evaluate the possibility to apply a modular concept in carrying out the cab structure.

For the applicability of the composite materials to the main structure, the operating conditions of the cab have been examined, in order to understand which were the conditions concerning the different components. This analysis has been based on searching materials with the best properties, among which the capacity of absorbing a high specific energy, for that specific application.

The modular approach philosophy is based on the possibility to carry out the cab in independent modules. In the specific case of the examined cab, the ideal splitting of the structure for detecting the different modules is suitable to the need of carrying out three absorption areas. The benefits from this solution concern different aspects of the problem, from production to maintenance. In fact, the production times are reduced due to the possibility to work on different parts at the same time, while, as for maintenance, in the event of damage due to differentiated impact of the three areas, there is the possibility to simply replace the damaged module and leave the remaining parts of the structure unchanged.



To make any modular solution promptly and generally applicable, the new cab has been developed starting from the existing one, by assuming, as modelling constraints, some specific points, such as: the external surface, which derives from previous aerodynamic studies, the position of the absorbers and the floor surface, as well as the connection points of the cab to the carbody. Other details have to be added, such as the position of the door and the lights.

Inside the space and the constraints as defined, different optimized solutions have been studied related to four basic components: lower absorption system, upper absorption system, cab framework and external surface.

As for the main structure, in the examined solution it is made up of a welded plate set constituting boxed elements, in order to ensure that the loads are transferred from the front area to the carbody (fig. 6.2). Inside this framework four elements can be found: the two boxed which define the cab's safety area and on which the upper absorbers are installed, and the two structures supporting the lower absorbers.

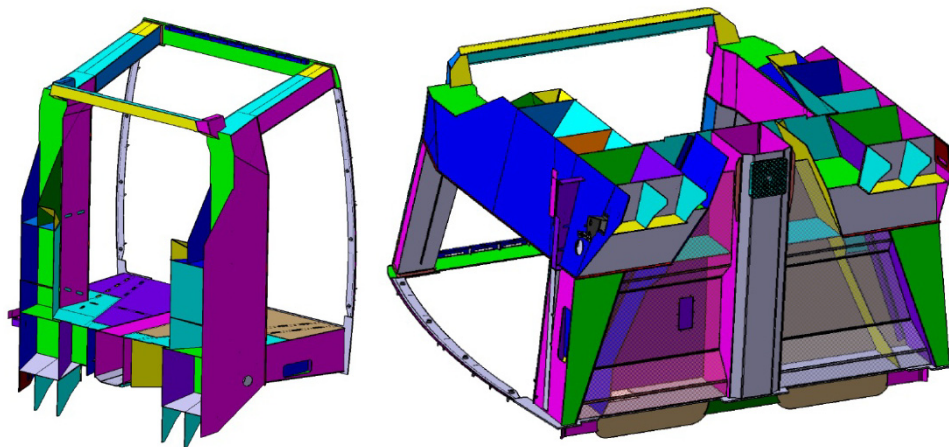


Fig. 6.2 – Proper cab main structure.

The first modelling phase concerns the individuation of the main structure critical areas, which are identified in the four above mentioned elements. Starting from the contour surfaces defined from these areas, the volumes have been found which will be subsequently filled up, in order to optimize their shape, as we will see later.

Because the coupler's central supporting beams are the supporting elements of this whole new structure, they have been not modified.

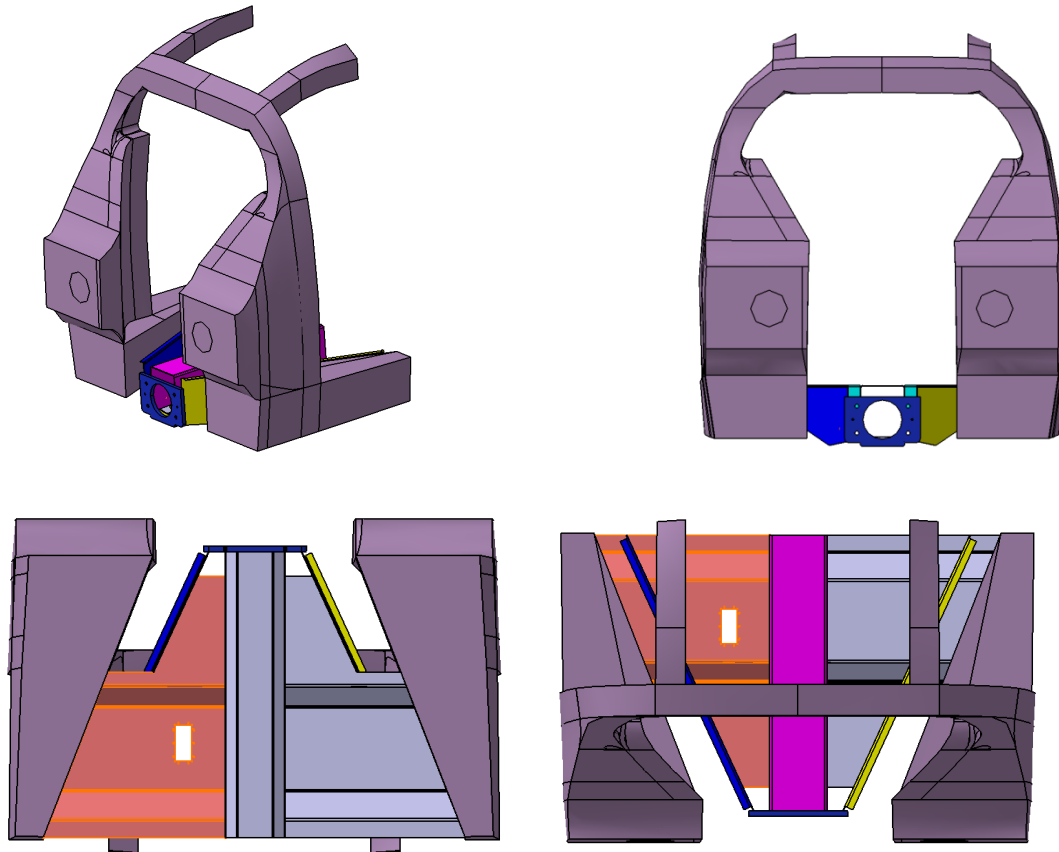


Fig. 6.3 – Location of the critical volumes.

In this structure three basic elements can be highlighted (fig. 6.3): 1) in the lower part we find the reactors, so called because they have to react to the axial load acting on the lower absorbers; 2) then, there is the upper structure, where the load, introduced in a different way through the front part elements, flows to the carbody; 3) and then the pillar, which is the closing element of the structure and to which the upper absorber is bound.

To this inner structure the external surface is added, which is part of the structure itself (differently from the previous solution, where it only works as a cab closure), thus actively participating to the absorption of the impact energy. For this purpose, the inner part is integrated to the external part, thus making a unique element.

The second phase concerns the study of the possible solutions to be adopted for carrying out the parts defined in the previous phase.

As for the so called reactor, it was decided to use polyurethane foam blocks wrapped in glass epoxy and joined to form a unique element, like that showed in fig. 6.4.

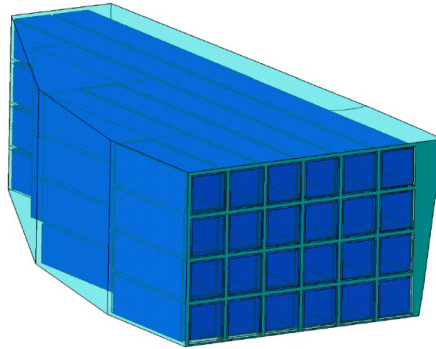


Fig. 6.4 – Reactor model.

Due to problems depending on the manufacture of such a system, we have examined an analogous solution which, however, should use GRP tubes filled with polyurethane foam and glued in order to form a single structure. The used tubular elements have a different length and are showed in fig. 6.5.

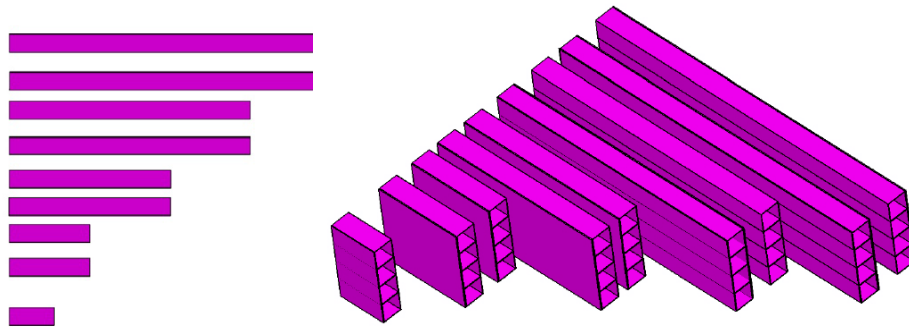


Fig. 6.5 – Detail of the reactor tubes.

To remove any sharp edges, the cavities due to length variations are filled with prismatic foam elements and covered with glass-fibre composite, in order to make the reduction of section gradual (fig. 6.6 ÷ 6.7).

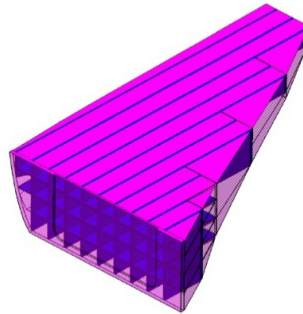


Fig. 6.6 – Section of the reactor.

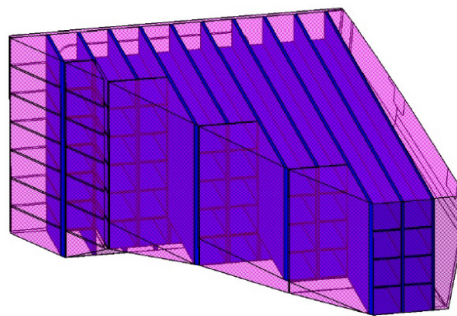


Fig. 6.7 – Tube detail.

For connecting the lower absorber to the reactor, the glass epoxy layer in the front part (fig. 6.8) is modelled in order to house the absorber backplate, while the joint is carried out with an appropriately thick glue layer. The pocket also works to reduce the cutting stresses in the glue due to the vertical component of the impact force, which can reach high levels.

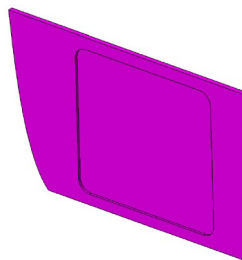


Fig. 6.8 – Front plate of the reactor.

The pillar structure consists of a series of polyurethane foam blocks alternated to glass epoxy layers, which give them an appropriate stiffness. Fig. 6.9 shows the optimized cad model of this structure. The inner delimitation surface has been found starting from the original model, in order to leave the free space inside the cab

unchanged. The first hypothesis showed a chipping less geometry with very mild gradations from the front to the rear area. Due to problems depending on carrying out such complex forms, we have chosen to use geometrically simpler models regardless of design, but with obvious benefits in terms of carrying out the prototype and of large-scale productions.

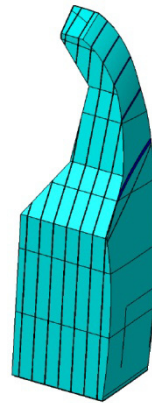


Fig. 6.9 – CAD model of the pillar, in view the foam volumes and the fiber layers

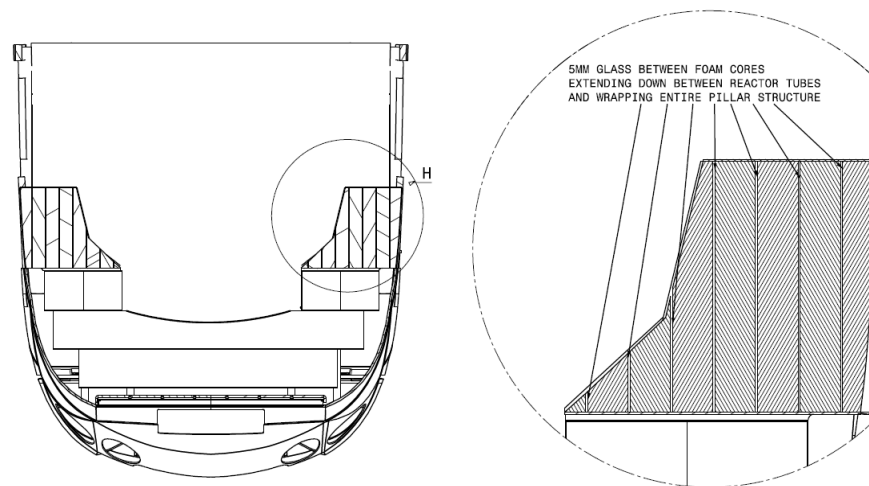


Fig. 6.10 – Horizontal section of the cab, with detail of the pillar

Blocks dimension has been chosen in line with the dimensions available on the market for the foam. Each layer thickness is 100 mm alternated to a 5 mm glass epoxy layer. The whole structural component, adhering to the cab's external structure (fig. 6.10.), fits its form in the contact area. To ensure a continuity between the pillar



and the reactor, the FRP layers are carried out seamless from an element to the other (fig. 6.11.).

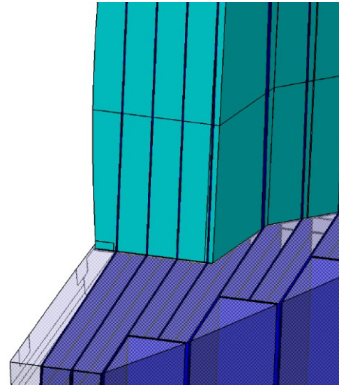


Fig. 6.11 – Detail of the connection area between pillar and reactor.

Furthermore, to ensure the load is transferred to the car in order to avoid that the pillar works like a cantilever embedded to the basis, we have introduced a supporting element in the upper part, whose shape is the same as the external surface and such as it can allow the transfer of the load in correspondence of the two upper connection points of the cab to the front plane of the carbody (fig. 6.12.).

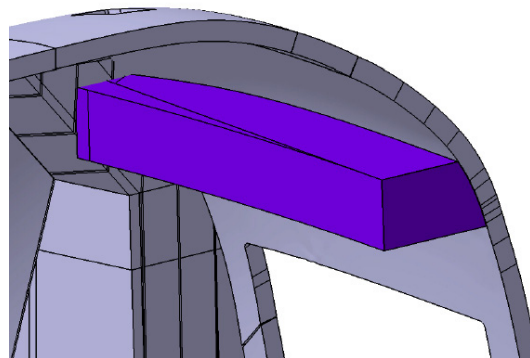


Fig. 6.12 – Beam element to transfer the load from the pillar to the carbody.

The planning choice to carry out the cab's absorption areas in independent modules has caused the pillar's front surface and the reactor's front surface to coincide, so that the absorption area, delimited by the absorber connection surface on the structure, could coincide with the ideal cutting plane between the second and the third module. This solution requested the introduction of a further interconnecting element, in order

to avoid that the upper absorber could interfere with the minimum space which had to be protected inside the cab, in the front part (fig. 6.13).

On the pillar's front surface a steel plate is glued, on which a box is fastened that is made of 4 balsa blocks (fig. 6.14), each one of them covered with a glass epoxy layer and kept together with a glue, and closed in a glass epoxy envelope. The upper absorber's backplate is glued to the aforementioned box.

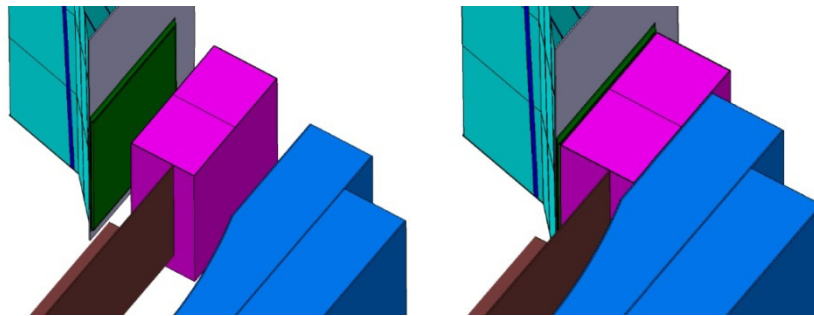


Fig. 6.13 – Assembly and exploded view of the connection area between upper absorber and pillar.

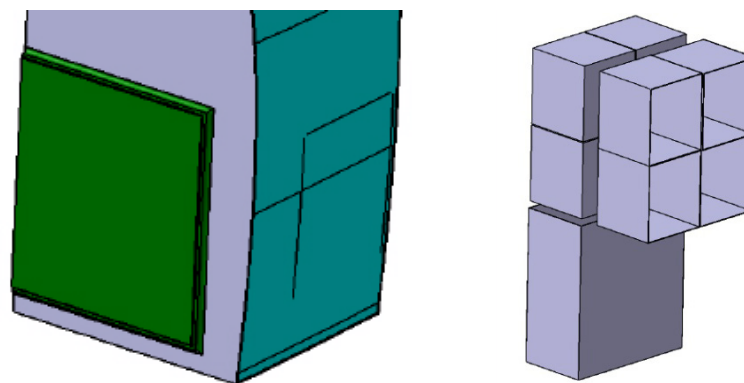


Fig. 6.14 – Front plate of the pillar and exploded view of the balsa box.

As for the external shell, we have used a sandwich consisting of a polyurethane foam core between two glass epoxy layers, as we already did for the pillar and the reactor. The thickness of the single layers is the result of an optimization process numerically conducted.

The modular division of the cabin also allowed finding three areas for the shell, with different resistance features (fig. 6.15). These three areas are: 1) nose, 2) secondary model, 3) tertiary model.

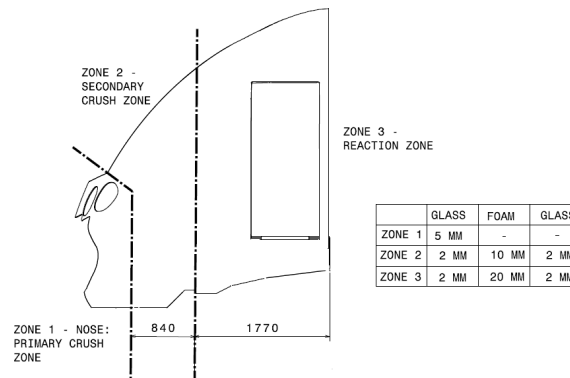


Fig. 6.15 – Section of the external shell.

As for the nose (fig. 6.16), this element is not assigned to absorb the energy and, in the event of an impact, has to be broken in order to release the absorbers and allow the engagement of the anticlimbers between the two impacting trains. For this reason, it has been assumed to consist of a 5 mm glass epoxy layer.

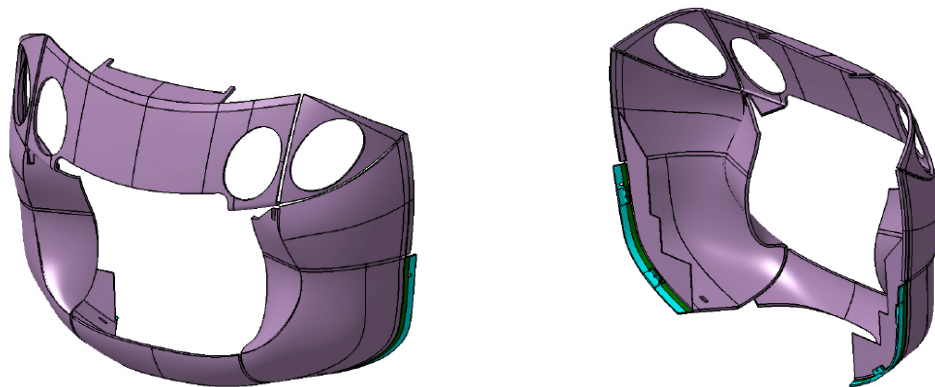


Fig. 6.16 – Front and rear view of the nose.

Furthermore, to reduce the free length of the absorber without compromising its performances, we have introduced an “ad hoc” shaped plate in the nose inner part (fig. 6.17), in order to support the absorber itself. For bolting this module to the secondary, perforated inserts have been enclosed in the inner edge of the component.

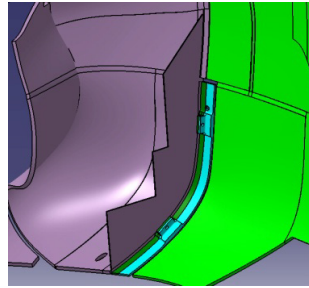


Fig. 6.17 – Detail of the connection plate of the lower absorber.

The secondary module (fig. 6.18) is carried out with a 14 mm thick sandwich made up of a 10 mm core and a 2 millimetre glass epoxy layer on each of the two faces (fig. 6.19).

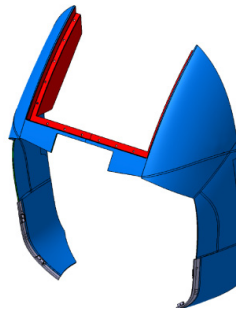


Fig. 6.18 – Assembly of the secondary module.

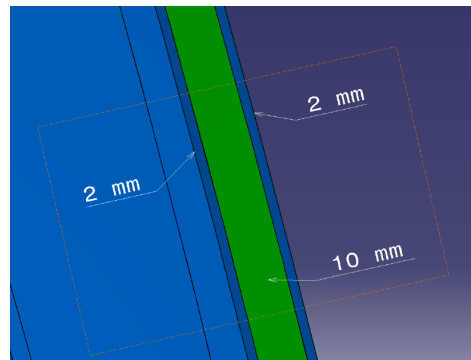


Fig. 6.19 – Detail of the external shell structure

Since this modules incorporates a part of the windscreen, there are strong-bending areas for which only one 5 mm glass epoxy layer has been used (fig. 6.20).

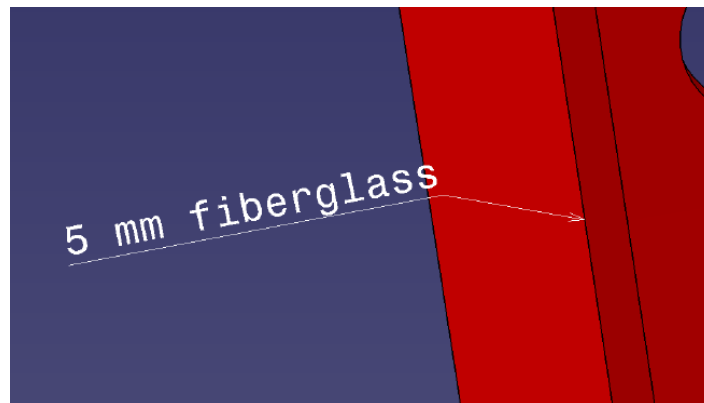


Fig. 6.20 – Detail of the area behind the windscreen.

The tertiary module is the driver's safety area and must resist to the impact without permanent plastic deformations. To design this module we have followed the same criteria as the secondary, assigning, however, a greater thickness to the different layers. The core thickness is 40 mm, while the external skins are 5 mm thick each, for a total thickness of 50 mm. Since a part of the windscreen, the lights and the door, is incorporated in the module, also in this case we have used a single 5mm fibreglass layer, in order to carry out the strong-bending areas (fig. 6.21).

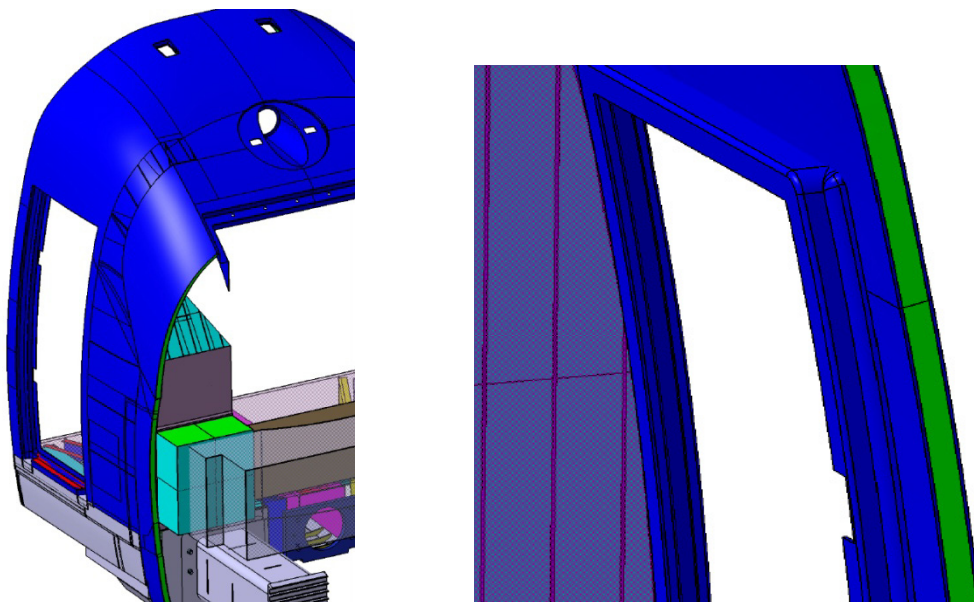


Fig. 6.21 – Assembly view of the CAD model and detail of the area behind the access door.

6.2. Performance requirements of the structure.

The complete structure obtained from the described optimization process must ensure the needed strength in order to support the static loads and the dynamic conditions provided in the standards. The verification for the dynamic conditions has been conducted by analysing the single absorption elements of the crash energy evaluating the absorbed energy and the obtained force levels. The check for the quality of the chosen solution in terms of stress and deformation has been only evaluated in static conditions using numerical simulations. With regard to EN12663, we have particularly evaluated the structural responses under the action of longitudinal and vertical loads.

As for the longitudinal loads, the loading conditions considered to be relevant for a PII-class vehicle are the four showed in fig 6.22.

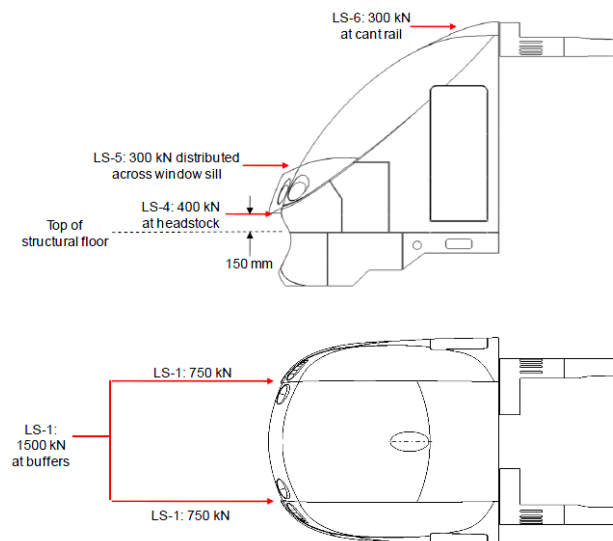


Fig. 6.22 – Schematic representation of the horizontal static load from EN12663.

Note that even if the reference standards [3] and [4] do define the verification of the structural response under vertical static loads, they do not prescribe any specific condition to verify the proper functioning of the anti-climb devices under the same loads. The “Railway Group Standard for the structural requirements of railway vehicles” (GM/RT2100 [24]) British standards provides the application of a 100 kN



load (fig. 6.23) in a vertical direction and in both ways, combined with a 1000 kN compression longitudinal load [25].

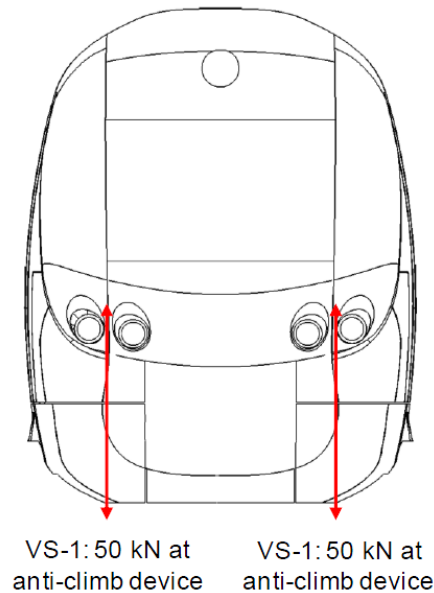


Fig. 6.23 – Schematic representation of the vertical static load.

The application of the above mentioned static loads should not cause stress levels in the tertiary module, such that they can generate permanent plastic deformations. As for the check of this condition, since the examined structure is completely made by composite materials, the EN 12663 is not enforceable because it only refers to metallic materials. For the specific application we have compared the maximum main stress obtained in the single components with the typical material ultimate stress divided by an appropriate safety coefficient.

6.3. FE Modelling

To create the finite elements model of the cab, we have used the HyperMesh code. The created model consists of 17713 shell elements, with Belytschko-Tsay formulation and 5 integration points through the thickness, as well as 350661 solid elements. The shell elements constitute the external envelope and the external tube of the lower absorber, while the solids the remaining part. Using the symmetry of the boundary conditions, we have modelled only half structure (fig. 6.24),. Furthermore,



since only the third module had been statically verified according to EN12663 regulations, the second module and the nose, concerning the only impact phase, have been omitted.

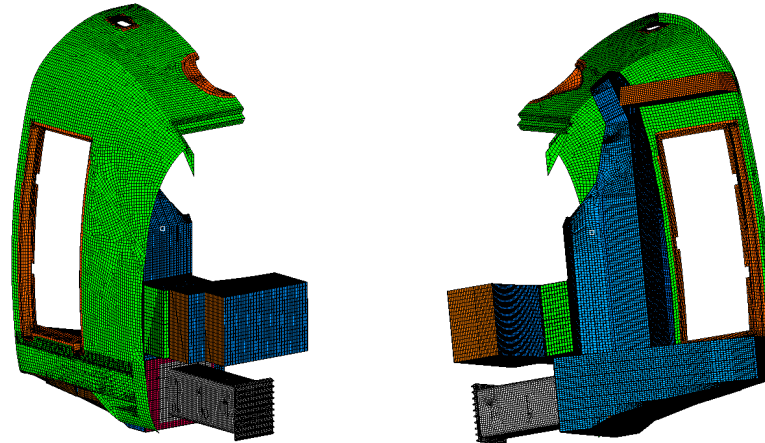


Fig. 6.24 – Front and rear view of the cab modelled in HyperMesh.

The external shell has been divided into two regions which are indicated in green and brown in fig. 6.25, and which are the areas carried out with the 50 mm sandwich and with a single 5 mm fiberglass layer.



Fig. 6.25 – Mesh detail of the external skin.

The discretization of this part with solid elements would have requested a remarkable calculation; therefore, we have preferred to use the shell elements. To assign the material properties to shell elements, in case of multi-layer composites, it is possible to follow different ways depending on the approach and the used calculation codes. As for the case examined in this thesis, since the numerical simulations have been conducted using the implicit LS-DYNA solver, there were only two ways to be



covered [26]. One way is the one using *Integration Shell, which allows defining the number of integration points through the thickness and assigning a different material and a different thickness to each point. Which makes the composite modelling possible, by assigning different orthotropic properties to the different thicknesses and in different directions from one layer to the other. The other way is to establish the equivalent constitutive properties of the composite being assigned to an element with a thickness equal to the total sandwich thickness. The last possibility has been chosen.

The equivalent properties of the material have been established by a software, developed at the Newcastle University, starting from the geometry and the properties of the materials of the layers constituting the shell.

As for the reactor and the pillar, the single layers have been modelled in detail, by assigning the concerning properties to each one of them.

The connection between shell elements and solid elements constituting the pillar and the reactor (fig. 6.26) has been carried out through constraint equations, by linking the translational degree of freedom of node pairs belonging to adjacent shell and solid elements.

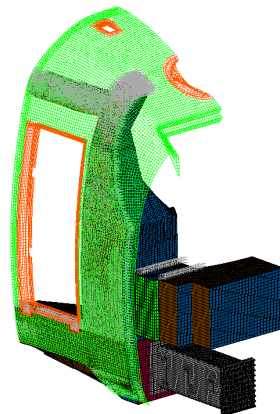


Fig. 6.26 – Detail of the constrained used to realize the connection of the external skin with the pillars and reactors.

As for the lower absorber, the external box and the backplate have been discretized with shell elements, while the honeycomb blocks, the interface plates between the



blocks and the anti-climb device have been discretized with solid elements. For modelling the interface contact between the pillar of aluminium honeycomb blocks and the external plates, we have used a *SURFACE-TO-SURFACE contact algorithm. The honeycomb has been discretized with an orthotropic model, by using the optimized parameters with the compression tests carried out on the honeycomb samples and showed in the chapter on the upper absorber.

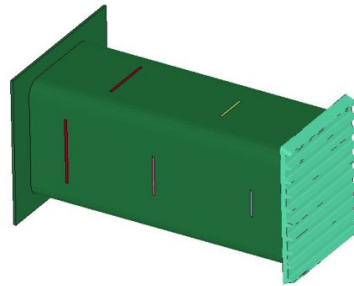


Fig. 6.27 – FE model of the lower absorber.

The connection between the backplate and the reactor (fig. 6.27) has been carried out by merging the interface nodes. To make the mesh more regular, some details related to connecting elements have been omitted and both the shape of the absorber plate and the related seat have been simplified (fig. 6.28).

For the aluminium external envelope we have used the viscoplastic model, while for the honeycomb we have used an anisotropic model.

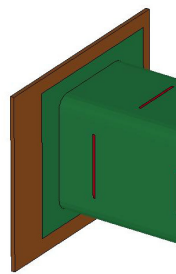


Fig. 6.28 – Detail of the connection between lower absorber and reactor.

As for the upper absorber, in the dynamic simulations, to evaluate the behaviour at the interfaces between the honeycomb blocks and the external plates, we have used a contact algorithm which took into account the stresses acting on the contact surfaces,

in order to introduce effects linked to decohesion. In this phase, the model has been carried out by merging nodes to interfaces, and these effects have been neglected since they were totally marginal. Furthermore, the mesh of the honeycomb blocks has been carried out by refining the element through the thickness in order to completely appreciate the stress gradient in this direction (fig. 6.29). The used constitutive models are the same described for the lower absorber.

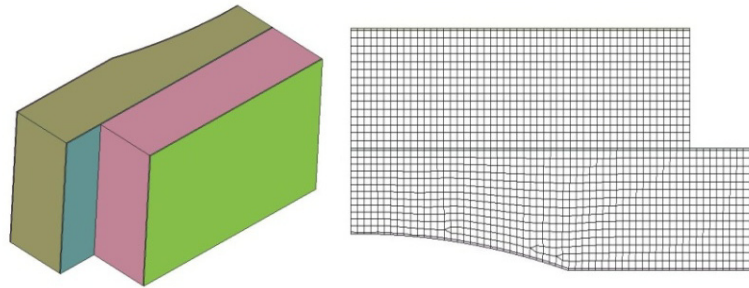


Fig. 6.29 – Detail of the mesh of the upper absorber.

As for the box carried out in balsa and fibreglass composite, the discretization has been conducted by using solid elements and merging the nodes of the surfaces contacting the parts which constitute the box (fig. 6.30). For the balsa wood, we have assumed an isotropic behaviour, while for the fibreglass composite parts the material has been modelled as orthotropic, by appropriately orientating the orthotropic axes of the material, mainly according to the fibre orientation.

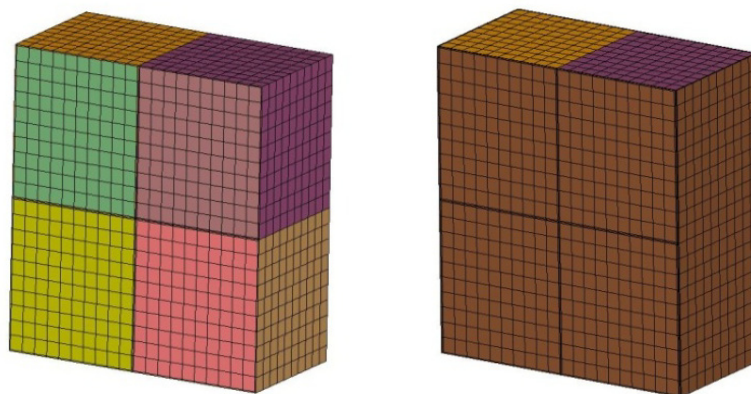


Fig. 6.30 – Detail of the mesh of the balsa box.



6.4. Calibration of Material Parameters

For calibrating the parameters of the material to be used in the numerical simulations and verifying the quality of the adopted solutions, compression tests have been conducted on representative elements and simulations at the finished elements with the ANSYS code.

As for the experimentation phase carried out at the Newcastle University labs, compression tests have been conducted using two different test machines: the Avery-Denison compression loading machine (5000 kN) and the DARTEC Universal Test Machine (± 100 kN) (fig. 6.31).



Fig. 6.31 – (a) Avery-Denison compression loading machine, (b) DARTEC Universal Test Machine.

The pictures below (fig. 6.32) show the tested items.



Fig. 6.32 – (a) GRP tubes, (b) Specimens made by polyurethane foam and glass epoxy.



Based on an evaluation of the forces transmitted by the lower absorber system to the reactor, we have evaluated that using a foam block with a section of $100 \times 100 \text{ mm}^2$, the force transmitted to each tube is 50 kN. Therefore, joining four blocks in a single element, this has to support a minimum load of 200 kN without collapsing. Furthermore, almost the whole compression load flows through the external covering of each block, since the foam stiffness is much lower. Moreover, to verify the validity of the solution with GRP tubes, compression tests have been performed on the single tube.

Tab. 6.1 summarizes the values registered during the compression tests on the blocks made by polyurethane foam and glass-epoxy.

Tab. 6.1 Compression test results of specimens (b)

	Mass	Density¹	Load rate (to 200kN)	Load rate (to failure)	Failure load
TR/DEL/1067-	(kg)	-	(kN/min)	(kN/min)	(kN)
01	3.7	266.8	40	1000	592
02	3.6	259.6	120	1000	488
03	3.7	266.8	240	1000	546

The average value for the maximum load obtained by the tests is 542 kN, against a requested minimum value of 200 kN. The following picture shows the collapse ways (fig. 6.33).

¹ Density calculated for entire test specimen, not for individual glass fibre or foam parts.



Fig. 6.33 – Detail of the failure occurred during compression tests on the FRP and polyurethane foam specimens.

All the tested specimens show an initial collapse on the tube gluing surface, but the structure final collapse is due to the external part collapsing.

As for the compression tests on the GRP tubes, the values of the registered maximum load are summarized in tab 6.2

Tab. 6.2 Test compression results on GRP tubes

	Mass	Density²	Load rate (to 100kN)	Load rate (to failure)	Failure load
TR/DEL/1067-	(kg)	-	(mm/sec)	(kN/min)	(kN)
04	0.530	1725.3	0.05	1000	165.0
05	0.531	1728.5	0.05	1000	164.8
06	0.530	1725.3	0.05	1000	157.1
07	0.542	1764.3	0.05	1000	161.6

The maximum average load is 162.5 kN, against a requested minimum value of 50 kN.

Fig. 6.34 shows the way the two tested items collapse

² Density calculated for GRP tubes only.

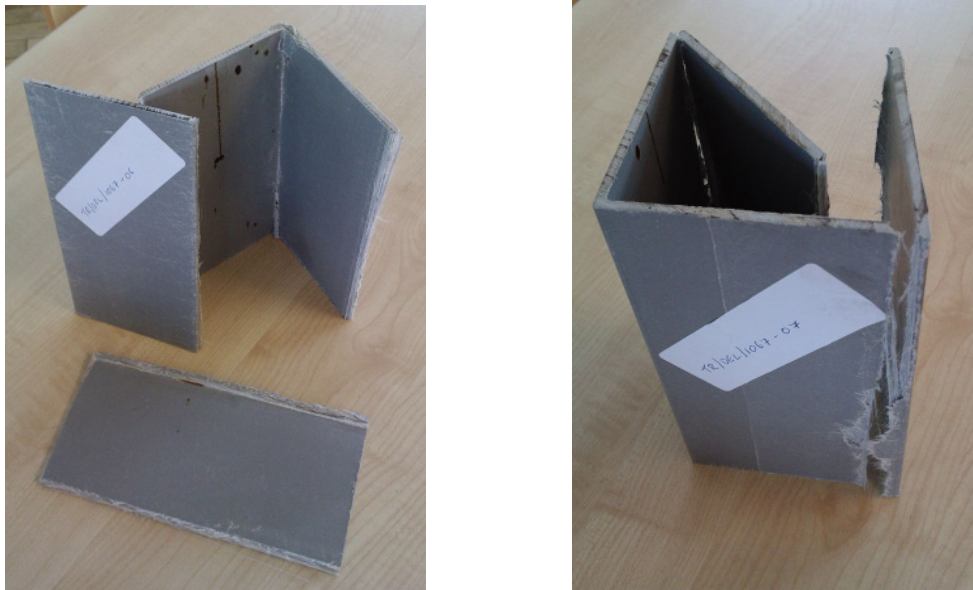


Fig. 6.34 – Detail of the failure mode on the GRP tubes.

For the component made up of foam blocks wrapped glass epoxy and for the GRP tube with a rectangular section, numerical simulations have been conducted in order to calibrate the material parameters to use for the next modelling of the whole cab. fig. 6.35 shows the models for the finished elements implemented in ANSYS.

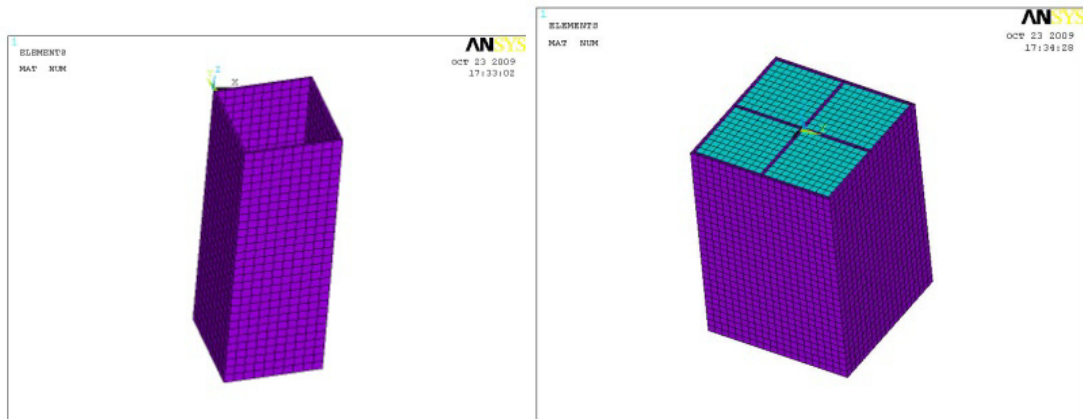


Fig. 6.35 – (a) FE model of the GRP tube, (b) FE model of the FRP and polyurethane foam specimens.

6.5. Results of the Static Analysis

With regard to fig. 6.36, the load conditions have been reproduced with the LS-Dyna code, by using the implicit algorithm.

For the simulation of the half-cab coupling on the head plane, we have restrained the nodes of the external surface rear edge, the nodes of the reactor rear surface and the nodes of the upper linking girder rear surface.

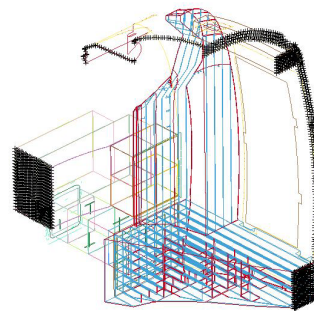


Fig. 6.36 – Boundary conditions for the simulations on the cab.

For applying the compression load LS1 at the buffer level (equal to 750 kN), we have created a node positioned on the box axis of the lower absorber and have stiffly linked it to the anti-climb device using a *Constrained Extra Nodes Node, in order to apply a load concentrated on the node and distribute it through the anti-climb device (fig. 6.37). The same procedure has been used for VS1.1 e VS1.2 load conditions.

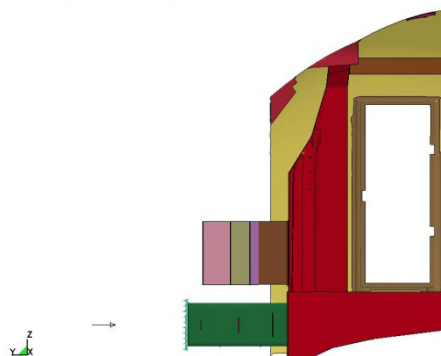


Fig. 6.37 – Compressive load applied on the buffer level on a single node rigid constrained to the anticlimber – LS1.

For the LS_4 and LS_5 conditions (fig. 6.38), the load has been applied as a pressure on the front plate of the upper absorber, on an element band, so that the resulting force could equal the related load.

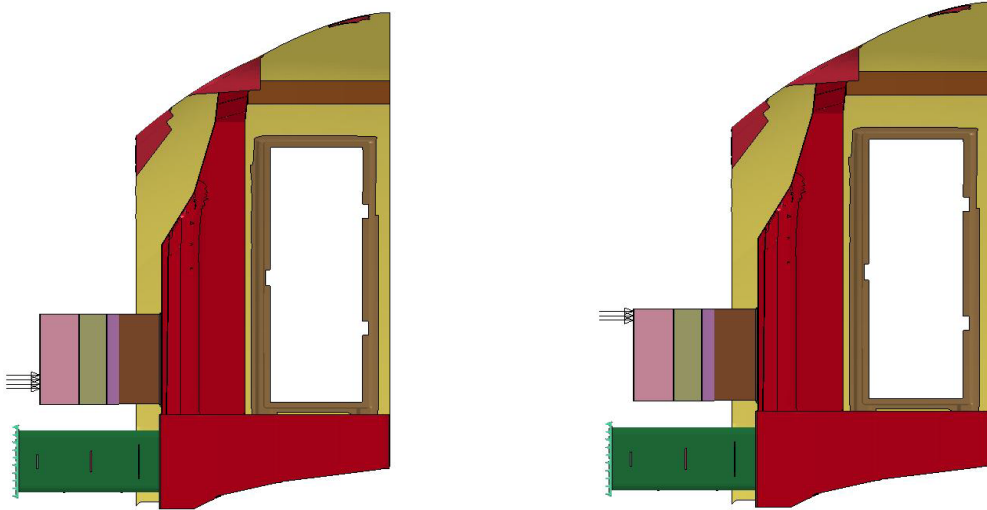


Fig. 6.38 – Pressure applied on the Upper Absorber corresponding to the LS4 and LS5.

For the LS_6 load condition (fig. 6.39), the total force has been uniformly distributed on more nodes.



Fig. 6.39 – Nodal Load applied at the level of the cant rail.



Regarding vertical load VS_1 and VS_2, fig 6.40 shows the concentrated loads applied on the lower absorber by the node constrained to the anticlimber.



Fig. 6.40 – Vertical load applied on the buffer level on a single node rigid constrained to the anticlimber – VS_1 (a) and VS_2 (b).

The conducted analyses have showed that the critical areas, as already expected in the preliminary study phase, are the hitch region between the pillar and the reactor, as well as the areas close to the access door, particularly for the LS_1 load condition and for the VS1.1 and VS1.2 load conditions.



The fig. 6.41 shows a map of the main stresses for the LS_1 condition related to the connecting area between pillar and reactor.

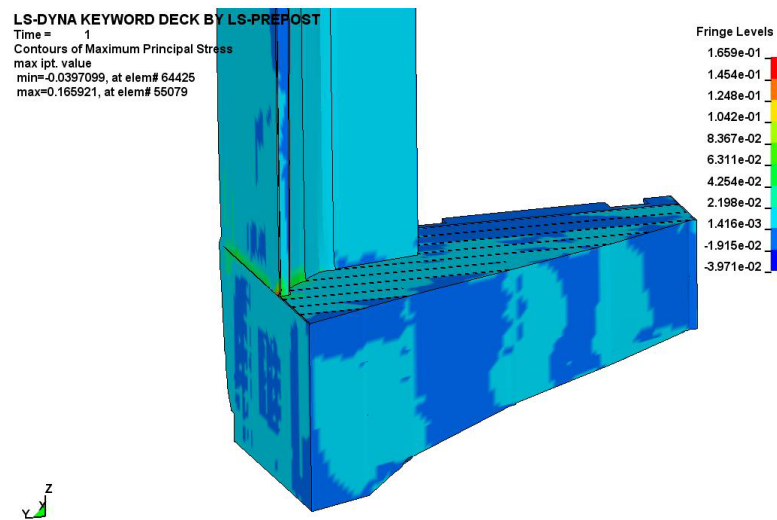


Fig. 6.41 –Maximum Principal Stress corresponding to LS_1 in the connection area between reactor and pillar.

By examining the stress contour plot and the levels reached by the main stresses in the single components, a positive judgement can be drawn about the project choices developed, both for the geometries and the found materials, since both of them can ensure a sufficient safety degree and a uniform stress distribution in the whole structure.



CONCLUSIONS

The subject of this thesis was the study of the applicability of composite materials to design to crash a train cab. The preliminary phase of work has involved the study of issues related to railway accidents and safety requirements for passengers imposed by Standards. It was noted that the breadth and diversity of accidents that may occur during operation, have led to the identification, by the legislator, of typical scenarios in respect of which it is necessary to ensure the required performance

The verification of compliance of a train passing through a testing phase which aims to verify that the design choices can assure, in case of an accident, a sufficient degree of security. Since, even if cut-down, the number of scenarios required a series of tests that would be very costly, the standards allow to support verification with virtual simulations, on condition to validate the numerical results by static and dynamic experimental tests on components of the 'whole structure.

The need to reproduce in simulations the behavior of individual components with a high degree of precision requires very thorough knowledge of the behavior of materials under both static and dynamic conditions. An important example is the design of energy absorption systems, whose mechanisms of failure require a thorough knowledge of the behavior of the materials used to be able to estimate with an error reduced the energy absorbed. This need has sensitized the scientific community towards deeper issues regarding the definition of constitutive material that describes the behavior at high strain rate.

The usual approach in the design of a cab provides identification of the initial geometry of the main structure on which is then fit the energy absorption systems. Since not all accidents involve the complete destruction of the cab, this approach would result in substantial costs during maintenance and repair, and in the manufacturing process. Moreover, since the absorption system should ensure a



relatively low deceleration levels for passengers, it is preferable that the cab is so arranged that the stiffness of the absorption components is increased gradually during the impact.

One of the solutions to the problems set out above can be represented by the modular approach. The cab is divided into several independent modules which can be prepared separately and then assembled. Also, to respond to the needs arising from the crash behavior of the structure, the detection of independent modules can help to satisfy the need to create separate sinks.

In carrying out this work has redesigned the structure of an existing cab, introducing the principles of the modular and simpler construction, seeking cost-effective solution to ensure, without compromising performance, reduced weight and a simplification in the number of components, in order to increase the payload and reduce manufacturing costs and maintenance. The objective of reducing the weights of individual components was achieved by adopting, for the various components, materials that are best suited to the particular performance.

To reduce the weight, it was considered appropriate to use composite materials, metallic and non, which are characterized by high specific energy absorption and, thanks to advanced development of manufacturing techniques, by a fit to carry out even complex geometries. For this purpose, different material characteristics were reviewed and applicability of each to a particular component was evaluated

The components on which it has operated, during the redesign, are the upper and lower absorption systems and the supporting structure.

For the lower absorption system, various solutions have been investigated using, as a benchmark for testing the goodness of the solution, the reaction force and energy absorbed profiles. This process led to the definition of a model composed of a honeycomb blocks inside an outer case made by aluminum. For the correct modeling of the behavior of the materials, in the preliminary stage, compression tests were conducted on mild steel tubes to characterize the behavior of them and to calibrate the needed parameters to define the constitutive model.



Regarding the Upper Absorption System the existing solution was replaced by a single element which, covering up the central area of the cab, allows to increase the level of safety for the driver and the energy dissipated by the system. Even in this case, to optimize the geometry and determine the material parameters an initial testing phase and a later phase of FE modeling with finite element codes have been carried out.

Regarding the main structure, the previous solution, which uses various steel plates welded to form a box, has been replaced by a very simple and compact structure made by FRP and polyurethane foam. The geometry of the outer surface, since it is the result of aerodynamic studies, has been left untouched but, unlike the previous solution, has been integrated into the structure in order to participate in the impact energy absorption.

The estimate of the goodness of the solutions obtained was carried out by numerical simulations, by characterizing the material behavior using different experimental tests. The next phase of the presented work will be the verification, by full-scale dynamic tests, of the designed structures, to verify the compliance between numerical and experimental results on the real components.



REFERENCES

- [1] J.J. HORST – “*Evacuation in case of an emergency*” TRAINSAFE ▪ Safe Vehicle Interiors ▪ April 2004 ▪ Belfry West Midlands UK
- [2] A SUTTON “*The development of Rail Vehicle Crashworthiness*” Proc Instn Mech Engrs Vol 216 Part F: J Rail and Rapid Transit, 2002.
- [3] EN12663 “*Structural Requirements of Railway Vehicle bodies*”.
- [4] EN15227 “*Railway Applications – Crashworthiness Requirements for Railway Vehicle Bodies*” September 2007.
- [5] ISTVÁN NÉMETH, KRISZTIÁN KOVÁCS, HANS GÜNTHER REIMERDES AND ISTVÁN ZOBORY, “*Crashworthiness study of Railway Vehicles Developing of Crash Elements*” 8th Mini Conf. on Vehicles System Dynamics, Identification and Anomalies, Budapest, Nov. 2002.
- [6] DAVID TYRELL, KRISTINE SEVERSON, A. BENJAMIN PERLMANN, BARRIE BRICKLE, CAROLINE VANLNGEN-DUNN, “*Rail Passenger Equipment Crashworthiness Testing Requirements and Implementation*” Int Mech Engineering Congress and Exposition, November 2000, Orlando, Florida.
- [7] ALASTAIR ERSKINE “*Structural crashworthiness literature search*” Rail Safety and Standard Board, REPORT NO. : ITLR-T12004-001 2003.
- [8] VILI PANOV “*Modeling of Behavior of Metals at High Strain Rates*” PhD Thesis, School of Engineering, Cranfield University, 2006.
- [9] HEXCEL COMPOSITES, HexWebTM Honeycomb Attributes and Properties, TSB 120, 1999.
- [10] JJ CARRUTHERS, JOHN H. PORTER, “*Determining the FEA Properties of Honeycomb for FMVSS201 Counter Measures for Headliners and Trim*” Auto Interiors Show, Detroit Michigan, 14-16 May 2002.
- [11] J. J. CARRUTHERS, “*Some Aspects of the Energy Absorption of Composite Materials*” Ph.D. Thesis, Department of Mechanical Engineering, University of Sheffield, September 1997.
- [12] ANDRE DA SILVA, STELIOS KYRIAKIDES – “*Compressive response and failure of balsa wood*”, Int. J of Solids and Structures 44 (2007) 8685–8717.
- [13] Coupling railway, Wikipedia, http://en.wikipedia.org/wiki/Coupling_%28railway%29.



- [14] V. TARIGOPULA, M. LANGSETH, O.S. HOPPERSTAD, A.H. CLAUSEN “*Axial crushing of thin-walled high-strength steel sections*” Int. J of Impact Engineering 32 (2006) 847–882.
- [15] ERIC MARKIEWICZ, PIERRE DUCROCQ and PASCAL DRAZETIC “*An Inverse Approach to Determine the Constitutive Model Parameters from Axial Crushing of Thin-Walled Square Tubes*” Int. J. Impact Engng Vol. 21, No. 6, pp. 433–449, 1998.
- [16] LSTC – LS-DYNA Keyword User's Manual Version 971, Livermore Software Technology Corporation, 2007.
- [17] HOPPERSTAD, OS, & REMSETH, S, *A return mapping algorithm for a class of cyclic plasticity models*, Int. J. for Numerical Methods in Eng., Vol. 38, pp. 549-564, 1995.
- [18] BERSTAD, T - *Material Modeling of Aluminium for Crashworthiness Analysis*, Dr. Ing. Dissertation, Norwegian University of Science and Technology, Trondheim, Norway, 1996.
- [19] BERSTAD, T, LANGSETH, M & HOPPERSTAD, OS - *Elastic-viscoplastic constitutive models in the explicit finite element code LS-DYNA3D*, Proc. of the Second International LS-DYNA3D Conference, San Francisco, 1994.
- [20] RONALD MAYVILLE, GABRIEL AMAR, J.W. LEE “*Development of a Multilevel Rail Car with Crash Energy Management for the U.S. Market*” Innovation in Passive Safety and Interior Design, 7th Int. Symposium on PASSIVE SAFETY, Berlin, 2008.
- [21] QINGWU CHENG, WILLIAM ALTENHOF, LI LI “*Experimental investigations on the crush behavior of AA6061-T6 aluminum square tubes with different types of through-hole discontinuities*” Thin-Walled Structures 44 (2006) 441–454.
- [22] S. SANTOSA, T. WIERZBICKI – “*Crash behavior of box columns filled with aluminum honeycomb of foam*”, Computers and Structures 68 (1998) 343-367.
- [23] C. O’NEILL, AND J. CARRUTHERS “*Design and analysis of a lightweight energy absorber to meet rail vehicle crashworthiness requirements*” MSE Postgraduate Conference, School of Mechanical and Systems Engineering Newcastle University.
- [24] RAILWAY GROUP STANDARD “*Requirements for Driving Cabs of Railway Vehicles*” GM/RT2161, Issue One, August 1995.



[25] J. CARRUTHERS “*Work Package 4F Rail Vehicle Driver’s Cab Task 4-F.2 Conceptual Design Rail Vehicle Cab Load Case Document*” NewRail, DE-LIGHT Transport Project.

[26] LS-Dyna support <http://www.dynasupport.com/howtos/material/define-composites/>.

-
- GILLES GARDIOL “*Impact assessment methodology for rolling stock Passive Safety in the Framework EU legislation*” Innovation in Passive Safety and Interior Design, 7th Int. Symposium on PASSIVE SAFETY, Berlin, 2008.
 - REBECCA LAWTON, NICHOLAS J. WARD – “*Systems analysis of the Ladbroke Grove rail crash*” Accident Analysis & Prevention Volume 37, Issue 2, March 2005, Pages 235-244.
 - ANSF “*Rapporto Annuale sulla Sicurezza della Circolazione dei Treni e dell’Esercizio Ferroviario*” Anno 2007.
 - S.-T. HONG A, J. PAN A, T. TYAN B, P. PRASAD B - *Quasi-static crush behavior of aluminum honeycomb specimens under non-proportional compression-dominant combined loads*, Int. J of Plasticity 22 (2006) 1062–108.
 - HAN ZHAO, GE RARD GARY - *Crushing behaviour of aluminium honeycombs under impact loadings*, Int. J. Impact Engng Vol. 21, No. 10, pp. 827–836, 1998.
 - JEOM KEE PAIK, ANIL K. THAYAMBALLI, GYU SUNG KIM - *The strength characteristics of aluminum honeycomb sandwich panels*, Thin-Walled Structures 35 (1999) 205–231.
 - JEOM KEE PAIK, ANIL K. THAYAMBALLI, GYU SUNG KIM “*The strength characteristics of aluminum honeycomb sandwich panels*” Thin-Walled Structures 35 (1999) 205–231.
 - M. VURAL, G. RAVICHANDRAN – “*Dynamic response and energy dissipation characteristics of balsa wood: experiment and analysis*”, Int. J of Solids and Structures 40 (2003) 2147–217.
 - V.L. TAGARIELLI, V.S. DESHPANDE, N.A. FLECK, C. CHEN - “*A constitutive model for transversely isotropic foams, and its application to the*



indentation of balsa wood”, Int. J of Mechanical Sciences 47 (2005) 666–686.

- S.R. REID and C. PENG – “*Dynamic uniaxial crushing of wood*”, Int. J of Impact Engng, Vol. 19, Nos. 5--6, pp. 531-570, 1997.
- LEE R. CALCOTE “*The Analysis of Laminated Composite Structures*” VAN NOSTRAND REINHOLD COMPANY 1969.
- XUE, X., SMITH, R. A. AND SCHMID, F. (2005) '*Analysis of crush behaviors of a rail cab car and structural modifications for improved crashworthiness*', Int. J. of Crashworthiness, 10:2, 125 — 136.
- ECKART JÄDE “*Development Process of a Side Bumper Crash Device*” Innovation in Passive Safety and Interior Design, 7th Int. Symposium on PASSIVE SAFETY, Berlin, 2008.
- A. ROSSI, Z. FAWAZ, K. BEHDINAN “*Numerical simulation of the axial collapse of thin-walled polygonal section tubes*” Thin-Walled Structures 43 (2005) 1646–1661
- W. ABRAMOWICZ, N. JONES “*Transition from Initial Global Bending to Progressive Buckling of Tubes Loaded Statically and Dynamically*” Int. J Impact Engng, Vol. 19, Nos. 5-6, pp. 415-437, 1997.
- T. WIERZBICHI, W. ABRAMOWICZ, “*On the Crushing Mechanics of Thin-Walled Structures*” J. Appl. Mech. -- December 1983 -- Volume 50, Issue 4a, 727-734.
- W. ABRAMOWICZ, T. WIERZBICHI, “*Axial Crushing of Multicorner Sheet Metal Columns*”, J of Appl. Mech., Volume 53, (1989) 113 – 120.
- M.D.WHITE, N. JONES, “*A theoretical analysis for the dynamic axial crushing of top-hat and double-hat thin-walled sections*”, Proceedings of the Institution of Mechanical Engineering, Part D: Journal of Automobile Engineering 213 (1999) (D4), pp. 307–325.
- A. A. N. ALJAWI, M. ABD-RABOU, AND S. ASIRI, “*Finite Element and Experimental Analysis of Square Tubes Under Dynamic Axial Crushing*” European Congress on Computational Methods in Applied Sciences and Engineering July 2004.
- B.P. DIPAOLO, P.J.M. MONTEIRO, R. GRONSKY “*Quasi-static axial crush response of a thin-wall, stainless steel box component*” Int. J of Solids and Structures 41 (2004) 3707–3733.



- JJ CARRUTHERS, AP KETTLE AND AM ROBINSON - “*Energy absorption capability and crashworthiness of composite material structures: A review*” Appl. Mech. Rev. October 1998 Volume 51, Issue 10, 635.
- G. PITARRESI, J.J. CARRUTHERS, A.M. ROBINSON, G. TORRE, J.M. KENNY, S. INGLETON, O. VELECELA, M.S. FOUND “*A comparative evaluation of crashworthy composite sandwich structures*” Composite Structures Volume 78, Issue 1, March 2007, Pages 34-44.
- Health and Safety Commission (HSC) and Health and Safety Executive (HSE) to the Office of Rail Regulation (ORR) “*The train collision at Ladbroke Grove 5 October 1999*”.